ANALYTICAL AND NUMERICAL STUDY OF CONVECTIVE HEAT TRANSFER IN POROUS MEDIA

By

P.V.S.N. MURTHY

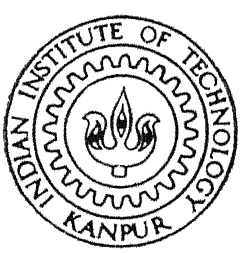

DEPARTMENT OF MATHEMATICS

INDIAN INSTITUTE OF TECHNOLOGY KANPUR

SEPTEMBER 1996

Analytical And Numerical Study Of Convective Heat Transfer In Porous Media

A Thesis Submitted in Partial Fulfilment of the Requirements
for the Degree of
DOCTOR OF PHILOSOPHY
by

P V S N MURTHY

to the

Department of Mathematics

Indian Institute of Technology Kanpur

SEPTEMBER 1996

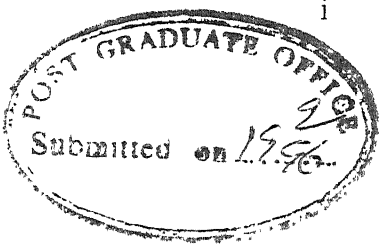

CERTIFICATE

It is certified that the work contained in the thesis entitled " *Analytical And Numerical Study Of Convective Heat Transfer In Porous Media* ", by **P.V.S.N. Murthy**, has been carried out under my supervision and that this work has not been submitted elsewhere for a degree.

Professor Punyatma Singh
Department of Mathematics
I.I.T. Kanpur
INDIA

19- September 1996.

Dedicated With Love

To My Parents

Sri. P.V. CHALAPATI SARMA

Smt. P. GAYATRI

ACKNOWLEDGEMENTS

It is my privilege to work with Professor Punyatma Singh, Chairman, Department of Mathematics, I.I.T - Kanpur. I sincerely record my gratitude for his invaluable guidance and constant encouragement throughout the preparation of this thesis. The amount of freedom I enjoyed during my research is unexpressible.

I am deeply indebted to the dynamic personality, Dr. B.V.Rathish Kumar, without whose help the numerical study presented in the thesis would not have been possible. I am very much thankful for his help and suggestions during the later part of my thesis work. I am thankful to the faculty, Department of Mathematics for their constant encouragement and suggestions at various committees like the comprehensive examination and the state of the art seminor etc. My special thanks are also due to Prof. J.B.Shukla for his critical observations at the Open Seminor presentation. I am also thankful to Prof. V.Raghavendra, Prof.Peeyush Chandra and Prof.Prawal Sinha for the concern they showed for the progress of my work.

I am extremely thankful to Professor Adrian Bejan, Dept of Mech Engg, Duke University, N.C, U.S.A, for his constant encouragement and also for sparing his precious time to review one of the chapters.

I thank all my friends, especially Appaji Rao, Bhadri, Balaji, Rajesh, Bera, Alok, Sri Jayaram Kumar and Dr. G.S.Narayanaji for being cooperative and also for making my stay in the campus enjoyable every moment.

To my parents, brother and sisters, I am indebted for the sacrifices they made for the sake of my education. Bhavani and Janakiram are gratefully acknowledged for their best wishes for my completion of research work. He has been a constant source of inspiration and encouragement through out my education, my heart felt gratitude to the personality, Sri. P.V.S.S.S.R.Krishna. I am grateful to my uncles, whose encouragement made possible this research. Happy to acknowledge my friends Raghu Ram and Subrahmanyam who are ever encouraging in all aspects of my life.

Financial assistance for this research work from I.I.T - KANPUR is gratefully acknowledged.

Date : 10 - 7 - 96

P.V.S.N. Murthy

SYNOPSIS

Convective heat transfer in porous media has been the challenging areas of research because of its various industrial and engineering applications. The work presented in the thesis can be broadly divided into two parts namely analytical (Chapters 2 - 5) and numerical (Chapters 6 & 7) study of convective heat transfer in porous media. In Chapters 2 & 3 the analysis of the combined effect of thermal dispersion and surface mass flux on Forchheimer free convection over semi-infinite flat plate and vertical cone pointing downwards is done using analytical techniques. The effect of viscous dissipation on non-Darcy natural convection over semi-infinite vertical flat plate has been initiated in Chapter 4. Forchheimer mixed convection over an isothermal vertical cone has also been done in Chapter 5. The free convection heat transfer from an isothermal sinusoidal vertical and horizontal wavy walls in a Darcian fluid saturated porous enclosure has been analysed in Chapters 6 & 7 using Bubnov - Galerkin finite element method numerically. Chapter 1 is introductory and contains a brief outline of the Darcy, Forchheimer and Brinkman flow models and their validity and limitations. To an extent the effect of thermal dispersion and viscous dissipation are also outlined. A review of the previous work of authors mainly related to present study is also included in this chapter.

In Chapter 2, the combined effect of surface mass flux and thermal dispersion on Forchheimer free convection from a horizontal flat surface is analysed when the surface heat flux remains constant. First, the effect of thermal dispersion on non-Darcy natural convection is analysed using integral technique. Then the combined effect of thermal dispersion and surface mass flux is analysed using similarity transformation. In both the cases, Forchheimer extension is considered in the flow equations and the coefficient of thermal diffusivity has been assumed to be the sum of molecular diffusivity and the dynamic diffusivity due to mechanical dispersion. The dynamic diffusivity varies linearly with the stream wise velocity component. Exponential profiles are chosen for the velocity and temperature distributions in the integral analysis. The closed form solutions for the boundary layer thickness, velocity and temperature distributions are obtained for the case when the wall heat flux is constant. The suction/injection velocity distribution has been assumed to have power function form Bx^l, similar to that of the wall temperature distribution Ax^n, x is the distance along the wall from the leading edge. For the problem of constant heat flux from the surface similarity solution is possible when the exponent l = -1/2. The obtained results in both the cases are

shown in the computer generated plots.

Chapter 3 is devoted to study the combined effect of thermal dispersion and lateral mass flux on Forchheimer natural convection over an isothermal vertical flat plate and a vertical cone pointing downwards. For the impermeable isothermal flat plate, two similarity transformations are possible for Forchheimer free convection, one by comparing the order magnitudes of the Darcy - buoyancy forces and the other by comparing that of the inertia - buoyancy forces. A correlation equation has been obtained to connect the Nusselt number results of both the cases. When Darcy law is used, the similarity solution is possible for a class of wall temperature variations and corresponding mass flux variations for the plane wall case. Because of the non-linearity in the Forchheimer flow model, this generality is reduced to the isothermal wall temperature variation with the fixed form of lateral mass flux $B\,x^{-1/2}$. In all the axi-symmetric configurations, it has been observed from the analysis that the similarity solution is possible only for vertical cone when the thermal dispersion effect is considered. The Nusselt number results are tabulated and the velocity and temperature distributions are plotted.

In chapter 4, the study of the effect of viscous dissipation on non-Darcy natural convection in porous medium is initiated. We considered the steady two-dimensional Forchheimer natural convection flow and heat transfer along an isothermal vertical wall with thermal dispersion and viscous dissipation effects. The inertia - buoyancy scaling is adopted and the effect of viscous dissipation in non-Darcy, intermediate and limit Darcy regimes is studied with and without thermal dispersion effects. The results show a significant decrease in the heat transfer rate with the inclusion of viscous dissipation effect. It is seen that as the value of dispersion parameter increases, the effect of viscous dissipation increases in all the three regimes and the percentage decrease in the value of the Nusselt number increases as one moves from the non-Darcy flow regime to the limit Darcy flow regime.

In chapter 5, similarity solution for non-Darcy mixed convection about an isothermal vertical cone pointing downwards in a fluid saturated porous medium for uniform free stream velocity is obtained. Similarity solution for the present problem is possible when curvature effects are neglected. The convection domain is divided into pure and mixed regions using the 5% deviation criteria. The effect of thermal dispersion is studied in both the aiding and opposing flows. Flow separation occurs when the forced and free convection act in opposite directions. It is interesting to note that when buoyancy effects are neglected,

similarity solution exists for all realistic power law variations of the wall temperature and for uniform free stream velocity, also a closed form solution is obtained for the isothermal wall temperature and uniform free stream. The overall heat transfer is enhanced due to the thermal dispersion effects. Chapter 6 deals with the heat transfer from the isothermal vertical sinusoidal wavy wall in the porous square enclosure. The other vertical wall is kept at the ambient temperature and the top and bottom walls are maintained adiabatic. Darcy's law is assumed to be valid in the enclosure. The governing parameters are the Rayleigh number based on the length of the wavy wall, the amplitude, phase of the wave and the number of waves considered per unit length. It has been observed that these four parameters have crucial effect on the global heat flux. The problem is solved using Galerkin finite element method. The results indicate that the Rayleigh number increases the global heat flux. The amplitude of the wave causes buoyancy loss in convection heat transfer and the increase in the number of waves per unit length further increases this loss. Hence the increase in the amplitude and number of waves per unit length decreases the global heat flux. The phase of the wave has got a significant effect on the heat transfer results.

In Chapter 7, the simulation of flow structure in the natural convection due to a uniformly heated horizontal wavy wall in a saturated porous enclosure is initiated. The wavy wall is assumed to be sinusoidal in structure. The numerical simulation is carried out by using Bubnov Galerkin Finite Element Method. The computational experiments are carried out for various values of the parameters and it is observed that the global heat flux decreases with increasing value of amplitude. The flow driving buoyancy force is seen to enhance the heat transfer into the system, at the same time, the intensified stream inside the separated region is seen to trap the heat and hinder the heat transfer. Because of this, only marginal changes could be seen in the heat transfer results with the increasing Rayleigh number. These results with varying amplitude, phase and Rayleigh number are clearly depicted through the computer generated plots for streamlines, isotherms and global heat flux.

LIST OF CONTENTS

Chapter 1

Introduction

1.1 Porous Medium - Heat Transfer

A porous medium may be defined as a solid matrix containing holes either connected or non-connected, dispersed within the medium in a regular or random manner provided such holes occur frequently in the medium. If these pores are saturated with a fluid, then the solid matrix with the fluid is called a fluid saturated porous medium. The flow of the fluid in a saturated porous material is possible only when some of the pores are interconnected. The interconnected pore space is termed as the *effective pore space* and the whole of the pore space is called the *total pore space*. If the package of the solid grains is regular, then it is called an *ordered porous material*, otherwise it is called a *random porous material*. Most natural and some of the artificial porous materials have random void structure. Natural porous media are ground soil, beach sand, rye bread, wood, human lung, etc., a few to quote.

Porosity of a porous material is defined as the fraction of the bulk volume of the porous material occupied by pores. This gives the total porosity of the medium. But the effective porosity ϕ is defined as fraction of the bulk volume of the material occupied by the interconnected pores. Depending on the structure of the porous medium, the fluid conductivity of the porous material i.e., the permeability K is defined as the ease with which a fluid may be made to pass through the material by an applied pressure gradient. The permeability depends on the microstructure of the medium and is independent of the properties of the

saturating fluid. Connecting this with the fluid property μ as $\frac{K}{\mu}$ gives the mobility of the fluid in the medium.

Heat propagation is meant the exchange in internal energy between individual elements or regions of the medium considered. It always occurs from higher temperature region to lower temperature region. There are three modes by which heat transfer is possible. Those are *Conduction*, *Convection* and *Radiation*. Conduction is because of molecular transport of heat in bodies (or between bodies) in the thermodynamical system considered. There is no actual displacement of particles from one place to another. Convection is concerned with the fluid medium and/or the fluid in the medium. The motion of a non-isothermal fluid is called convection. Here, the transport of heat is mainly because of the movement of fluid from one region to the other region in the medium. Pure conduction can be observed in solids where as heat transfer by convection is always accompanied by conduction and this is observed in fluid media. This combined process of heat transfer by conduction and convection is referred to as convective heat transfer. The conversion of the internal energy of a substance into radiation energy is referred to as radiation heat transfer. It propagates by means of electromagnetic waves depending on the temperature and on the optical properties of the emitter.

The interest of the present thesis is to study the convective heat transfer in fluid saturated porous media. Convective heat transfer is further classified as *Forced Convection*, *Free Convection* and *Mixed Convection*. Forced convection originates due to an external agent which induces the flow of fluid over the heated body where as the motion in natural convection arises only because of density variations which come into play due to temperature and concentration changes in material phases and other effects in the body force field. The natural flow developed is relatively weak with relatively small velocities when compared with the forced flows. Also the governing equations will become coupled in the natural convection process where as in the forced convection process, flow field can be solved independently first and then used to solve the energy equation for finding the temperature distribution. In mixed convection the order magnitude of the buoyancy force is comparable with the externally maintained pressure drop to force the flow. If the buoyancy force has component in the direction of the free stream, then it is called an *aiding flow* and if buoyancy opposes the free stream, then it is called an *opposing flow*.

Thus to understand the convective heat transfer in a porous medium, the flow field in

the porous medium has to be understood properly first. Attempts were made to understand the flow through such a complicated labyrinth in two ways, by *postulation* and *averaging* approaches. In the postulation approach one develops balance equations for each phase by writing the conservation laws directly in terms of the average quantities. Constitutive behavior, including the transport coefficients and the interactions between them, are then deduced from experiments. The final product is a closed set of equations in which the dependent variables are averages of the microscopic field variables such as velocity, pressure and temperature. In the averaging approach one starts by writing the microscopic balance equations for each phase in differential form. These are the familiar equations of fluid mechanics and heat transfer. One then takes the phase average of each equation to produce an averaged balance equation. Most of the analytical studies in porous medium use the former approach.

1.2 Equation of Continuity

For the solid part, equation of continuity holds since the solid in the medium is stationary (we consider consolidated solid structure). For the fluid medium we can derive the equation of continuity as : the mass instantaneously trapped inside the control volume is equal to the net flow rate (in - out). This implies

$$\frac{\partial \rho}{\partial t} + \nabla \cdot \rho \mathbf{V} = 0 \tag{1.1}$$

where ρ is the density of the fluid and $\mathbf{V}$ is the area averaged velocity vector. Usage of the area averaged quantities in deriving this equation makes it to look similar to the equation of continuity for the clear fluids. The concept of area averaged velocity was introduced precisely in order to be able to apply the pure fluids mathematical tools to flows through porous media (see Bejan [2]). When the density of the fluid is constant the above equation for two dimensional flow becomes

$$\nabla \cdot \mathbf{V} = 0 \tag{1.2}$$

1.3 Equation of Motion

The governing equation for fluid motion in a vertical porous column was first given by Darcy (1856). His experimental observation was that the volume flow rate Q' of the fluid in the fluid saturated sand column is proportional to the difference in the peizometric head $\triangle h$ and the cross-sectional area A of the sand column and inversely proportional to the thickness of the sand column $\triangle s$. The proportionality constant, he called it as the hydraulic conductivity K_c. In mathematical form it is given as

$$Q' = \frac{K_c A \triangle h}{\triangle s} \tag{1.3}$$

The pressure head h is equal to $(z + \frac{P}{\rho g})$ where z is the elevation, P is the pressure and ρ is the density of the fluid. Further, experiments revealed that the hydraulic conductivity is proportional to the density and inversely proportional to the viscosity of the fluid. Expressing the above equation in terms of the space averaged velocity (or Darcian velocity), we have

$$v = -\frac{K}{\mu}\frac{d}{ds}(P + \rho g z) \tag{1.4}$$

where K is the (intrinsic) permeability of the medium and is given by $K = \frac{\mu K_c}{\rho g}$. The relation between the permeability and the porosity of the medium is given by $K = \frac{d^2\phi^3}{(1-\phi)^2}$ for the porous medium composed of solid spheres, d is the diameter of the spheres. The '-' sign indicates that the fluid velocity is in the opposite direction of increasing pressure gradient. This equation has been generalized to higher dimensions. In vector form, this equation can be written as

$$\mathbf{V} = -\frac{K}{\mu} \bigtriangledown (P - \rho \mathbf{g}) \tag{1.5}$$

where $\mathbf{g}$ = (0,0,-g). The permeability K is constant for an isotropic medium. Here we assumed the medium is isotropic. But for anisotropic porous medium, K will be a second order tensor whose components depend on the direction of the experiment from which it is measured. The above equation represents a balance of viscous force, gravitational force and pressure gradient. This model does not take inertial effects into consideration. So this model is valid for seepage flows only i.e., for flows with $O(Re) < 1$, where Re is the Reynolds number defined as $\frac{uK^{1/2}}{\nu}$, $K^{1/2}$ is used as the length scale in porous medium. For $O(Re) < 1$, the friction factor f_k which is defined as

$$f_k(Re) = \frac{-\left(\frac{dp}{dx}\right) K^{1/2}}{\rho u^2} \tag{1.6}$$

becomes equal to $\frac{1}{Re}$. Also, this friction factor relation is observed to be violated for O(Re) ≥ 1.

At moderate and high velocities, inertial effects become appreciable, causing an increase in the form drag due to which the fluid velocity gets reduced. Forchheimer (1901) was the first person to propose a correction to the Darcy's law to consider the inertial effects. He conducted experiment to study the flow at O(Re) ≥ 1. He considered horizontal flow at moderate velocities and proposed that as the velocity of the fluid is increased, form drag developed (because of the inertial effects offered through the solid matrix) is proportional to the square of the velocity. So at moderate velocities, the breakdown in linearity in the Darcy's law is understood to be due to the fact that the form drag due to the solid obstacles which is comparable with the surface drag due to friction. So the appropriate modification to the Darcy's equation at moderate velocities will be

$$B(q)\mathbf{V} = -\frac{K}{\mu}[\nabla P - \rho \mathrm{g}] \tag{1.7}$$

where the local velocity q is given by $(u^2 + v^2)^{1/2}$, u and v are the velocity components and $B(q)$ is given by

$$B(q) = \left[1 + \frac{C\sqrt{K}}{\nu} q\right], \tag{1.8}$$

C is the dimensionless form drag coefficient and it varies with the nature of the porous medium. Using this model, the friction factor results are observed to fit more closely with the experimental data. The coefficients of Darcy and Forchheimer terms contain both the fluid properties and the micro-structure of the porous medium. The validity of this model has been confirmed by a number of experimentalists. $f_k(Re)$ in this case is

$$f_k(Re) = \frac{1}{Re} + C \tag{1.9}$$

where C is an empirical constant approximately equal to 0.55 (Bejan [2]).

Under the assumption that the flow through an isotropic porous medium with high permeability must reduce to the viscous flow limit, Brinkman (1948) corrected Darcy's equation with the addition of Laplace term. Brinkman felt the need to account for the viscous force exerted by a flowing fluid on a dense swarm of spherical particles embedded in a porous mass and added the term $\mu' \nabla^2 \mathbf{V}$ to balance the pressure gradient. Here μ' is the effective viscosity $\mu' = \mu(1 + 2.5(1 - \phi))$. The validity of the Brinkman model is restricted to the high porosity medium (as confirmed by the experiments) and most naturally occurring porous

medium have porosities less than $\phi < 0.6$. So for high porosity medium (when convective inertia is negligible) the equation of motion will be

$$-(\nabla P - \rho g) = \frac{\mu}{K}\mathbf{V} + \mu' \nabla^2 \mathbf{V} \tag{1.10}$$

Another model which considers both Forchheimer and Brinkman term with no-slip boundary conditions is :

$$-\nabla P = \frac{\mu}{K}\mathbf{V} + \frac{C\rho|\mathbf{V}|}{\sqrt{K}}\mathbf{V} - \frac{\mu'}{\phi}\nabla^2 \mathbf{V}. \tag{1.11}$$

Yet another model in which the convective term has been considered along with these two effects has also been proposed to study the flow of fluid in the porous medium :

$$\rho \frac{D\mathbf{V}}{Dt} = -\nabla P - \frac{\mu}{K}\mathbf{V} - \frac{C\rho|\mathbf{V}|}{\sqrt{K}}\mathbf{V} + \frac{\mu'}{\phi}\nabla^2 \mathbf{V} \tag{1.12}$$

The validity and limitations of these models are well discussed in Nield and Bejan [7].

1.4 Energy Equation

Two options exist for deriving the energy equation. One is the two phase model and the other one which is widely used, is local equilibrium model. In the former case the fluid and solid are treated separately with respect to temperature. In the later case, solid and fluid are assumed to have the same local average temperature. When the temperature difference between solid and fluid phases is very high, the local equilibrium model becomes invalid, but the two phase model is a little complicated and controversial (see Tucker and Dessenberger [6]).

In the local equilibrium model, we consider the energy equations for both the fluid and solid phases separately first. For solid phase, the energy equation is

$$(\rho c)_s \frac{\partial T_s}{\partial t} = \nabla.(k_s \nabla T_s) \tag{1.13}$$

where ρ is the density, c is the specific heat, $(\rho c)_s$ is the heat capacity of the solid phase, T_s is the temperature of the solid phase, k_s is the thermal conductivity of the solid.

The energy equation for the fluid phase is

$$(\rho c_p)_f \frac{\partial T_f}{\partial t} + (\rho c_p)_f (\mathbf{V}.\nabla) T_s = \nabla.(k_f \nabla T_f) + \mu\Phi \tag{1.14}$$

$(\rho c_p)_f$ is the heat capacity of the fluid phase, V is the space averaged velocity of the fluid, T_f is the temperature of the fluid phase, k_f is the fluid thermal conductivity and μ is the kinematic viscosity of the fluid, Φ is the dissipation function. The internal heating associated with viscous dissipation is represented by the term Φ. This dissipation term equals the mechanical power needed to extrude the viscous fluid through the pore (see Bejan [2] and Tucker and Dessenberger [6]), this power requirement is equal to the mass flow rate times the externally maintained pressure drop divided by the fluid density. In-turn the pressure drop is proportional to the velocity of the fluid in Darcy law and proportional to B(q) in Forchheimer flow model. Integrating the above energy equations over the spaces occupied by the respective phases, adding both the equations and taking the volume average over a representative volume element of the porous medium, we obtain the energy equation as

$$\sigma \frac{\partial T}{\partial t} + \mathbf{V}.\bigtriangledown T = \bigtriangledown.(\alpha_e \bigtriangledown T) + \frac{\nu}{K c_p} B(q)(\mathbf{V})^2 \tag{1.15}$$

where σ is the heat capacity ratio and α_e is the effective thermal conductivity of the medium.

As we already noticed, in the porous medium, some of the pores may be non connected. The fluid entering these pores turns back and rejoins the main stream. Some of the pores are connected throughout. Also because the solid particles (obstacles) in the medium are randomly placed, the flow direction differs from point to point in the medium. Thus the tortuous nature of the porous matrix leads to the mixing of the fluid at the pore level. This hydrodynamic mixing of fluid at the pore scale is called the mechanical dispersion. Thus in the study of convective heat transfer in porous medium, in addition to the molecular diffusion, diffusion due to the thermal dispersion has also been incorporated to consider the effect of hydrodynamic mixing. The thermal dispersion term represents the contribution of joint variations in temperature and velocity to the transport of heat.

The effect of thermal dispersion can be understood from the simple situation : consider the uniform flow of fluid in a porous channel confined between two long parallel plates. The top wall is at temperature T_1 and the bottom wall is kept at higher temperature T_2 such that the conduction takes place in the upward normal direction of the bottom wall. Suppose the plates are long enough that the flow is fully developed in the x- direction (i.e., along the plates) implies $\frac{\partial}{\partial x}$ of any average quantity is zero. So in the energy equation convection term will be zero. However, one observes a larger heat flux when the fluid is flowing than when it is not. This is due to the dispersion effect.

Physically, dispersion occurs because the microscopic fluid velocities and temperatures

are different from the average values. Even though the average fluid motion in the normal direction in the above example is zero, on the microscopic scale the fluid moves up and down in the normal direction as it goes around the solid particles in the porous matrix. If the fluid experiences a temperature gradient at the same time it will then convect heat locally and if these temperature gradients are different from the gradient of the average temperature, then there will be net heat flux. In many cases, convection due to microscopic velocity deviations are not negligible.

The form of D_{ij}, the dispersivity tensor in the particular cases of very small and very large velocities has been discussed by Poreh [55]. From the physical and dimensional considerations it has been concluded that D_{ij} has a quadratic dependence on the velocity components for very small Reynolds and Peclet numbers and a linear dependence on the velocity components for large Reynolds numbers.

1.5 Boundary Conditions

Various types of boundary conditions used in the study of convective heat transfer in a fluid saturated porous medium (for boundary layer and enclosure flows) are discussed in Cheng [12] and Nield and Bejan [7]. In the study of heat transfer from impermeable walls, the condition of impermeability of the wall is used. Outside the boundary layer, the flow in the mainstream direction is assumed to be zero in the natural convection flows and in the mixed convection flows either constant or a power function form for the free stream can be assumed. A power function form of the suction or injection velocity at the wall can be assumed for permeable walls in case of non-zero surface mass flux. In the enclosure problems, the four walls may be assumed to be impermeable. The wall temperature is assumed to be greater than the ambient temperature. Isothermal and non isothermally heated walls are used. Outside the boundary layer, the temperature may be assumed to be equal to that of the ambient temperature. In enclosures walls can be isothermal or non-isothermal or adiabatic or of constant heat flux.

1.6 Literature

Owing to the complex structure of the porous medium, idealized models are employed to understand the flow and transport phenomenon in the porous medium. None of the models till today could give the clear picture of the transport mechanism in porous medium, but still some of the mechanisms like wall channelling and the thermal dispersion effects were described efficiently.

To begin with Darcy's law was used as the governing equation of motion and coupled it with the energy equation to study the convective heat transfer in the porous medium. The heat source has been assumed to be either vertical wall or horizontal wall (wall can be a flat plate or axi-symmetric or arbitrary shaped bodies, arbitrary shapes cannot be expressible in terms of mathematical equations) or a point source or a line source etc. These studies are very important because free convection about vertical/horizontal surfaces in a saturated porous medium has many interesting geophysical and engineering applications.

Porous materials are used in heat exchangers, building thermal insulators, porous insulators for fire fighting etc.. In the nuclear waste disposal industry, to model a suitable canester is very essential for the safety analysis . Axi-symmetric bodies are utilized as canesters. Their disposal to the sea bed or to the earth's crust needs a better understanding of the convection phenomenon in the porous medium. The extraction of petroleum to the last drop from the oil reservoirs in the earth's crust needs a nice knowledge of the convection mechanism and thorough understanding of the miscible displacement techniques in porous medium.

With the occurrence of volcanism, magmatic intrusions may occur at the shallow depths in the earth's crust. Meteoric water with which the earth is saturated, percolates down to the depth in the permeable formation and gets heated directly or indirectly by the intruded magma. Because of the density variations, this fluid is driven buoyantly upwards to the top of the aquifer. Hot fluids from thus formed aquifers are continuously withdrawn by a down-hold pump. For geothermal power generation, the hot fluids are then piped to a geothermal power plant to drive the turbine directly or indirectly. It is understood that the geothermal energy *can* replace all other forms of energy but the *identification* of geothermal reservoir and *extraction* of geothermal energy needs more sophisticated technology.

The whole process may be identified as the natural convection from a vertical wall in a

saturated porous medium. When a hot intrusive like molten magma is trapped in an aquifer, its cooling rate is governed by heat convection. Intrusives (such as natural rocks such as lava and other igneous rocks have a high total pore space but essentially no effective pore space), are being modeled as vertical or horizontal impermeable hot walls to understand the basic level behaviour of such complex situations. Since the source temperature is very high, the water adjacent to the intrusive may be vaporized during the initial stage of intrusion. The vaporization process ceases to exist when the intrusive is cooled to a temperature below the boiling point of water corresponding to its pressure. Thus to understand the complete convection phenomenon about a dike, one must consider the transient nature, change of phase of the ground water and the magma, non-uniform wall temperature distribution and the anisotropy of the rock formation. But to understand the basic mechanism this phenomenon has been modeled as the natural convection heat transfer from a vertical wall in a homogeneous and isotropic fluid saturated porous medium which will give the basic level solution. This will provide the information about the rate of cooling of vertical intrusions trapped in an aquifer as well as the rate of heat loss from underground energy transport.

One more interesting application of convection heat transfer in porous medium is in the Resin Transfer Molding. R T M is the process of producing fibre reinforced polymeric parts in final shape. Reinforced fibre is placed in a closed mold and resin is injected into the mold to fill up the pores. This is then cooled and cured and the fibre shapes are taken out from the mold in final form. With isothermal or non-isothermal resin filled into the pores, the cooling process needs an understanding of the convective phenomenon in fluid saturated isotropic porous medium.

Very recently, researchers are seeing the utility of the porous layers for transpiration cooling by water for fire fighting. Some more interesting applications on heat transfer in porous media can be found in Shenoy [3].

When the dimensions of the convective system is large ie., in convective heat transfer from infinite or semi-infinite walls or from an infinite line of heat source is tackled, it has been the common practice in all analytical studies to go for all possible simplifications without loss in the physics of the problem. Boundary layer approximations provide sufficient mathematical simplifications to tackle the problems analytically and gives clear understanding of the convective mechanism in the continuum fluid flows. The possibility of boundary layer simplifications in the fluid saturated porous medium is discussed for the first time by

Wooding [68]. He developed boundary layer analogy for the steady vertical convection from a point source of heat in fluid saturated porous medium. He observed that the diffusion effects can be neglected except in regions where the gradients of fluid properties are very large.

Since then, boundary layers on bodies immersed in saturated porous medium for both free and mixed convection have been the interest of several researchers. In natural convection heat transfer in porous medium the flow equations get coupled with the energy equation through the body force term, which is absent in the forced convection heat transfer. This complication has been successfully overcome (upto certain accuracy) by using the Boussinesq approximation which is given by

$$\rho = \rho_\infty[1 - \beta(T - T_\infty)]. \tag{1.16}$$

This clearly says the density linearly varies with the temperature. This approximation for density is used only in the body force term in the momentum equation as the density variations through other terms in the continuity and energy equations become negligible under the conditions at which the above relation holds good Gebhart [1].

Different mathematical tools are employed for solving these boundary layer equations: Some of these tools are similarity solution technique, integral method, Meskyn's series solution technique, local similarity and local non-similarity methods, Keller's box method, finite difference and finite element techniques.

Similarity analysis is used to investigate the conditions under which the solutions of a particular boundary value problem have similar forms for different values of the independent variables. In two - dimensional flow problems, if similarity exists, then the independent variables can be merged into a single similarity variable and the governing partial differential equations are reduced into ordinary differential equations. This is a considerable mathematical simplification. The classical way of obtaining the similarity transformation (Sparrow et al, [34]) is now replaced by the scale analysis (Bejan [2]). In the analytical study done here we use this new technique. Thus reduced ordinary differential equations allows the usage of the generalized techniques developed for solving ordinary differential equations. The motivation for seeking similar solutions is of three fold. Firstly, the results may be directly usable in important technical applications. Secondly, the similar solutions provide a standard of comparison against which approximate methods may be checked. Once verified, the approximate methods may then be used in studying more complex flow situations where the

conditions of similarity solutions are not satisfied. Finally, the general trends may provide valuable insight in understanding the physical occurrences which take place in complicated flows.

Approximate methods like Karman - Pohlhausen integral technique has also been used in the study of convection heat transfer problems in cases where similarity solutions is not possible. The main aim of this method is also suppressing of one of the independent variable by integrating the momentum and energy equations across the boundary layer. Thus obtained integral forms of the equations are solved by suitably choosing the profile shapes for the velocity and temperature distributions. This process sometimes might reduce these equations into algebraic equations, which can be solved very easily. Though it is an approximate solution technique, this method is very famous since it is easy to handle the problem using this method and computational expenses are negligible when compared with the other methods. Sometimes this method leads to the closed form solutions for velocity and temperature profiles.

When similarity solution is not possible, then the coefficient which contains the independent variable other than the similarity variable may be made as a parameter ϵ and the dependent function is expanded in a series form in-terms of this parameter and the unknown function form of the similarity variable. Since the series will converge for $\epsilon < 1$, the solution obtained in this way is accurate for small values of the parameter. The basic level solution will be the solution of the differential equations with ϵ^o term. Then this system is augmented with ϵ^1 equations and thus obtained solution will give first order effects of the parameter. To know the higher order effects, one should proceed solving the augmented system of equations with higher order terms of the parameter ϵ.

Other approximate analytical methods are local similarity technique and local non-similarity technique and are well described in Rogers [8].

Bejan [2] discusses clearly the external and internal convection in Darcian fluid saturated porous medium. A very recent book by Nield and Bejan [7] is a researcher's literature survey book giving every minute detail about the happenings in the field of convective heat transfer in porous medium upto the year 1992. Cheng [12] discusses about convective heat transfer aiming at the extraction of geothermal energy using governing equations in porous medium. In Sahimi [11], the flow and transport in porous media and fractured rock has been discussed and various applications of the flow through porous media such as miscible displacement and

nmiscible displacement techniques are also discussed.

Johnson and Cheng [73] reviewed all possible similarity solutions for free convection djacent to flat plates which were dealt with the Darcy model. A more general similarity ·ansformation was proposed by Nakayama and Koyama [17] for free convection and [18])r combined convection over a non-isothermal body of arbitrary shape embedded in a fluid ıturated porous medium. In addition to the similarity analysis, integral technique has lso been employed by Nakayama and Koyama [17]. These arbitrary shaped bodies include ertical flat plate, horizontal ellipse and ellipsoids with different minor-to-major axis ratios, ertical wedge, vertical cone, horizontal circular cylinder and a sphere.

Vafai and Tien [49] discussed the boundary and inertia effects on flow and convective eat transfer in porous medium to study the presence of the solid boundary. Using the local olume averaging technique they averaged the microscopic forms of the governing equations ver a representative volume element of the porous medium. Thus obtained surface integrals ·ere explained to give a measure of the flow resistance offered by the solid matrix and arrived t the Forchheimer and Darcian terms as the resisting forces for fluid flow. Keeping in mind, ıe special feature of high porosity medium, the flow equations should tend to the viscous ow equations, they retained the Brinkman viscous term in the flow equation. They solved ıe resulting equations and observed that both the inertia and boundary forces decrease the)nvective heat transfer rate since both are flow resisting forces.

Later Plumb and Huenefeld [56] studied the non-Darcy natural convection over a vertical ·all in a saturated porous medium. They used the Ergun model as the momentum equation. Inlike in the Darcy case, the similarity solution was possible only for isothermal wall. They sed Darcy-buoyancy force comparison in the scale analysis and obtained the similarity ·ansformation. Results reveal that the inertial effects thicken the boundary layer thickness nd resist the heat transfer. For the vertical heated surfaces the deviation of the heat transfer esults from its Darcian counterpart is less than 5% for the modified Grashoff number less han 0.1 and when it is greater than 0.1 the deviation increases rapidly.

By considering inertia and buoyancy force comparison in scale analysis Bejan and Poulikakos 16] proposed new scales for boundary layer thickness and stream function. This analysis ; effective at large Reynolds number limit where Darcy law is invalid and inertial effects re important. A new non-dimensional group G was identified which takes the flow field :om non-Darcy to intermediate and to the limit Darcy at $G = 0$, $G = O(1)$ and $G \to \infty$

respectively. This transformation permits similarity solution for isothermal wall and also in the case when surface heat flux is constant when the Darcian term is neglected. The Nusselt number result indicates the reduced heat transfer because of the quadratic drag term.

The results obtained by using these two different scales in the analysis of non-Darcy natural convection from vertical wall lead to two different Nusselt number expressions. In chapter 3, we give a correlation equation which behaves like a bridge between these two Nusselt number results. Chen and Ho [48] studied this problem for all power function variations of the wall temperature using local non-similarity technique. An integral treatment was given for non-Darcy natural convection over a flat plate and a cone in Nakayama et al [20]. A one parameter family of third degree polynomial is used to describe the velocity field. The Nusselt number results were in good agreement with the similarity results. Lai and Kulacki [35] studied the inertial effects on convection from horizontal impermeable surface. When the surface heat flux is uniform, similarity solution is possible for free convection case and in the mixed convection case, the free stream should be maintained at uniform velocity.

Ingham [30] gave a similarity transformation for non-Darcy free convection boundary layer on axi-symmetric and two dimensional bodies of arbitrary shape. He completely neglected the Darcian effects in this study. As in the Darcy case, a more general transformation for Forchheimer free convection over a non isothermal body of arbitrary shape was given by Nakayama et al [21]. This analysis is also confined to non-Darcy regime only since they neglect the over all Darcian effect on heat transfer.

In all the above studies the wall is assumed to be impermeable. However the influence of fluid suction and injection on convective heat transfer in porous medium have also been analysed. Influence of lateral mass flux on free convection from a vertical wall was studied by Cheng [12]. Similarity solution was possible when the suction/injection velocity varies in a specific relation with the power law variation of wall temperature. A more realistic case of isothermal wall variation and uniform suction/injection was analysed by Merkin [43] for the vertical wall. Series solution technique was used. It has been observed that fluid suction enhances the heat transfer rate where-as the fluid injection decreases it.

More recently Hooper et al [77] studied the influence of surface injection/suction on the mixed convection from a vertical plate. Using free and forced convection parameters they described a single governing parameter which dictates the whole mixed convection domain. The resulting non-linear differential equations were solved using the finite difference method.

respectively. This transformation permits similarity solution for isothermal wall and also in the case when surface heat flux is constant when the Darcian term is neglected. The Nusselt number result indicates the reduced heat transfer because of the quadratic drag term.

The results obtained by using these two different scales in the analysis of non-Darcy natural convection from vertical wall lead to two different Nusselt number expressions. In chapter 3, we give a correlation equation which behaves like a bridge between these two Nusselt number results. Chen and Ho [48] studied this problem for all power function variations of the wall temperature using local non-similarity technique. An integral treatment was given for non-Darcy natural convection over a flat plate and a cone in Nakayama et al [20]. A one parameter family of third degree polynomial is used to describe the velocity field. The Nusselt number results were in good agreement with the similarity results. Lai and Kulacki [35] studied the inertial effects on convection from horizontal impermeable surface. When the surface heat flux is uniform, similarity solution is possible for free convection case and in the mixed convection case, the free stream should be maintained at uniform velocity.

Ingham [30] gave a similarity transformation for non-Darcy free convection boundary layer on axi-symmetric and two dimensional bodies of arbitrary shape. He completely neglected the Darcian effects in this study. As in the Darcy case, a more general transformation for Forchheimer free convection over a non isothermal body of arbitrary shape was given by Nakayama et al [21]. This analysis is also confined to non-Darcy regime only since they neglect the over all Darcian effect on heat transfer.

In all the above studies the wall is assumed to be impermeable. However the influence of fluid suction and injection on convective heat transfer in porous medium have also been analysed. Influence of lateral mass flux on free convection from a vertical wall was studied by Cheng [12]. Similarity solution was possible when the suction/injection velocity varies in a specific relation with the power law variation of wall temperature. A more realistic case of isothermal wall variation and uniform suction/injection was analysed by Merkin [43] for the vertical wall. Series solution technique was used. It has been observed that fluid suction enhances the heat transfer rate where-as the fluid injection decreases it.

More recently Hooper et al [77] studied the influence of surface injection/suction on the mixed convection from a vertical plate. Using free and forced convection parameters they described a single governing parameter which dictates the whole mixed convection domain. The resulting non-linear differential equations were solved using the finite difference method.

The influence of surface mass flux and lateral mass flux on the Forchheimer free and mixed convection over horizontal and vertical walls was given in Ramanaiah and Malarvizhi [39] and [38] respectively. For the axi-symmetric body, the increase in the non-Darcy parameter decreases the heat transfer rate in both suction and injection domains. In the mixed convection case, the increase in the value of the mixed convection parameter increased the local heat flux in the suction and injection domains. As the surface temperature increases, the heat transfer rate increases as one moves from injection to suction domain.

At moderate flow velocities, the thermal dispersion effects are observed to become prevalent. For the first time, dispersion effect was considered by Cheng [60] and later by Plumb [57] in the study of non-Darcy natural convection over a vertical flat plate. Thermal dispersion has components in longitudinal and transverse directions. Cheng [60] assumed that dispersion coefficients are proportional to the velocity components and to the Forchheimer coefficient. He found that thermal dispersion decreases the surface heat flux.

Plumb [57] assumed that the longitudinal dispersion was negligible and the transverse dispersion was proportional to the stream-wise velocity component and gave the linear relation as $\alpha_{td} = \gamma d u$ where γ is the mechanical dispersion coefficient which has to be determined from the experimental results, d is the grain diameter. His expression for Nusselt number differs from that used in Cheng [60]. He observed that the inertial effect decreases the heat transfer where as thermal dispersion enhances it.

Hong and Tien [46] analysed the thermal dispersion effects on vertical free convection boundary layer in a porous medium. He took the boundary effects into consideration along with the no-slip boundary condition. Owing to the high porosity near the wall and thereby wall channelling effect heat transfer is more in a very small region near the wall. The singular perturbation solution revealed that the combination of no-slip boundary effects and dispersion effects results in large temperature gradients near the wall while it decreases a small distance away from the wall.

Since the no-slip wall effect is negligible for low porosity medium and it decreases as the value of the Rayleigh number increases (see Hong et al [47], Hsu and Cheng [25]), Lai and Kulacki studied the thermal dispersion effects on non-Darcy convection over Horizontal surface [36] and vertical wall [37] in a saturated porous medium. They obtained similarity solution in both the cases. Darcy-buoyancy comparison is used in the scale analysis. In the horizontal wall case, for the free convection problem the similarity solution is possible only

for the constant surface heat flux constant case and for mixed convection, the free stream should remain at uniform velocity. For the vertical wall case, the isothermal wall permits similarity solution when the free stream velocity remains constant.

Fand et al [71] observed from their experiment that the effect of viscous dissipation is significant when the saturating fluid is silicon oil. Using the one dimensional flow model and incorporating the viscous dissipation effects in the energy equation they observed that a decrease in the value of Nusselt number results. More recently, Nakayama and Pop [22] analysed the effect of viscous dissipation on the free convection over a non-isothermal body in a porous medium. They used the Karman-Pohlhausen integral technique in their study. It was observed that the viscous dissipation lowers the level of heat transfer rate.

The study of natural convection in confined porous media is fueled by interesting and important engineering applications. Natural convection in porous enclosures can be studied in two ways. One way is the natural convection in a layer with vertical sides maintained at different temperatures, and the other is natural convection in a porous layer heated from below. First configuration is widely used in the preparation of porous insulation layers oriented vertically, as in building technology, industrial cold storage installation and cryogenic engineering. The study of configuration is analogous to the Rayleigh-Benord convection which is known as the Morton-Rogers-Lapwood problem, which is useful to understand the functioning of geothermal systems and fibrous insulations of the type used in attics. Unlike the external free convection boundary layers that is caused by the heat transfer interaction between a single wall and porous medium extended semi-infinitely or infinitely in all the directions, natural convection in an enclosure is the result of complex interaction between a finite size fluid saturated porous matrix in thermal communication with all the walls that confine it. Review of all those articles on natural convection in porous enclosures can be found in Cheng [12] and Nield and Bejan [7].

All these works till today assume plane walls as the sides of the enclosures. The present thesis, however, investigates the fundamental behaviour of the fluid flow and the natural convection heat transfer in a fluid saturated porous enclosure with sinusoidal wavy wall as one of the boundaries of the enclosures. Both the basic problems of heating from side and from below of the enclosure are addressed. This non-linear geometry is attacked by the classical Bubnov-Gelarkin finite element technique. In addition to the flow driving Rayleigh number, the geometrical parameters due to the wavy nature of the wall arise and the effect

of all these parameters on the natural convection is analysed.

The work presented in the thesis can be broadly divided into two parts namely analytical (Chapters 2 - 5) and numerical (Chapters 6 & 7) study of convective heat transfer in porous media. In Chapters 2 & 3 the analysis of the combined effect of thermal dispersion and surface mass flux on Forchheimer free convection over semi-infinite flat plate and vertical cone pointing downwards is done using analytical techniques. The effect of viscous dissipation on non-Darcy natural convection over semi-infinite vertical flat plate has been initiated in Chapter 4. Forchheimer mixed convection over an isothermal vertical cone has also been done in Chapter 5. The free convection heat transfer from an isothermal sinusoidal vertical and horizontal wavy walls in a Darcian fluid saturated porous enclosure has been analysed in Chapters 6 & 7 using Bubnov - Galerkin finite element method numerically.

The various directions in which one can work to study the convection heat transfer in porous medium are : (1) the effect of viscosity variation with temperature (2) effect of porosity variation (3) effect of wall channelling (4) thermal dispersion (5) double diffusion (6) conjugate convection (7) viscous dissipation (8) anisotropy (9) relaxing the condition of local thermal equilibrium etc., independently and then examining their combined effects over the complex porous structure.

Chapter 2

Thermal Dispersion Effects On Non-Darcy Natural Convection Over Horizontal Flat Surface [1]

2.1 Introduction

Study of convective heat transfer in porous media has been the interest of several researches owing to its wide applicability in engineering and geophysical problems such as in oil recovery technology, in the use of fibrous materials for thermal insulations, in the design of aquifers as an energy storage system and also in Resin Transfer Molding process in which fiber reinforced polymeric parts are produced in final shape. A plethora of literature is available on convection in porous media using various flow models depending on their applicability and limitations. Most of the works dealing with convective heat transfer in porous media have been motivated by geothermal applications. Understanding the formation of geothermal reservoirs and its utilization for energy extraction needs thorough understanding of the convection in porous media. Inspite of the fact that many of the geothermal reservoirs are known to be fracture dominated, the studies based on the idealization of geothermal reservoir as a saturated porous medium can provide considerable insight into the physical process involved.

The study of free convection in a saturated porous medium above a heated horizontal

[1] Integral analysis has been accepted for publication in the journal "**Heat and Mass Transfer**"

surface (heated bedrock) or below a cooled horizontal surface (cooled cap-rock) with surface injection and suction of fluid has important geothermal applications. Energy extraction from magma which is defined as molten hot rock at a temperature in excess of $650°C$ lying beneath the earth's crust is done by injection of cold water down in one well, circulating through the artificially fractured zone while absorbing heat and is recovered as hot water or steam from the other well. Even though, it has been thought that the utilization of magma energy will not be feasible in very near future due to various technical difficulties, considerable attention has been paid to estimate the strength of the magma chamber. Cheng [12] gives a nice description of the geothermal heat sources and its proper utilization.

The literature regarding the past works in this direction has been briefed in the Chapter 1. After Wooding [68] proposed and used the boundary layer analogy for convection heat transfer in porous medium, several investigators used Darcy flow model and many others used non-Darcy flow models with boundary layer approximations in their study. The solution procedures mostly move around similarity, local similarity, local non-similarity, Meksyn's series method, finite difference and finite element methods. However, some of the studies were concentrated on the approximate Karman-Pohlhausen integral method also. Cheng [59] used integral method to obtain local heat transfer results for a number of heat transfer problems where similarity solutions exist. Later Nakayama and Koyama [17] studied the more general problem of free convection heat transfer over a non-isothermal body of arbitrary shape in a Darcian fluid saturated porous medium. Nakayama and Koyama [18] studied the heat transfer from horizontal surface when the surface heat flux remains constant. Integral method has been successfully employed by Singh and Sharma [67] and Bejan [2] to study the free convection from a vertical flat plate in a thermally stratified porous medium, where the similarity solutions were not possible.

Integral method has been successfully employed for the non-Darcy (Forchheimer) natural convection heat transfer in porous medium also inspite of the non-linearity of this model. Nakayama et al [20], Bejan and Poulikakos [16] presented integral solution for non-Darcy free convection over an isothermal vertical flat plate. A one parameter family of third order polynomial was employed in the former case where as exponential decay profiles were used in the later case for velocity and temperature distributions. When inertial effects are prevalent, thermal dispersion effects (due to the hydrodynamic mixing of the fluid in the pore scale) become important as observed by Plumb [57], Hong and Tien [46] and Lai and Kulacki [36], Nield and Bejan [7]. It has been observed that because of this effect, the heat transfer rate

is greatly increased.

The aim of the present chapter is to study the combined effect of surface mass flux and thermal dispersion on non-Darcy free convection from a horizontal flat surface when the surface heat flux remains constant. First, the effect of thermal dispersion on non-Darcy natural convection is analysed using integral technique. Then the combined effect of thermal dispersion and surface mass flux is analysed using similarity solution technique. In both the cases, Forchheimer extension is considered in the flow equations and the coefficient of thermal diffusivity has been assumed to be the sum of molecular diffusivity and the dynamic diffusivity due to mechanical dispersion. The dynamic diffusivity varies linearly with the stream wise velocity component. Exponential profiles are chosen for the velocity and temperature distribution in the integral analysis. The closed form solutions for the boundary layer thickness, velocity and temperature distribution are obtained for the case when the wall heat flux remains constant. The suction/injection velocity distribution is assumed to have power function form Bx^l, similar to that of the wall temperature distribution Ax^n, x is the distance from the leading edge. For the problem of constant heat flux from the surface similarity solution is possible when the exponent l takes the value -1/2. The obtained results in both the cases are analysed and are shown in the computer generated plots.

2.2 Governing Equations

Consider the problem of non-Darcy natural convection flow and heat transfer over a semi-infinite horizontal surface in a fluid saturated porous medium as shown in the Figure (2.1). The heated wall can be impermeable with $v_w(x) = 0$ or can be permeable which permits a surface mass flux in the normal direction in the form $v_w(x) = B\ x^l$. $x = 0$ represents the leading edge of the hot wall. The temperature of the wall is assumed to be of the form $T_w(x) = A\ x^n$. The governing equations for the flow and heat transfer are given by

$$\frac{\partial u}{\partial x} + \frac{\partial v}{\partial y} = 0 \tag{2.1}$$

$$u + \frac{C\sqrt{K}}{\nu}u^2 = -\frac{K}{\mu}\left(\frac{\partial p}{\partial x}\right) \tag{2.2}$$

$$v + \frac{C\sqrt{K}}{\nu}v^2 = -\frac{K}{\mu}\left(\frac{\partial p}{\partial y} + \rho g\right) \tag{2.3}$$

$$u\frac{\partial T}{\partial x} + v\frac{\partial T}{\partial y} = \frac{\partial}{\partial x}\left(\alpha_x \frac{\partial T}{\partial x}\right) + \frac{\partial}{\partial y}\left(\alpha_y \frac{\partial T}{\partial y}\right) \tag{2.4}$$

$$\rho = \rho_\infty[1 - \beta(T - T_\infty)] \tag{2.5}$$

along with the boundary conditions

$$\left.\begin{array}{lll} y = 0: & v_w(x) = B\,x^l, & T_w(x) = T_\infty + A\,x^n \\ y \to \infty: & u = 0, & T \to T_\infty \end{array}\right\}. \tag{2.6}$$

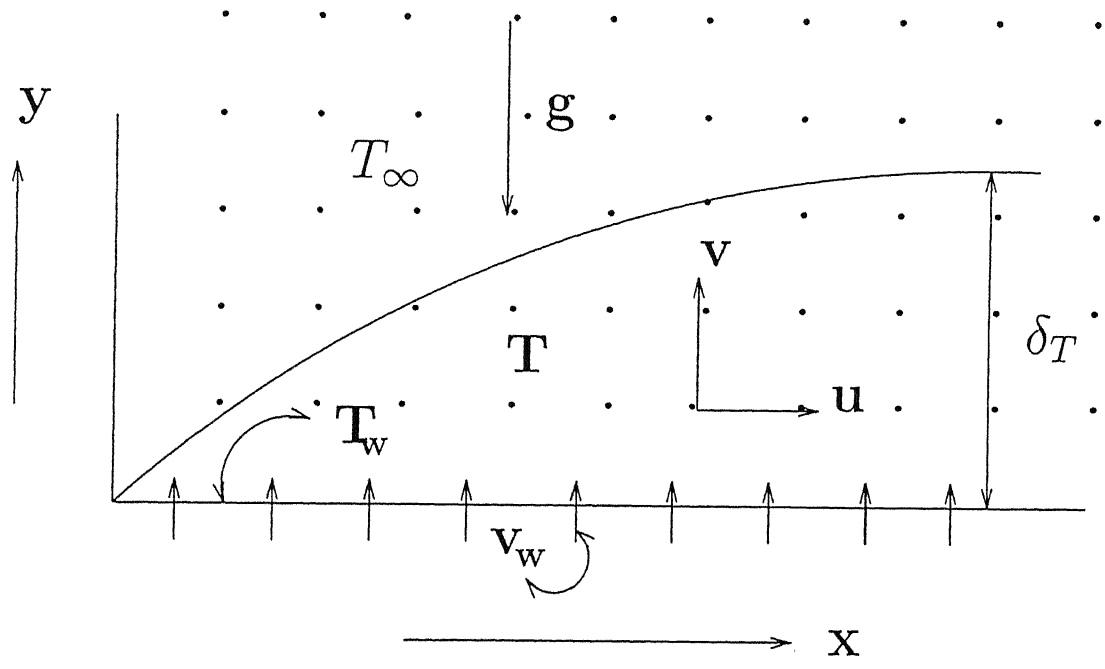

Figure 2.1: Coordinate system

Here x and y are the Cartesian coordinates, u and v are the Darcian velocity components in x and y directions, T is the temperature, ρ is the density, p is the pressure, β is the coefficient of thermal expansion, μ is the viscosity of the fluid, ν is the kinematic viscosity of the fluid, K is the permeability constant, C is an empirical constant, g is the acceleration due to gravity, α_x and α_y are the components of thermal diffusivity in x and y directions. The suffix w and ∞ indicate the conditions at the wall and at the outer edge of the boundary layer respectively. A,B,n and l are fixed real constants.

Experimental and numerical studies on convective heat transfer in a porous medium show that thermal boundary layers exist adjacent to the heated or cooled walls. When the thermal

boundary layer is thin (i.e., $x >> y \sim \delta_T$, δ_T is the boundary layer thickness), boundary layer approximations analogous to classical boundary layer theory can be applied [7]. Near the boundary, the normal component of seepage velocity is small compared with the other component of the seepage velocity and the derivatives of any quantity in the normal direction are large compared with derivatives of the quantity in the direction of the wall. Under these assumptions, the equations (2.1)-(2.4) become

$$\frac{\partial u}{\partial x} + \frac{\partial v}{\partial y} = 0 \tag{2.7}$$

$$u + \frac{C\sqrt{K}}{\nu} u^2 = -\frac{K}{\mu}\left(\frac{\partial p}{\partial x}\right) \tag{2.8}$$

$$\frac{\partial p}{\partial y} = -\rho g \tag{2.9}$$

$$u\frac{\partial T}{\partial x} + v\frac{\partial T}{\partial y} = \frac{\partial}{\partial y}\left(\alpha_y \frac{\partial T}{\partial y}\right) \tag{2.10}$$

Eliminating the pressure and invoking the Boussinesq approximations, the equations (2.8)-(2.10) become

$$\frac{\partial u}{\partial y} + \frac{C\sqrt{K}}{\nu}\frac{\partial u^2}{\partial y} = -\left(\frac{Kg\beta}{\nu}\right)\frac{\partial T}{\partial x} \tag{2.11}$$

$$u\frac{\partial T}{\partial x} + v\frac{\partial T}{\partial y} = \frac{\partial}{\partial y}\left(\alpha_y \frac{\partial T}{\partial y}\right) \tag{2.12}$$

Here α_y is a variable quantity which is the sum of molecular thermal diffusivity α and dispersion thermal diffusivity α_d. Following Plumb [57], the expression for dispersion thermal diffusivity α_d will be $\alpha_d = \gamma\, d\, u$, where γ is the mechanical dispersion coefficient whose value depends on the experiments, and d is the pore diameter.

2.3 Impermeable Wall: Integral Solution

Integrating the resulting equations (2.11) and (2.12) across the boundary layer (see eq.33 in [59]) to yield

$$\left(u + \frac{C\sqrt{K}}{\nu}u^2\right)|_{y=0} = \frac{Kg\beta}{\nu}\frac{d}{dx}\left(\int_0^\delta (T - T_\infty)dy\right) \tag{2.13}$$

and

$$\frac{d}{dx}\int_0^\delta u(T - T_\infty)dy = -\left[(\alpha + \gamma du)\frac{\partial T}{\partial y}\right]|_{y=0} \tag{2.14}$$

where $u_{|y=0} = u_w$ is the slip velocity at the wall, which remains to be determined. In obtaining the above equations, we have implicitly assumed that the thermal and velocity boundary layers are of same thickness (see [59]). The velocity and temperature profiles are assumed to be of the form

$$\left.\begin{aligned} u &= u_w e^{\frac{-\lambda y}{\delta}} \\ (T - T_\infty) &= (T_w - T_\infty) e^{\frac{-y}{\delta}} \end{aligned}\right\} \tag{2.15}$$

where λ is yet another unknown parameter to be determined. Clearly these profiles satisfy the boundary conditions (2.6). Substituting equation (2.15) into equations (2.13) and (2.14) we get,

$$\frac{C\sqrt{K}}{\nu} u_w^2 + u_w = \frac{Kg\beta}{\nu} \frac{d}{dx}(Ax^n \delta) \tag{2.16}$$

and

$$\frac{d}{dx}\left[u_w A x^n \frac{\delta}{\lambda + 1}\right] = (\alpha + \gamma d u_w) \frac{Ax^n}{\delta} \tag{2.17}$$

At this juncture we are left with two equations for obtaining the explicit forms for three unknowns δ,u_w and λ. Previous studies [17],[18],[20] which used integral method as the solution technique provide us a clue to have an additional constraint. To have the additional relation we evaluate the momentum and energy equations at the wall and club these two conditions. The resulting condition is

$$\lambda\left[u_w + \frac{C\sqrt{K}}{\nu} u_w^2\right] = \frac{Kg\beta}{\nu} \frac{1}{u_w}\left[(\alpha + \gamma d u_w)\frac{Ax^n}{\delta} + \gamma d \frac{\lambda A x^n}{\delta}\right] \tag{2.18}$$

So from equations (2.16),(2.17) and (2.18), we can obtain the three unknown functions u_w,δ and λ. The closed form solution of equations (2.16),(2.17) and (2.18) is be possible only when $n = 1/2$. In this case, δ may be written as

$$\delta = \left(\frac{\alpha\nu}{Kg\beta A}\right)^{1/3} x^{1/2}\delta^* \tag{2.19}$$

and slip velocity u_w becomes

$$u_w = \frac{P}{2C\sqrt{K}/\nu} \tag{2.20}$$

where P $= [(1 + 4Gr\delta^*)^{1/2} - 1]$ and Gr $= \frac{C\sqrt{K}\alpha}{\nu}\left[\frac{Kg\beta A}{\alpha\nu}\right]^{2/3}$. Here δ^* is the non-dimensional boundary layer thickness. Making use of equations (2.19) and (2.20), equations (2.17) and (2.18) reduce to the following algebraic equation in δ^* along with the flow and field parameters Gr,Ra_d and γ

$$(P^3 + P^2)[P\delta^{*3} - \delta^*(2Gr + DsP)] - 4Gr^2(2Gr + DsP) - 2GrDsP^2\delta^{*2} = 0 \tag{2.21}$$

where $Ra_d = \frac{Kg\beta(T_w - T_\infty)d}{\alpha\nu}$ and $Ds = \gamma Ra_d^{2/3}$ is the dispersion parameter.

2.3.1 Results and Discussion

In the above algebraic equation of degree 5 in δ^*, the parameter Gr represents the inertia effects on the natural convection, Ra_d is the modified Rayleigh number in terms of the por diameter d and γ is the mechanical dispersion coefficient. The parameter Gr can be rewritte as $F_o Ra_d^{2/3}$ where $F_o = \frac{C\sqrt{K}\alpha}{d\nu}$ is the fluid inertia parameter which reflects the structure an thermophysical properties of the porous medium. The quantity $\gamma Ra_d^{2/3}$ is defined to be th dispersion parameter which signifies the thermal dispersion effects. When γ=0, the problen reduces to the case without thermal dispersion effects.

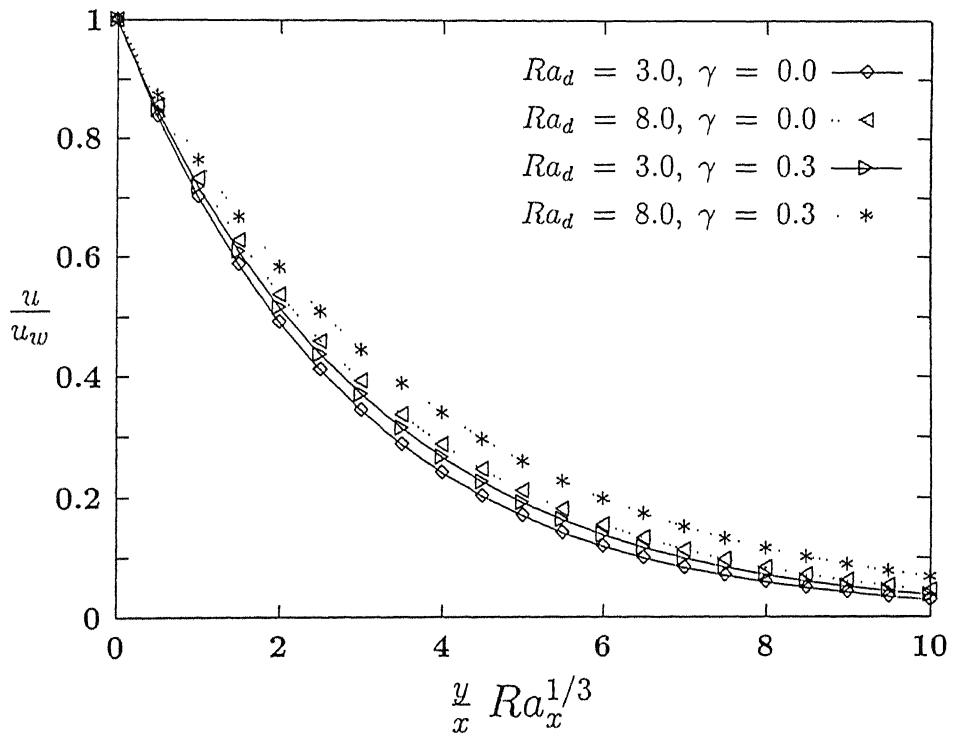

Figure (2.2): Effect of thermal dispersion on the non-dimensional velocity component when $F_o = 0.4$.

For fixed values of Ra_d, F_o and γ, equation (2.21) gives the appropriate value of δ^*, usin which u_w can be found from the equation (2.20). Then the value of λ can be determined fror equations (2.17) and (2.18). The non-dimensional velocity and temperature distribution ca be obtained from equation (2.15) and the obtained results are plotted in Figure (2.2) an Figure (2.3). In both the figures, abscissa is taken as $\frac{y}{x} Ra_x^{1/3}$ and the figures are plotte for fixed value of $F_o = 0.4$. Experimental studies on thermal dispersion confirm that th mechanical dispersion coefficient depends on the structure of the porous medium and th

solid grains [25]. Also, it is to be noted that γ takes values from the range 1/7 to 1/3. Fo all calculations, γ is taken to be 0.3 to signify the thermal dispersion effects. From both th Figure (2.2) and Figure (2.3) it is clear that for a fixed value of inertial parameter F_o, th increase in the value of the Rayleigh number thickens profile in both the cases of $\gamma = 0$ and $\gamma = 0.3$. Also when F_o and Ra_d are fixed, the increase in the value of thermal dispersion parameter increases the thickness of the velocity and temperature profiles.

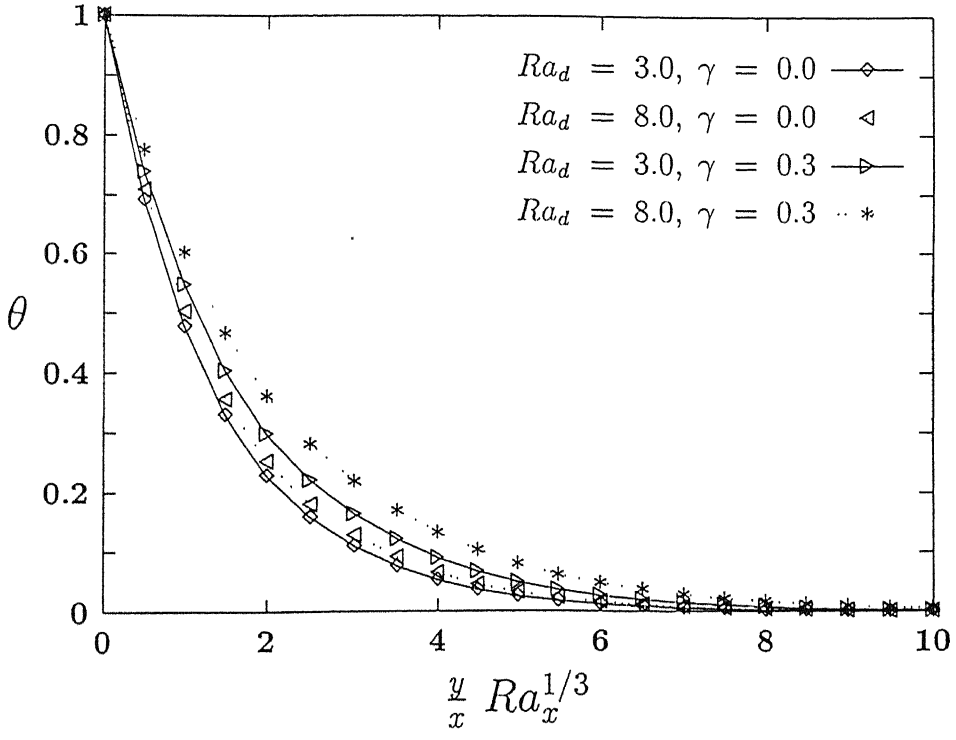

Figure (2.3): Effect of thermal dispersion on non-dimensional temperature distribution when $F_o = 0.4$.

The local heat transfer rate which is the primary interest of the study is given by

$$q = -k_e \frac{dT}{dy}|_{y=0} = -[k + k_d]\frac{dT}{dy}|_{y=0} \tag{2.22}$$

where k_e is the effective thermal conductivity of the porous medium which is the sum of th molecular thermal conductivity k and the dispersion thermal conductivity k_d. This can b rewritten as

$$q(x) = -k\left[(1 + \frac{\gamma P}{2F_o})\right]\frac{\partial T}{\partial y}|_{y=0} \tag{2.23}$$

The local heat flux in terms of Nusselt number is given by

$$\frac{Nu}{Ra_x^{1/3}} = -\left[(1 + \frac{\gamma P}{2F_o})\right]\frac{1}{\delta^*} \tag{2.24}$$

	$\frac{Nu}{Ra_x^{1/3}}$ when $\gamma = 0.3$	
Ra_d	$F_o = 0.1$	$F_o = 0.5$
1.0	1.0233	0.9129
5.0	1.2983	0.9895
10.0	1.4910	1.0411
25.0	1.8174	1.1312
10.0	2.1132	1.2186

Table 2.1: Nusselt number results when $\gamma = 0.3$

The Nusselt number results are plotted in Figure (2.4). When $\gamma = 0.3$ the Nusselt number results are given in Table (2.1) for various values of Rayleigh number with two values of the inertial parameter F_o. From Figure (2.4) it is obvious that when γ=0, increase in the value of the inertial parameter decreases the value of the Nusselt number and when γ is non zero, dispersion enhances the heat transfer rate and this decreases with increase in the inertial parameter.

Comparing with the similarity results, the present integral method results using simple exponential profiles for velocity and temperature distributions are in good agreement (deviation is about 5%). For the case when γ=0, the comparison results are plotted in Figure (2.5). This proves that even with simple exponential profiles for velocity and temperature distributions along with an additional parameter in the profiles yields a better approximation to the exact solution.

Thus the present investigation shows that the simple approximate Karman - Pohlhausen integral method can be used without hesitation for solving convective heat transfer problems in porous medium even for non-linear Forchheimer model along with the thermal dispersion effects upto the required accuracy.

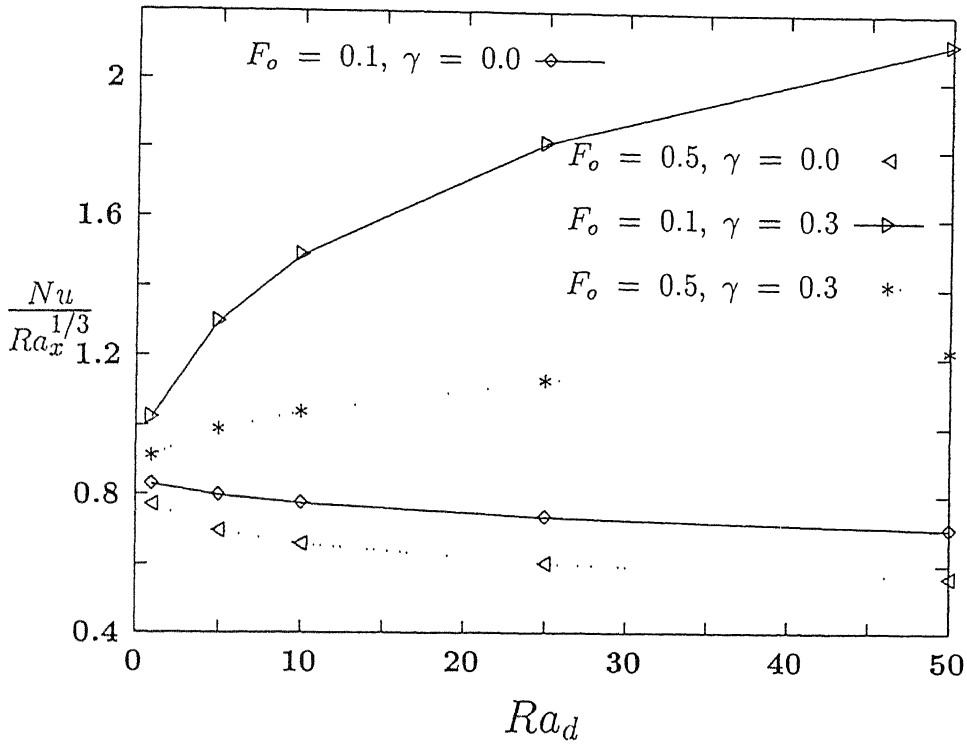

Figure (2.4): Inertial and Thermal dispersion effects on the Nusselt number results.

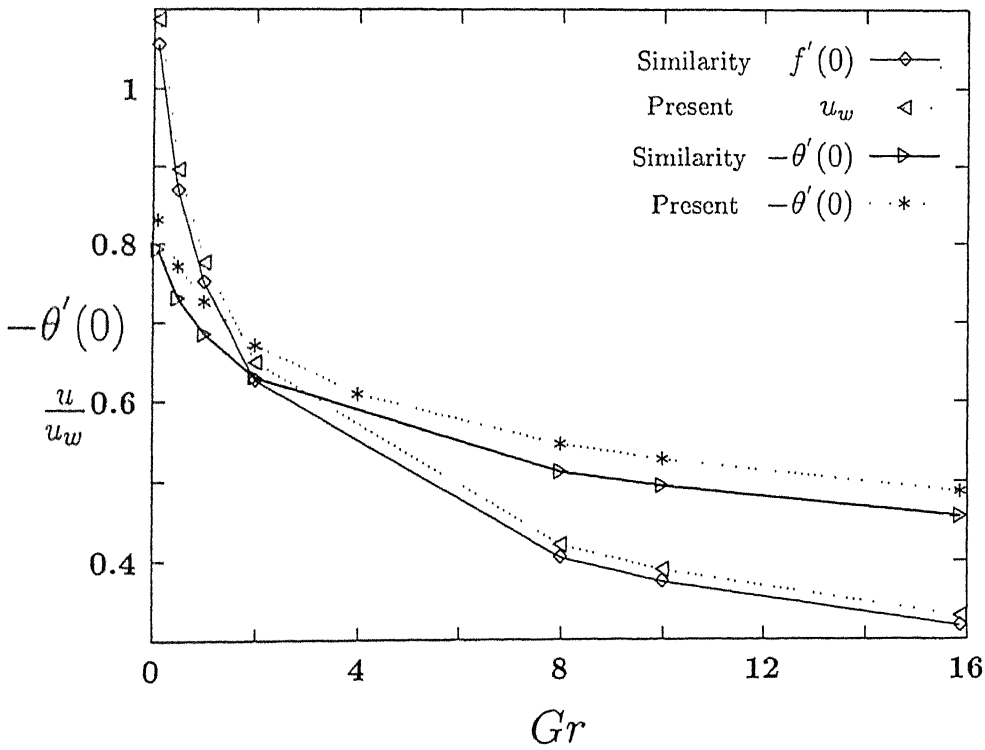

Figure (2.5): Comparison of Integral solution with the similarity solution for $\frac{u}{u_w}$ and $-\theta'(0)$.

2.4 Permeable Wall: Similarity Solution

First we represent the governing equations (2.11) and (2.12) in terms of stream function and temperature formulation. The velocity components u and v can be written in terms of stream function ψ as: $u = \frac{\partial \psi}{\partial y}$ and $v = -\frac{\partial \psi}{\partial x}$. This representation is valid since the expressions for velocity components clearly satisfy the continuity equation. Now the resulting equations are

$$\frac{\partial^2 \psi}{\partial y^2} + \frac{C\sqrt{K}}{\nu} \frac{\partial}{\partial y} \left(\frac{\partial \psi}{\partial y} \right)^2 = -\frac{Kg\beta}{\nu} \frac{\partial T}{\partial x} \tag{2.25}$$

$$\frac{\partial \psi}{\partial y} \frac{\partial T}{\partial x} - \frac{\partial \psi}{\partial x} \frac{\partial T}{\partial y} = \frac{\partial}{\partial y} \left(\alpha_y \frac{\partial T}{\partial y} \right) \tag{2.26}$$

Comparing the order magnitudes of Darcy and buoyancy terms in the momentum equation, we get the order magnitude estimate for ψ as

$$\psi \sim Ra_x \; \alpha \; \frac{\delta_T^2}{x^2} \tag{2.27}$$

where Ra_x is the modified Rayleigh number, $Ra_x = \frac{Kg\beta(T_w - T_\infty)x}{\alpha\nu}$. The energy equation gives the order magnitude estimate for ψ as

$$\psi \sim \frac{\alpha x}{\delta_T} \tag{2.28}$$

From the above estimates for ψ, we get an estimate for the boundary layer thickness δ_T as

$$\delta_T \sim x Ra_x^{-1/3}. \tag{2.29}$$

Now, the similarity variable η which is defined as

$$\eta = \frac{y}{\delta_T} \tag{2.30}$$

will become

$$\eta = \frac{y}{x} Ra_x^{1/3}. \tag{2.31}$$

Then from the above expressions, we obtain the non-dimensional stream function as

$$f(\eta) = \frac{\psi}{\alpha Ra_x^{1/3}} \tag{2.32}$$

and write the non-dimensional temperature distribution as

$$\theta(\eta) = \frac{T - T_\infty}{T_w - T_\infty}. \tag{2.33}$$

Now equations (2.31), (2.32) and (2.33) constitute the similarity transformation if this set transforms the governing partial differential equation into ordinary differential equations with x being eliminated from the governing equations and boundary conditions explicitly. Then from the definition of the stream function, the velocity components become

$$u = \frac{\alpha}{x} Ra_x^{2/3} f'(\eta), \tag{2.34}$$

$$v = -\frac{\alpha}{3x} Ra_x^{1/3} \left[(n+1)f + (n-2)\eta f'\right], \tag{2.35}$$

Applying the similarity transformation to the governing equations (2.11) and (2.12), we get

$$f'' + \frac{C\sqrt{K}\alpha}{\nu}\left[\frac{Kg\beta A}{\alpha\nu}\right]^{2/3} x^{\frac{(2n-1)}{3}} \left(f'^2\right)' + n\theta + \frac{(n-2)}{3}\eta\theta' = 0 \tag{2.36}$$

$$\theta'' + \frac{(n+1)}{3} f\theta' - nf'\theta + \gamma d x^{\frac{(2n-1)}{3}} \left[\frac{Kg\beta A}{\alpha\nu}\right]^{2/3} (f''\theta' + f'\theta'') = 0 \tag{2.37}$$

and the boundary conditions (2.6) are transformed to

$$\left.\begin{aligned} \eta = 0 &: f = f_w,\ \theta = 1 \\ \eta \to \infty &: f' = 0,\ \theta = 0 \end{aligned}\right\}. \tag{2.38}$$

A close observation of equations (2.36) and (2.37) reveal that the coefficients of all the terms become constant when n takes the value 1/2. In the boundary conditions $f = f_w =$ constant is applied to preserve the x-independency in equation (2.35), because it is necessary for the similarity solution to exist. Now we have from equation (2.35),

$$v_w(x) = -\frac{\alpha}{3x} Ra_x^{1/3} (n+1) f_w \tag{2.39}$$

and the particular value of l for which v_w will be free from x is l = -1/2. The negative power distribution for injection/suction will lead to infinite injection/suction at the leading edge, which is unrealistic, but the method of similarity solution will still give accurate results sufficiently far from the leading edge.

Now equations (2.36) and (2.37) for constant wall heat flux case (i.e., $n = 1/2$) will become

$$f'' + Grf'^{2'} + \frac{\theta}{2} - \frac{\eta\theta'}{2} = 0 \tag{2.40}$$

$$\theta'' + \frac{f\theta'}{2} - \frac{f'\theta}{2} + Ds(f''\theta' + f'\theta'') = 0 \tag{2.41}$$

where $\mathrm{Gr} = \frac{C\sqrt{K}\alpha}{\nu}\left[\frac{Kg\beta A}{\alpha\nu}\right]^{2/3}$ is the inertial parameter, and $Ds = \gamma Ra_d^{2/3}$ is the dispersion parameter, $Ra_d = \frac{Kg\beta\theta_w d}{\alpha\nu}$. Note that $Gr = 0$ corresponds to the Darcian free convection and $Ds = 0$ represents the case where the thermal dispersion effect is neglected.

2.4.1 Results and Discussion

The resulting ordinary differential equations (2.40) and (2.41) with the corresponding boundary conditions (2.38) are solved by numerical integration using the fourth-order Runge-Kutta method and Newton-Raphson technique by giving proper guess values for $f'(0)$ and $\theta'(0)$. The present results are accurate upto the sixth decimal place. To understand the effect of various parameters on the free convection process, in the present analysis the inertial parameter Gr is varied form 0 to 1.0, the dispersion parameter Ds assigned values 0, 0.1, 0.5 and the mass flux parameter f_w varied from -1.0 to 1.0. $f_w = 0$ corresponds to the impermeable surface, $f_w > 0$ corresponds to suction and $f_w < 0$ corresponds to injection of the fluid into the porous medium. The flow field and the temperature distribution are presented in terms of the non-dimensional velocity component in the x-direction $f'(\eta)$ and non-dimensional temperature distribution $\theta(\eta)$ in Figures (2.6 - 2.9).

Figures (2.6) and (2.7) correspond to $f'(\eta)$ with η for $Gr = 0$ and $Gr = 1.0$ respectively. From these figures it is clear that the increase in the inertial effects decrease the value of $f'(0)$ and there by decreasing the velocity of the fluid in the medium. From both these figures it can also be observed that the increase in the value of the dispersion parameter increases the value of $f'(\eta)$. Also, for fixed Gr and Ds, the increase in the value of the mass flux parameter decreases the thickness of the velocity component profile. Similarly it can be seen from the non-dimensional temperature distribution presented in the Figures (2.8) and (2.9) (for $Gr = 0$ and $Gr = 1.0$ respectively) that the increase in the inertial parameter decreases the temperature distribution, where as the increase in the value of the dispersion parameter favors the convection process.

The boundary layer thickness δ_T as a function of the mass flux parameter is plotted in the Figure (2.10) for Gr and for various values of Ds. The value of the similarity variable at which $\theta(\eta)$ becomes equal to 0.001 is noted as the boundary layer thickness. From equation (2.29), it is noted that the boundary layer thickness varies inversely as 1/3 power of the Rayleigh number. From the definition of the dispersion parameter it is clear that Ds varies directly as 2/3 power of the Rayleigh number. For all numerical calculations here, γ is taken to be 0.3. It is clearly seen that the increase in the value of the dispersion parameter decreases the boundary layer thickness. Also, the boundary layer thickness decreases as the mass flux parameter moves from the injection domain to the suction domain.

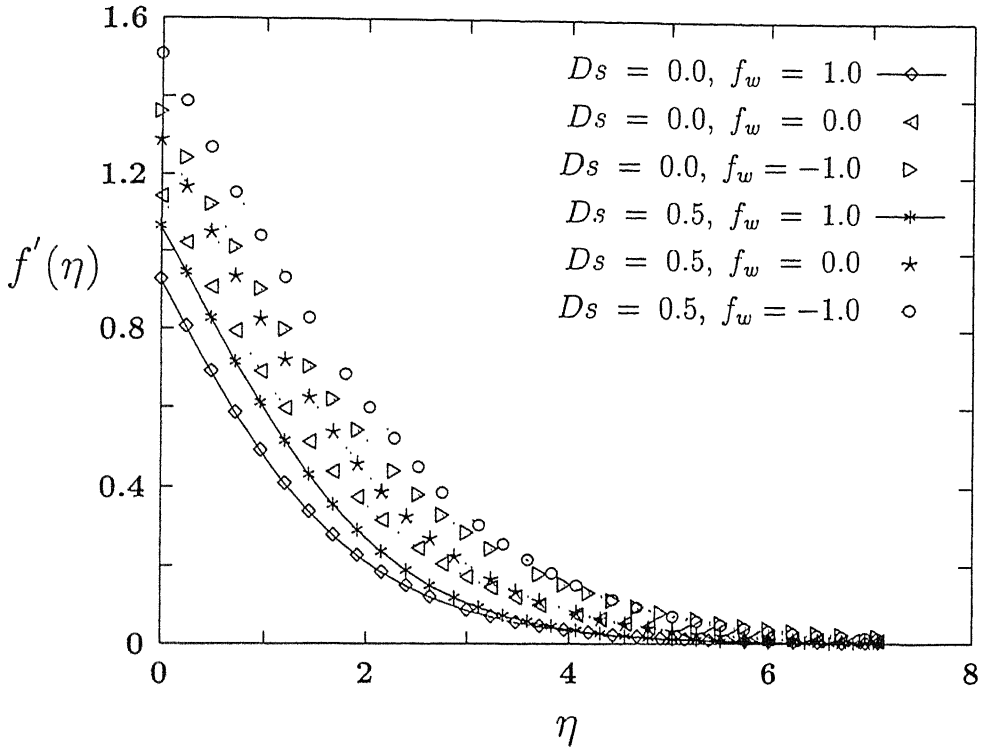

Figure (2.6): Variation of $f'(\eta)$ with the similarity variable η for $Gr = 0$ for various dispersion amd mass flux parameter values.

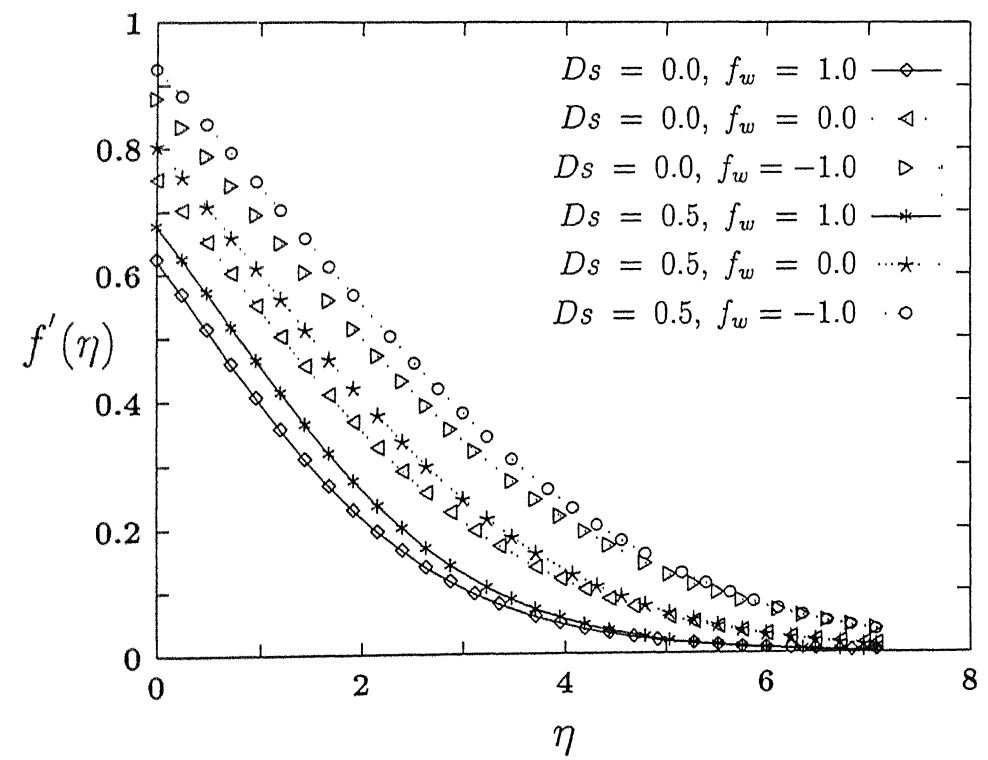

Figure (2.7): Variation of $f'(\eta)$ with the similarity variable η for $Gr = 1.0$ for various dispersion and mass flux parameter values.

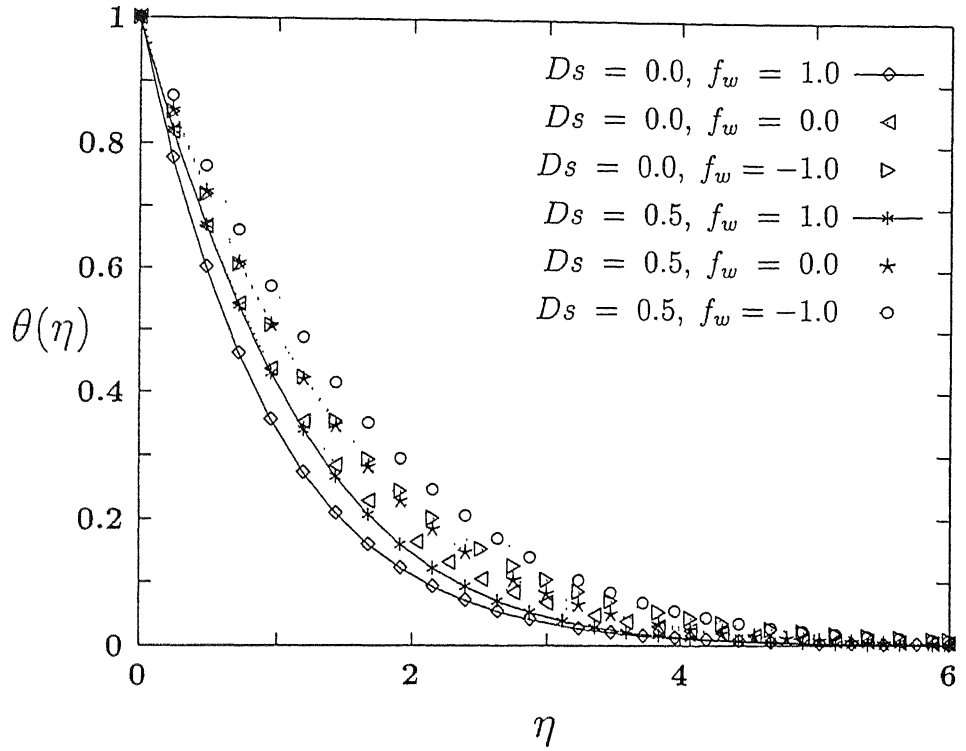

Figure (2.8): Variation of $\theta(\eta)$ with the similarity variable for $Gr = 0$ for various dispersion and mass flux parameter values.

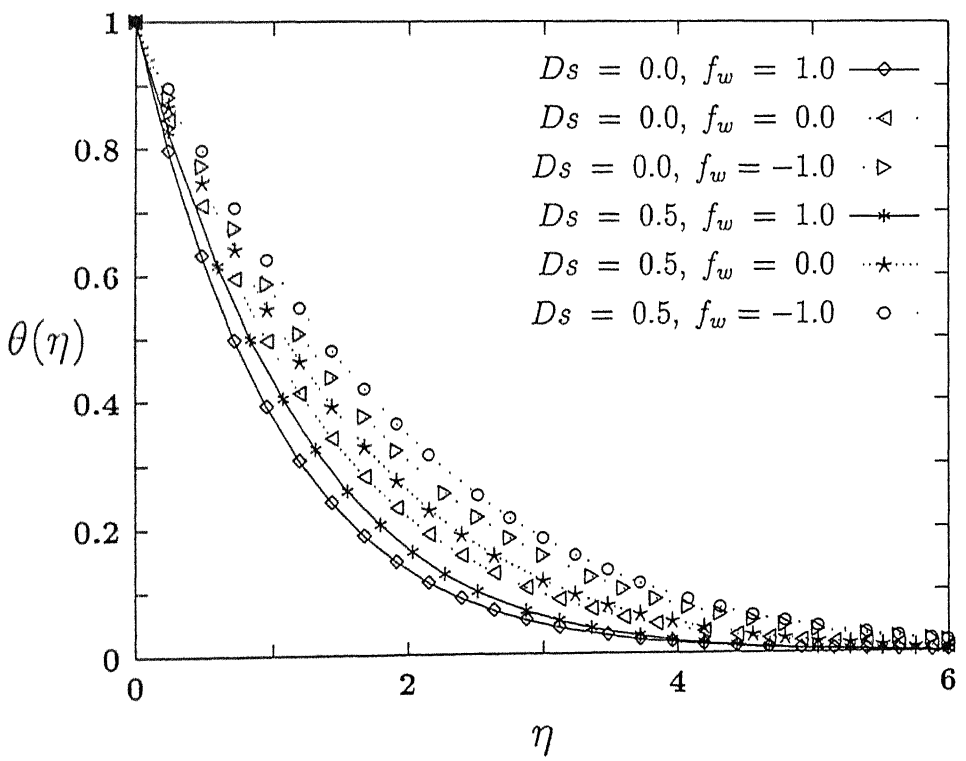

Figure (2.9): Variation of $\theta(\eta)$ with the similarity variable η for $Gr = 1.0$ for various dispersion and mass flux parameter values.

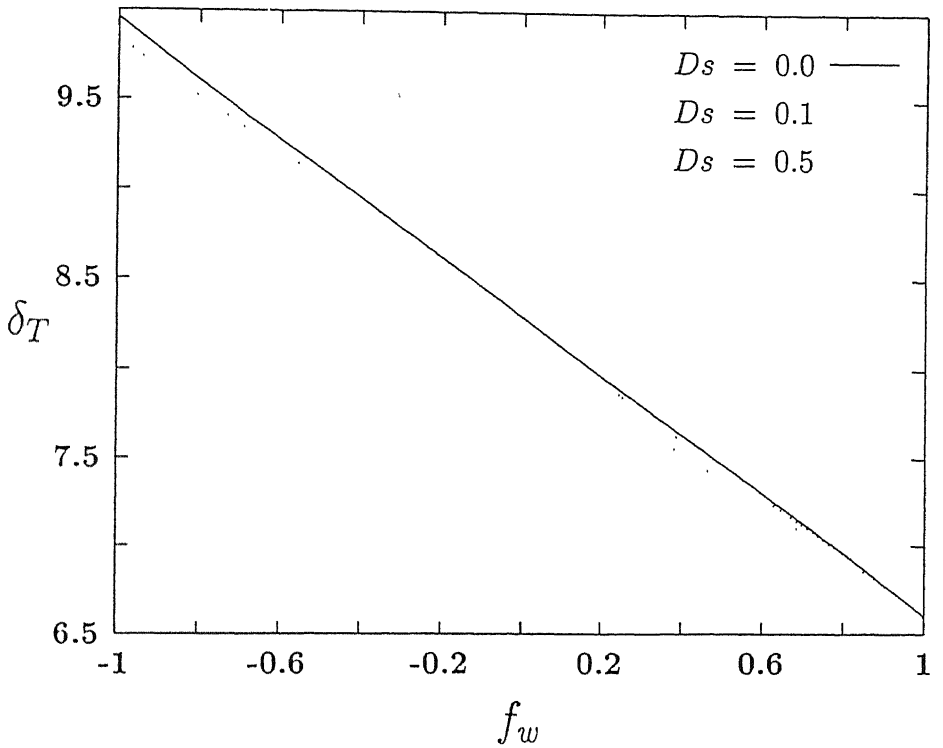

Figure (2.10): Variation of δ_T with f_w in the non-Darcy porous medium for various dispersion parameter values.

The heat transfer coefficient in terms of Nusselt number is given by

$$\frac{Nu}{Ra_x^{1/3}} = [1 + Ds\, f'(0)]\,[-\theta'(0)] \tag{2.42}$$

Nusselt number results for varying values of the inertial and dispersion parameters are presented in Table (2.2). Since the value of $f'(0)$ is always positive, dispersion always enhances the heat transfer coefficient. In Figure (2.11) the Nusselt number results are plotted as a function of mass flux parameter for varying inertial and dispersion parameters. From this figure, it is clear that the value of the Nusselt number increases as the non-dimensional mass flux parameter moves from the injection domain to suction domain. Moreover, the increase in the value of the dispersion parameter enhances the heat transfer. Also the inertial effects decreases the heat transfer rate. The combined effect of thermal dispersion and surface mass flux on natural convection heat transfer over the horizontal wall in porous medium is that the Nusselt number increases as the mass flux parameter moves from injection domain to suction domain. But the relative increase in the Nusselt number values of injection, no injection/no

suction and suction is observed to be lowered with the increase in the value of the inertial parameter.

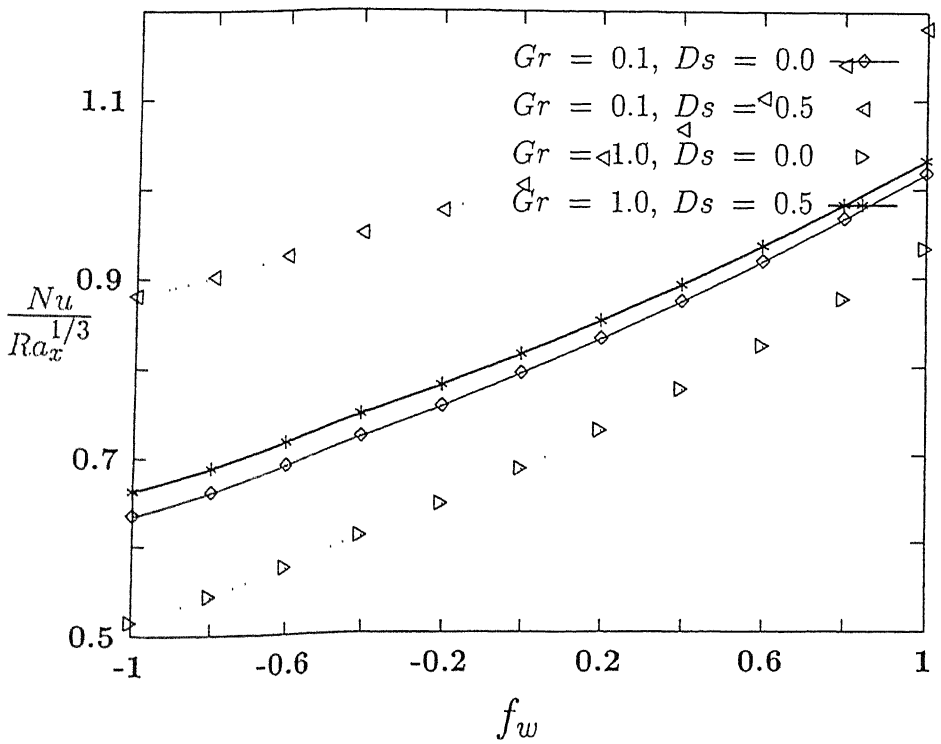

Figure (2.11): Variation of Nusselt number with mass flux parameter for various inertial and dispersion parameter values.

	$\frac{Nu}{Ra_x^{1/3}}$ when Ds=0			$\frac{Nu}{Ra_x^{1/3}}$ when Ds=0.5		
Gr	$f_w = -1$	$f_w = 0$	$f_w = 1$	$f_w = -1$	$f_w = 0$	$f_w = 1$
0	0.6632	0.8165	1.0360	0.9439	1.053	1.2174
0.1	0.6337	0.7921	1.0180	0.8806	1.0035	1.1813
1.0	0.5145	0.6848	0.9331	0.6625	0.8141	1.033

Table 2.2: Combined effect of thermal dispersion and surface mass flux on Nusselt number results.

Chapter 3

Thermal Dispersion Effects On Non-Darcy Natural Convection Over A Vertical Flat Plate And A Cone

3.1 Introduction

Because of the important and interesting applications of convective heat transfer in porc media in nuclear waste disposal, in underground heat exchangers for energy storage a recovery, temperature controlled reactors, packed beds and the utilization of porous lay for transpiration cooling by water for fire fighting, in the storage of food grains, and also Resin Transfer Molding process in which fiber reinforced polymeric parts are produced final shape, etc., it has gained the attention of many researchers in the past decades.

As mentioned in Chapter 1, most of the works dealing with convective heat transfer porous media have been motivated by geothermal applications. Also designing a suitab canester for the nuclear waste disposal into the depths of the earth or into the sea bec demands a thorough understanding of the convective mechanism in porous medium in ord to take care of the safety of the all living begins. In this direction, one needs to stu the convective heat transfer from different geometries. To begin with, axi-symmetric bodi such as cone, horizontal and vertical cylinders and spheres are amicable for the fundament study using the standard analytical techniques. Depending on the flow and field conditio

different flow models are being employed.

In this direction, Merkin [43] analysed the free convection about a general two dimen sional and axi-symmetric heated body of arbitrary shape in a Darcian fluid saturated porou medium. The free convection about a vertical cylinder embedded in a porous medium ha been analysed by Minkowycz and Cheng [78]. Cheng et al [66], Pop and Cheng [41] studie the free convection heat transfer from a vertical cone pointing downwards in a fluid sat urated porous medium. In the first case, the curvature effects are neglected and a loca non-similarity solution has been obtained for the frustum of cone and the similarity solu tion was possible when the full cone has been considered. In the later case, using integra analysis, it has been shown that the curvature effects will become insignificant as the buoy ancy effects dominate. Ingham and Pop [31] studied the free convection from a horizonta cylinder in a fluid saturated porous medium. Fand et al [71] experimentally analysed the free convection over a horizontal cylinder and observed that the results are consistent with the analytical results. Nakayama et al [17] gave a more general transformation for the free convection heat transfer from non-isothermal two dimensional and axi-symmetric body o arbitrary shape in a Darcian fluid saturated porous medium. They developed a more genera similarity transformation which takes care of all possible geometries.

A class of similarity solutions were obtained by Cheng [58] in the study of the effect of lat eral mass flux on the free convection heat transfer from a vertical hot wall in a fluid saturate porous medium. This problem has applications to injection of hot water in a geotherma reservoir. The practical case of constant discharge velocity at uniform temperature has beer treated using different methods by Merkin [44] and Minkowycz and Cheng [79]. The effect of suction/injection on the free convection over an axi-symmetric body (vertical cylinder) has been studied by Huang and Chen [51], and they concluded that suction increases the rate of heat transfer.

When the pore diameter dependent Reynolds number is high enough for the Darcy mode to break down, several investigators used the Forchheimer flow model to account for the inertial effects offered by the porous structure. Plumb and Huenefeld [56] studied the natura convection from vertical impermeable heated surface in saturated porous medium using Ergun model. Later Bejan and Poulikakos [16] studied the same case using a new scaling based on buoyancy-fluid inertia force comparison. An integral analysis has been presented by Nakayama et al [20] to understand the Forchheimer free convection from an isotherma

vertical flat plate and a cone. Ingham [30] studied the non-Darcy natural convection on axi-symmetric and two dimensional bodies of arbitrary shape for isothermal wall variation. Forchheimer free convection over a non-isothermal body of arbitrary shape has been studied by Nakayama et.al., [21]. They obtained similarity solutions for different geometries with varying wall temperature. Both these studies on axi-symmetric bodies are confined to pure non-Darcy regime (i.e., Darcy term has been neglected completely).

When inertial effects are prevalent, thermal dispersion effects (due to the hydrodynamic mixing of the fluid in the pore scale) become important as observed by Plumb [56], Hong and Tien [46] and Lai and Kulacki [37], Nield and Bejan [7]. It has been observed that because of this effect, the heat transfer rate is greatly increased. Hong and Tien [46] studied non-Darcy natural convection along a vertical flat plate in which thermal dispersion effects were included along with the Brinkman term in the momentum equation with no-slip boundary conditions. Plumb [57] studied this problem by neglecting wall effects, and assuming a linear relation between dispersion thermal diffusivity and the stream wise velocity component.

In the present chapter, we analyse the combined effect of thermal dispersion and lateral mass flux on Forchheimer natural convection over an isothermal vertical flat plate and a vertical cone pointing downwards. When Darcy law is used, the similarity solution is possible for a class of wall temperature variations and corresponding mass flux variations for the plane wall case. Because of the non-linearity in the Forchheimer flow model, this generality is reduced to the isothermal wall temperature variation with the fixed form of lateral mass flux $B\ x^{-1/2}$. In all the axi-symmetric configurations, it has been observed from the analysis hat the similarity solution is possible only for vertical cone when the thermal dispersion effects are considered. The Nusselt number results are tabulated and the velocity and temperature distributions are plotted.

3.2 Governing Equations

Consider a vertical flat plate and a vertical cone pointing downwards in a fluid saturated porous medium as shown in Figure (3.1). For the flat plate, x-axis is along the plate and y-axis is normal to it, $x = 0$ being the leading edge. The cone is placed with its axis of symmetry vertical and x-measures the distance along the surface of the cone from the apex, and y measures distance normally outwards. ξ is the cone apex half anlge. The body in both

the cases is held at a temperature T_w = constant, greater than the ambient temperature T_∞. The hot body may be impermeable $v_w(x) = 0$ or permeable with lateral mass flux $v_w(x) = B\, x^l$.

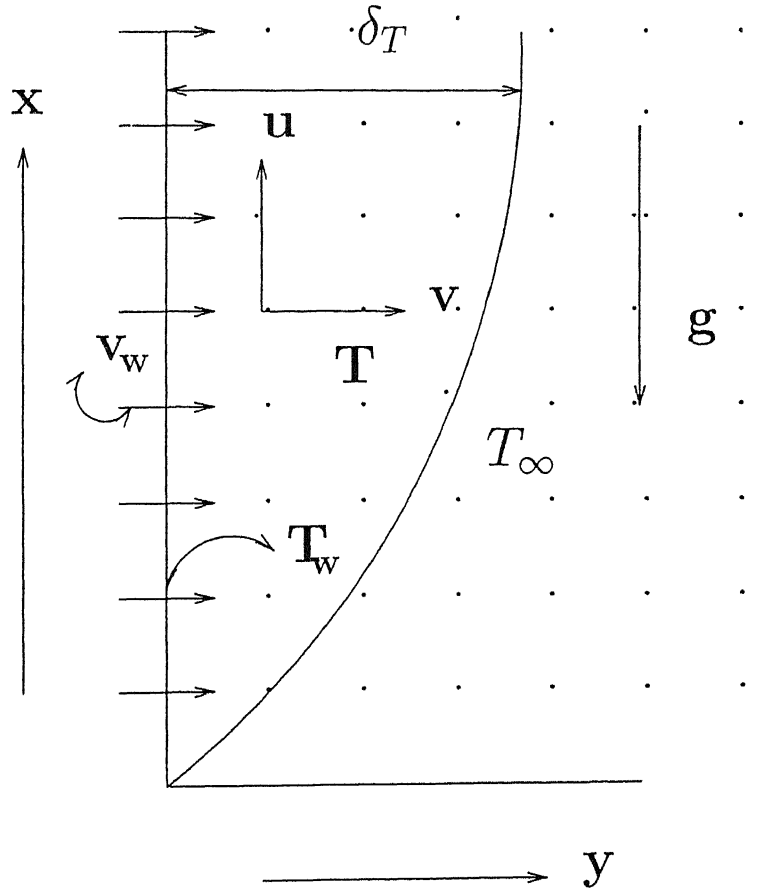

Figure 3.1: Vertical wall - coordinate system

The governing equations for the flow and heat transfer from the wall $y = 0$ into the fluid saturated porous medium $x \geq 0$ and $y > 0$ are given by

$$\frac{\partial(ru)}{\partial x} + \frac{\partial(rv)}{\partial y} = 0 \tag{3.1}$$

$$u + \frac{C\sqrt{K}}{\nu}u^2 = -\frac{K}{\mu}\left(\frac{\partial p}{\partial x} + \rho g_x\right) \tag{3.2}$$

$$v + \frac{C\sqrt{K}}{\nu}v^2 = -\frac{K}{\mu}\left(\frac{\partial p}{\partial y}\right) \tag{3.3}$$

$$u\frac{\partial T}{\partial x}+v\frac{\partial T}{\partial y}=\frac{\partial}{\partial x}\left(\alpha_x\frac{\partial T}{\partial x}\right)+\frac{\partial}{\partial y}\left(\alpha_y\frac{\partial T}{\partial y}\right) \tag{3.4}$$

along with the Boussinesq approximation

$$\rho=\rho_\infty[1-\beta(T-T_\infty)] \tag{3.5}$$

where

$$r(x)=\begin{cases} 1 & for\ plane\ flows \\ xsin\xi & for\ cone \end{cases} \tag{3.6}$$

and

$$g_x=g\left[1-\left(\frac{\partial r}{\partial x}\right)^2\right]^{1/2} \tag{3.7}$$

and the boundary conditions are

$$\left.\begin{array}{l} y=0:\ v_w(x)=B\,x^l,\ T_w=constant \\ y\to\infty:\quad u=0,\qquad T\to T_\infty \end{array}\right\}. \tag{3.8}$$

Here x and y are the Cartesian coordinates, u and v are the Darcian velocity components in x and y directions respectively, T is the temperature, ρ is the density, p is the pressure, β is the coefficient of thermal expansion, μ is the viscosity of the fluid, ν is the kinematic viscosity of the fluid, K is the permeability, C is an empirical constant, g is the acceleration due to gravity, α_x and α_y are the components of thermal diffusivity in x and y directions, r is the curvature of the cone and ξ is the cone apex half angle. The suffix w and ∞ indicate the conditions at the wall and at the outer edge of the boundary layer respectively. A,B,n and l are fixed real constants.

Experimental and numerical studies on convective heat transfer in a porous medium show that thermal boundary layers exist adjacent to the heated or cooled bodies. When the thermal boundary layer is thin (i.e., $x >> y \sim \delta_T$, δ_T is the boundary layer thickness), boundary layer approximations analogous to classical boundary layer theory can be applied [7]. Near the boundary, the normal component of seepage velocity is small compared with the other component of the seepage velocity and the derivatives of any quantity in the normal direction are large compared with derivatives of the quantity in the direction of the wall. Under these assumptions, the equations (3.1)-(3.4) become

$$\frac{\partial(ru)}{\partial x}+\frac{\partial(rv)}{\partial y}=0 \tag{3.9}$$

$$u + \frac{C\sqrt{K}}{\nu}u^2 = -\frac{K}{\mu}\left(\frac{\partial p}{\partial x} + \rho g_x\right) \tag{3.10}$$

$$\frac{\partial p}{\partial y} = 0 \tag{3.11}$$

$$u\frac{\partial T}{\partial x} + v\frac{\partial T}{\partial y} = \frac{\partial}{\partial y}\left(\alpha_y \frac{\partial T}{\partial y}\right) \tag{3.12}$$

Eliminating the pressure and invoking the Boussinesq approximations, the equations (3.10)-(3.12) become

$$\frac{\partial u}{\partial y} + \frac{C\sqrt{K}}{\nu}\frac{\partial u^2}{\partial y} = -\left(\frac{Kg_x\beta}{\nu}\right)\frac{\partial T}{\partial y} \tag{3.13}$$

$$u\frac{\partial T}{\partial x} + v\frac{\partial T}{\partial y} = \frac{\partial}{\partial y}\left(\alpha_y \frac{\partial T}{\partial y}\right) \tag{3.14}$$

Here α_y is a variable quantity which is the sum of molecular thermal diffusivity α and dispersion thermal diffusivity α_d, ($\alpha_d = \gamma\ d\ u$), where γ is the mechanical dispersion coefficient, and d is the pore diameter.

First we represent the governing equations (3.13) and (3.14) in terms of stream function and temperature formulation. The velocity components u and v can be written in terms of stream function ψ as : $u = \frac{1}{r}\frac{\partial \psi}{\partial y}$ and $v = -\frac{1}{r}\frac{\partial \psi}{\partial x}$. This representation is valid since the expressions for velocity components clearly satisfy the continuity equation (3.9). Now the resulting equations are

$$\frac{1}{r}\frac{\partial^2 \psi}{\partial y^2} + \frac{1}{r^2}\frac{C\sqrt{K}}{\nu}\frac{\partial}{\partial y}\left(\frac{\partial \psi}{\partial y}\right)^2 = -\frac{Kg_x\beta}{\nu}\frac{\partial T}{\partial y} \tag{3.15}$$

$$\frac{1}{r}\frac{\partial \psi}{\partial y}\frac{\partial T}{\partial x} - \frac{1}{r}\frac{\partial \psi}{\partial x}\frac{\partial T}{\partial y} = \frac{\partial}{\partial y}\left([\alpha + \frac{\gamma d}{r}\frac{\partial \psi}{\partial y}]\frac{\partial T}{\partial y}\right) \tag{3.16}$$

Following Plumb and Huenefeld [56], comparison of the order magnitudes of Darcy and buoyancy terms in the momentum equation, we get the order magnitude estimate for ψ as

$$\psi \sim \alpha\ r\ Ra_x\ \frac{\delta_T}{x} \tag{3.17}$$

where Ra_x is the modified Rayleigh number, $Ra_x = \frac{Kg_x\beta(T_w - T_\infty)x}{\alpha\nu}$. The energy equation gives the order magnitude estimate for ψ as

$$\psi \sim \frac{\alpha x\ r}{\delta_T} \tag{3.18}$$

From the above estimates for ψ, we get an estimate for the boundary layer thickness δ_T as

$$\delta_T \sim xRa_x^{-1/2}. \tag{3.19}$$

Now, define the similarity variable η as

$$\eta = \frac{y}{\delta_T} \tag{3.20}$$

implies

$$\eta = \frac{y}{x} Ra_x^{1/2}. \tag{3.21}$$

Then from the above expressions, we obtain the non-dimensional stream function as

$$f(\eta) = \frac{\psi}{\alpha\, r\, Ra_x^{1/2}}. \tag{3.22}$$

and the non-dimensional temperature distribution as

$$\theta(\eta) = \frac{T - T_\infty}{T_w - T_\infty}. \tag{3.23}$$

Now equations (3.21),(3.22) and (3.23) constitute the similarity transformation if this set transforms the governing partial differential equations (3.15) and (3.16) into ordinary differential equations, with x being eliminated from ordinary differential equations and the boundary conditions. Then from the definition of the stream function, the velocity components become

$$u = \frac{\alpha}{x} Ra_x f'(\eta), \tag{3.24}$$

$$v = -\frac{\alpha}{2x} Ra_x^{1/2} \left[If - \eta f' \right]. \tag{3.25}$$

where

$$I = \begin{cases} 1 & flat\ \ plate \\ 3 & for\ \ cone \end{cases} \tag{3.26}$$

On the wall ($\eta = 0$) equation (3.25) becomes

$$v_w(x) = -\frac{I\alpha}{2x} Ra_x^{1/2} f_w \tag{3.27}$$

and the particular value of l for which v_w will be free from x is l = -1/2 and this assures that the boundary conditions are also free from x. Applying the similarity transformation to the governing equations (3.15) and (3.16), we get

$$f'' + 2F_o Ra_d f' f'' - \theta' = 0 \tag{3.28}$$

$$\theta'' + \frac{I}{2} f\theta' + \gamma Ra_d (f'\theta')' = 0 \tag{3.29}$$

and the boundary conditions (3.8) transform into

$$\left.\begin{array}{l} \eta = 0 : \ f = f_w, \ \theta = 1 \\ \eta \to \infty : \ f' = 0, \ \theta = 0 \end{array}\right\}. \tag{3.30}$$

Thus the resulting ordinary differential equations with the boundary conditions can be solved using the generalized techniques for solving ordinary differential equations. The negative power distribution for injection/suction will lead to infinite injection/suction at the leading edge, which is unrealistic, but the method of similarity solution will still give accurate results sufficiently far from the leading edge.

3.3 Results and Discussion

The governing equations (3.28) and (3.29) along with the boundary conditions (3.30) are solved using shooting and matching technique along with fourth order Runge-Kutta method for integration by giving proper guess values for $f'(0)$ and $\theta'(0)$. The results are observed upto the accuracy $5X10^{-6}$ using the NAG software. Before proceeding to solve these equations, we look at the other transformation given by Bejan and Poulikakos [16] for the case of impermeable vertical flat plate without thermal dispersion effect.

3.3.1 Correlation equation

Following Bejan and Poulikakos [16], comparison of order-magnitudes of inertia-buoyancy forces in the momentum equation gives the order magnitude estimate for ψ as

$$\psi \sim \alpha \, R_x^{1/2} \, \frac{\delta_T}{x} \tag{3.31}$$

where R_x is the Rayleigh number defined as, $R_x = \frac{\sqrt{K}g\beta(T_w - T_\infty)x^2}{C\alpha^2}$. The estimate for ψ from the energy equation remains same as equation (3.18) and the boundary layer thickness δ_T will become

$$\delta_T \sim x R_x^{-1/4}. \tag{3.32}$$

Now, the similarity variable η will become

$$\eta = \frac{y}{x} R_x^{1/4}. \tag{3.33}$$

Then from the above expressions, we obtain the non-dimensional stream function as

$$f(\eta) = \frac{\psi}{\alpha \, R_x^{1/4}}. \tag{3.34}$$

Now write the non-dimensional temperature distribution as

$$\theta(\eta) = \frac{T - T_\infty}{T_w - T_\infty}. \tag{3.35}$$

This similarity transformation reduces the governing equations into

$$Gf' + f'^2 = \theta \tag{3.36}$$

$$\theta'' + 1/2\, f\theta' = 0. \tag{3.37}$$

The governing parameters with this transformation are the non-dimensional group G, and the modified Rayleigh number R_x which has been interpreted as the "large Reynold's number limit" Rayleigh number. It is worth mentioning the use of the second transformation set that when the value of the parameter $G = 0$, the results correspond to the Forchheimer regime, where the Darcian effects are completely neglected (thus provide an upper bound for the heat transfer results), $G \to$ O(10) correspond to the near Darcy and $G \to$ O(1) correspond to the intermediate regime.

The transformation due to Plumb and Huenefeld [56] reduces the governing equations as

$$f' + Gr\, f'^2 = \theta \tag{3.38}$$

$$\theta'' + 1/2\, f\theta' = 0 \tag{3.39}$$

The governing parameters in this case are the Grashof number Gr and the modified Darcy-Rayleigh number Ra_x.

Now the first and fundamental interest of the study of convective heat transfer is to find out the expression for the heat transfer coefficient in-terms of the Nusselt number. The local heat flux from the wall is given by

$$q = -k\frac{dT}{dy}_{y=0} \tag{3.40}$$

where k is the thermal conductivity of the porous medium. Heat transfer coefficient in-terms of Nusselt number is written as

$$Nu_x = \frac{hx}{k} \tag{3.41}$$

where h is the convective heat transfer coefficient. Using these two transformations, we get two different expressions for Nusselt number as $Nu(Gr, Ra_x)$ and $Nu(G, R_x)$ as

$$\frac{Nu(Gr, Ra_x)}{Ra_x^{1/2}} = [-\theta'(0)]. \tag{3.42}$$

$Gr' = G^{-2}$	-$\theta'(0)$	-$\theta'(0)$	-$\theta'(0)$	-$\theta'(0)$
Gr'	[56]	Eqn (3.44)	present analysis	[16]
0.01	0.44232	0.13987	0.1402	
0.04	0.4376	0.1957		0.1980
0.1	0.42969	0.24163	0.2421	
1.0	0.36617	0.36617	0.3658	0.3700
10.0	0.25126	0.44681	0.4457	
25.0	0.2076	0.46421	0.4625	0.4630
100.0	0.15186	0.4802	0.4778	

Table 3.1: Nusselt number correlation using equation (3.44) for vertical wall.

and

$$\frac{Nu(G, R_x)}{R_x^{1/4}} = [-\theta'(0)]. \tag{3.43}$$

Solving the set of equations (3.36),(3.37) and (3.38), (3.39) with the impermeable boundary conditions give us two different values for $\theta'(0)$. Here, we obtained a correlation equation which behaves like a bridge between these two expressions. In the case of vertical wall, the parameter G is nothing but equal to $Gr^{-1/2}$ and this allows us to connect equations (3.42) and (3.43) as

$$\frac{Nu}{R_x^{1/4}} = \frac{Nu}{Ra_x^{1/2}} Gr^{1/4} \tag{3.44}$$

This equation behaves as a bridge for the Nusselt number results using inertia-buoyancy comparison and Darcy-buoyancy comparison. In Table (3.1) we compare these values of Nusselt number results obtained using the correlation equation (3.44)

3.3.2 Permeable Wall

The governing parameters are identified as F_o, Ra_d and Ds. The parameter $F_o = \frac{C\sqrt{K}\alpha}{\nu d}$ represents the structural and thermophysical properties of the porous medium, $Ra_d = \frac{Kg\beta(T_w - T_\infty)d}{\alpha\nu}$ is the pore diameter dependent Rayleigh number which describes the relative intensity of the buoyancy force, and the dispersion parameter $Ds = \gamma Ra_d$ represents the thermal dispersion effects, γ is the mechanical dispersion coefficient. In general γ should be found out

from experiments and observations reveal that its value lies between 1/7 and 1/3. For all calculations, γ is assigned a value 0.3 in the present study.

Note that $F_o = 0$ corresponds to the Darcian free convection and $\gamma = 0$ represents the case where the thermal dispersion effects are neglected. It has been observed that the similarity solution is possible for the problem under consideration with the above transformation only for the case of isothermal vertical flat plate and cone with fixed apex half angle. For plane flows r(x) = 1, then g_x = g and ξ becomes 0°, the problem will become the natural convection over an isothermal vertical wall and it has been tackled by Lai and Kulacki [37]. By neglecting thermal dispersion effects, Plumb and Huenefeld [56] studied this problem using Darcy-buoyancy force comparison.

The present analysis consists of two related problems. Those are
(a) the effect of lateral mass flux on the Forchheimer free convection and
(b) the combined effect of thermal dispersion and lateral mass flux on Forchheimer free convection in a fluid saturated porous medium.
To understand the effect of various parameters on the free convection process, in the present analysis, the parameter F_o is varied form 0 to 1.0, the Rayleigh number Ra_d is varied from 1.0 to 10. The mass flux parameter f_w is varied from -1.0 to 1.0. It is clear from the analysis that $f_w = 0$ correspond to the impermeable surface, $f_w > 0$ corresponds to suction and $f_w < 0$ correspond to injection of the fluid through the wall into the porous medium.

The flow field and the temperature distribution are presented in terms of the non-dimensional velocity component in the x-direction, $f'(\eta)$ and non-dimensional temperature distribution $\theta(\eta)$. Figures (3.2) and (3.3) correspond to $f'(\eta)$ and $\theta(\eta)$ versus the similarity variable η by considering and neglecting the thermal dispersion effects for three different values of the non-dimensional mass flux parameter f_w, for fixed value of $F_o = 0.1$ and $Ra_d = 5.0$. In both the cases, the velocity and temperature profiles thicken as the mass flux parameter passes from the suction domain to the injection domain. Also it is worth noting here that the increase in the value of the parameter F_o will thicken these profiles, because the Forchheimer term accounts for the form drag in the porous medium.

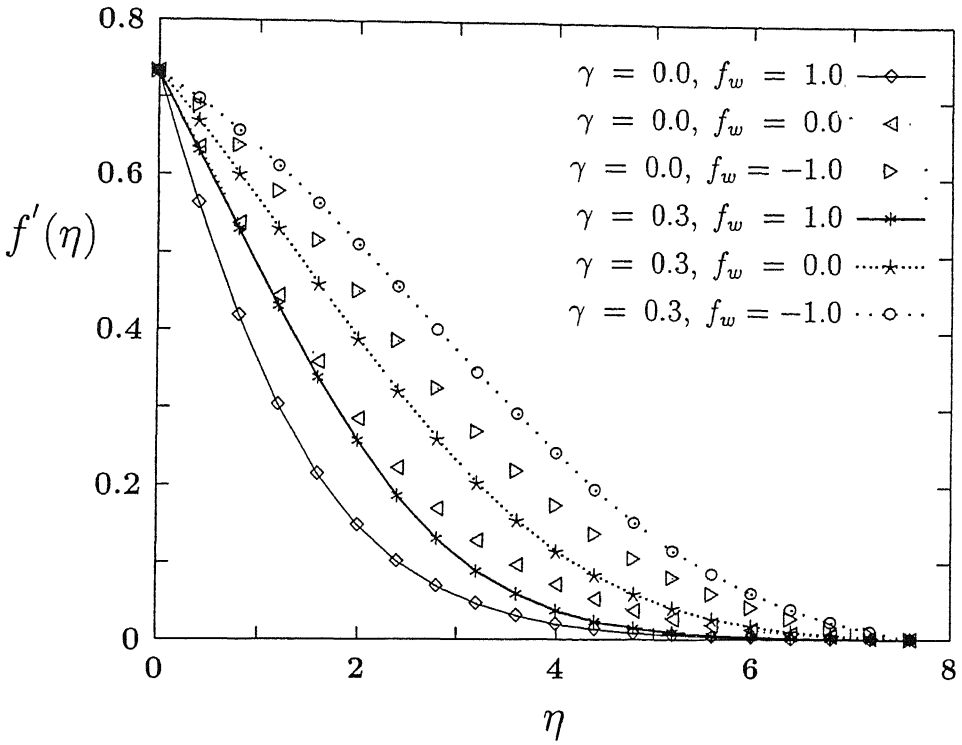

Figure (3.2): Variation of $f'(\eta)$ with the similarity variable for $F_o = 0.1$, $Ra_d = 5.0$ for various dispersion and mass flux parameter.

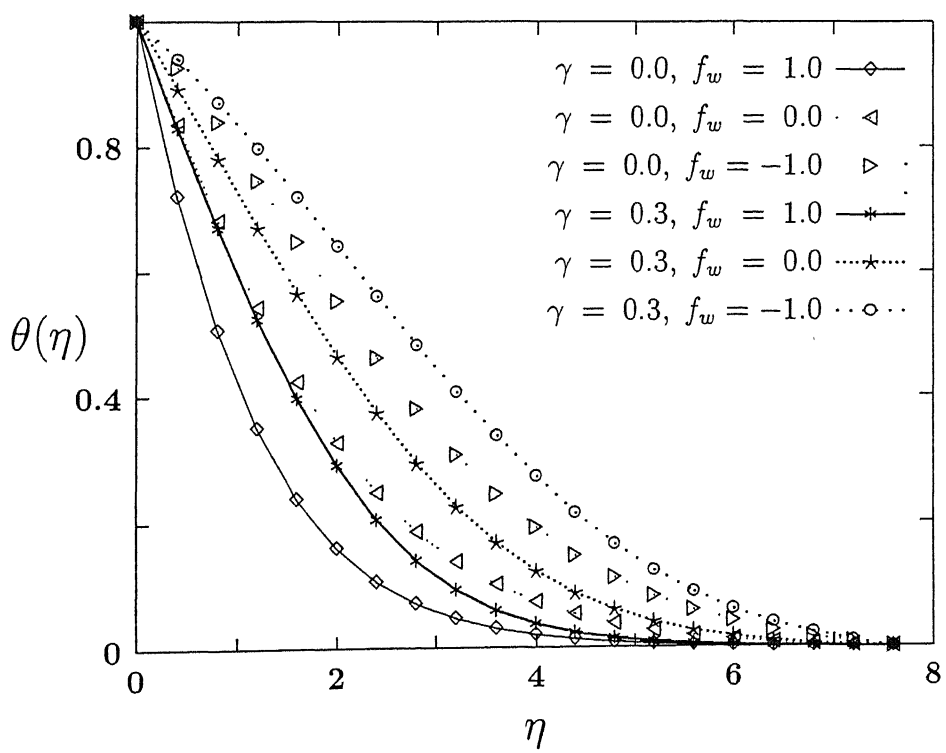

Figure (3.3): Variation of $\theta(\eta)$ with the similarity variable η for $F_o = 0.1$, $Ra_d = 5.0$ for various dispersion and mass flux parameter values.

The boundary layer thickness δ_T as a function of the mass flux parameter is plotted in the Figure (3.4) for various values of the dispersion parameter The value of the similarity variable at which $\theta(\eta)$ becomes equal to 0.01 is noted as the boundary layer thickness. From equation (3.19), it is noted that the boundary layer thickness varies inversely as 1/2 power of the Rayleigh number. From the definition of the dispersion parameter it is clear that Ds varies linearly with the Rayleigh number. By fixing $F_o = 0.1$ and $Ra_d = 5.0$, the increase in the value of γ (0 - 0.3) is observed to increase the boundary layer thickness as seen from the Figure (3.4). Also, the boundary layer thickness decreases as the mass flux parameter moves from the injection domain to the suction domain.

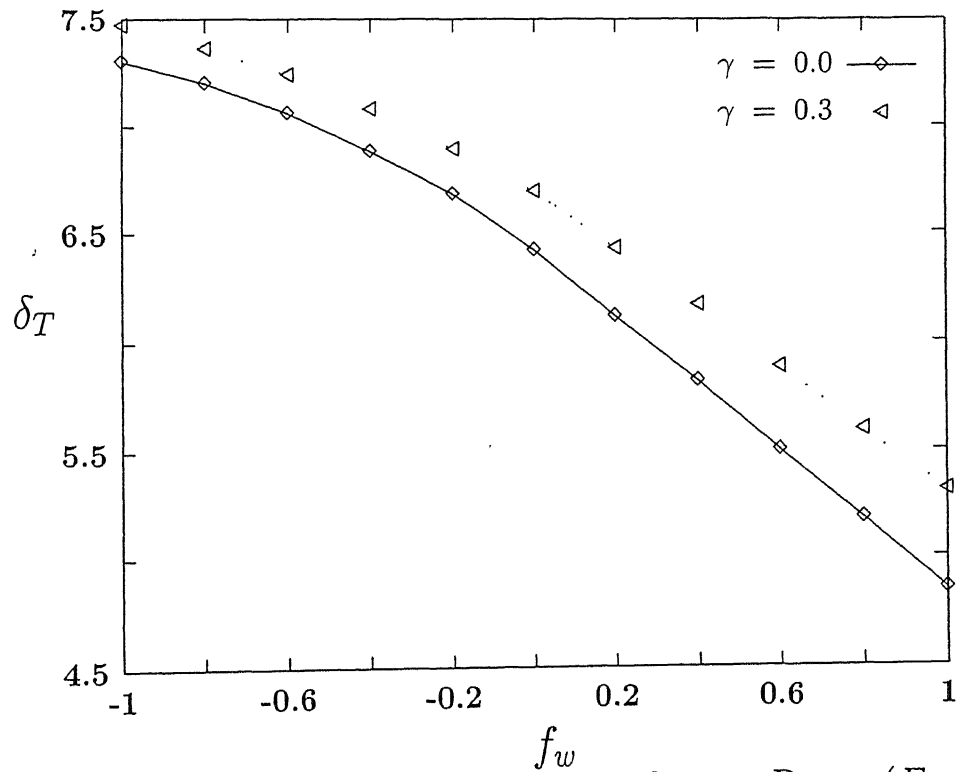

Figure (3.4): Variation of δ_T with f_w in the non-Darcy ($F_o = 0.1$, $Ra_d = 5.0$) porous medium for various dispersion parameter values.

The local heat flux which is the primary interest of the study is given by

$$q = -k_e \frac{dT}{dy}|_{y=0} = -[k + k_d]\frac{dT}{dy}|_{y=0} \tag{3.45}$$

where k_e is the effective thermal conductivity of the porous medium which is the sum of the molecular thermal conductivity k and the dispersion thermal conductivity k_d.

The heat transfer coefficient in terms of Nusselt number is given by

$$\frac{Nu}{Ra_x^{1/2}} = [1 + Ds\, f'(0)]\,[-\theta'(0)] \tag{3.46}$$

Nusselt number results for various values of the F_o and Ra_d (for the case of vertical flat plate) are presented in Table (3.2) for $\gamma = 0$ and $\gamma = 0.3$. The results for the case of vertical cone can also be obtained from the same formula, but the values of $f'(0)$ and $\theta'(0)$ will be different in this case. Since the value of $f'(0)$ is always positive, it can be noticed from the equation (3.46) that dispersion always enhances the heat transfer coefficient.

	$\frac{Nu}{Ra_x^{1/2}}$ when $\gamma = 0$.			$\frac{Nu}{Ra_x^{1/2}}$ when $\gamma = 0.3$		
Ra_d	$f_w = -1$	$f_w = 0$	$f_w = 1$	$f_w = -1$	$f_w = 0$	$f_w = 1$
1.0	0.1909	0.4295	0.7740	0.2293	0.4709	0.8103
2.0	0.1804	0.4180	0.7641	0.2479	0.4911	0.8284
5.0	0.1579	0.3929	0.7424	0.2847	0.5308	0.8646

Table 3.2: Combined effect of thermal dispersion and surface mass flux on Nusselt number results.

In Figure (3.5) the Nusselt number results are plotted as a function of mass flux parameter for varying Ra_d fixing γ at 0.3. From this figure, it is clear that the value of the Nusselt number increases as the non-dimensional mass flux parameter moves from the injection domain to suction domain. Moreover, it has been observed that the increase in the value of the dispersion parameter enhances the Nusselt number. Also, the increase in the value of the the parameter F_o decreases the heat transfer rate.

The combined effect of thermal dispersion and surface mass flux on natural convection heat transfer over the vertical wall in porous medium is that the Nusselt number increases as the mass flux parameter moves from injection domain to suction domain. But the relative increase in the Nusselt number values of injection, no injection/no suction and suction is observed to be enhanced with the increase in the value of Ra_d.

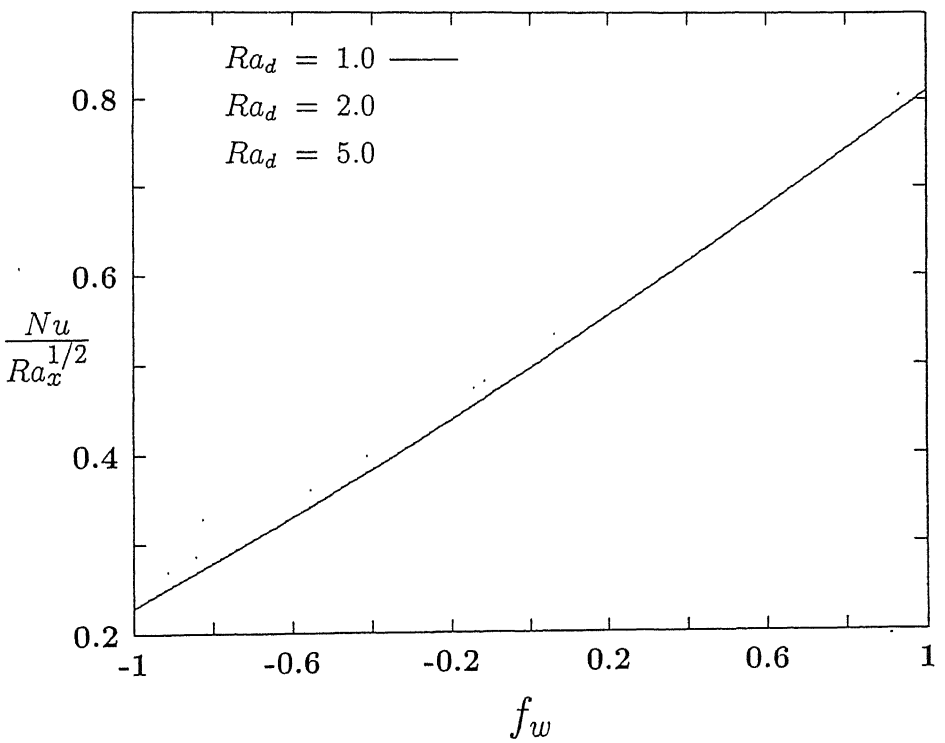

Figure (3.5): Variation of Nusselt number with mass flux parameter for fixed $F_o = 0.1$, $\gamma = 0.3$ and various values of Ra_d.

Chapter 4

Effect Of Viscous Dissipation On Non-Darcy Natural Convection Regime [1]

4.1 Introduction

Natural convection flow and heat transfer in a saturated porous media has gained more attention from the past two decades because of its wide range of applicability in packed bed reactors, porous insulation, beds of fossil fuels, nuclear waste disposal, usage of porous conical bearings in lubrication technology, geophysics and energy related engineering problems, etc. A nice review of buoyancy driven boundary layer flows in Darcian fluid is given in Nield and Bejan [7]. When the pore Reynolds number is high enough for the Darcy flow model to breakdown, Plumb and Huenefeld [56] studied the fundamental problem of non-Darcy natural convection from heated vertical wall in saturated porous medium. Later Bejan and Poulikakos [16], Bejan [15] by dividing the flow regime into non-Darcy and intermediate regimes, studied the same problem using fluid inertia-buoyancy scaling and defined large Reynolds-number- limit Rayleigh number Ra_∞. The new dimensionless group G defined in their analysis has been understood to be the number which describes the "extent to which the flow departs from Darcy law" by the successors, Fand et.al., [71]. The non-similar boundary

[1] Accepted for publication in "**International Journal of Heat and Mass Transfer**"

layer equations resulting from the Forchheimer natural convection from a power law wall variation were analysed by Chen and Ho [48].

In the case when inertia effects are prevalent, the transverse thermal dispersion effects will become important, and the analysis is dealt in length in works by Plumb [57], Cheng [60], Hong and Tien [46], Hong et.al.,[47], Cheng and Vortmeyer [62], Amiri and Vafai [14] etc. All these works confirm importance of thermal dispersion effect. Except for Cheng and Vortmeyer [62], all other works use the linear dependence of dispersion diffusivity on stream wise velocity . In order to correlate the available experimental data concerning the packed beds Cheng and Vortmayer [62] introduced wall function term also into the term of dispersion diffusivity.

The effect of viscous dissipation in natural convection in clear fluids has been studied by Gebhart [23] for power law vertical wall variation and obtained a perturbation solution in terms of a parameter which could not be expressed in terms of both the Rayleigh number as well as Prandtle number, and observed its increasing effect as the Prandtl number increases. Later Gebhart and Mollendorf [24] obtained the similarity solution for the same problem when exponential wall temperature variation is used and similar trend was observed. A comment was made by Fand and Brucker [70] that the effect of viscous dissipation might be significant in the case of natural convection in porous medium in connection with their experimental correlation for heat transfer in external flows. The validity of the comment was tested for Darcy model by Fand et.al., [71] both experimentally and analytically while estimating the heat transfer coefficient from a horizontal cylinder embedded in a saturated porous medium. Their mathematical analysis is confined to studying the dissipation effect using steady, one-dimensional energy equation, the basis of the equation is from the analogy given in Bejan [2] for the inclusion of viscous dissipation effects.The influence of viscous dissipation can be seen from the analogy given in Tucker and Dessenberger [6] to model the heat transfer and fluid flow through porous media in studying the Resin Transfer Molding (R.T.M) for producing fiber reinforced polymeric parts in final shape. Recently, Nakayama and Pop [22] studied the effect of viscous dissipation on the Darcian free convection over a non-isothermal body of arbitrary shape embedded in a saturated porous medium using the integral method. Their results indicate that the viscous dissipation lowers the level of heat transfer rate.

In the present chapter, we study the effect of viscous dissipation on non-Darcy natural

convection in porous medium. We consider the steady two-dimensional Forchheimer natural convection flow and heat transfer along an isothermal vertical wall with thermal dispersion and viscous dissipation effects. The scaling proposed by Bejan and Poulikakos [16] is adopted and the effect of viscous dissipation in non-Darcy , intermediate and limit Darcy regimes is studied with and without thermal dispersion effects. The results show a significant decrease in the heat transfer rate with the inclusion of viscous dissipation effect. It is seen that as the value of dispersion parameter increases, the effect of viscous dissipation increases in all the three regimes and the percentage decrease in the value of $\frac{Nu}{R_x^{1/4}}$ increases with the value of G.

4.2 Governing Equations

Consider the problem of natural convection from an isothermal vertical wall embedded in a saturated porous medium, and the pore Reynolds number is high enough for the departure of the flow from the Darcy's law. At higher velocities, inertial effect become appreciable, causing an increase in the form drag, in-addition to the bulk damping resistance due to the porous structure. Viscous resistance due to the solid boundary is neglected because the present study is assumed to be valid for low permeability and porosity. So the pressure drop is proportional to the linear combination of flow velocity and the square of the velocity. Both the thermal dispersion and viscous dissipation terms are retained in the energy equation. So, the governing equations for the flow and heat transfer are

$$\nabla \cdot V = 0 \tag{4.1}$$

$$B(q)\ V = \frac{K}{\mu}(-\nabla p + \rho\, \mathbf{g}) \tag{4.2}$$

$$(V \cdot \nabla T) = \nabla \cdot (\alpha_e \nabla T) + \frac{1}{\rho c_p} V\ (-\nabla p + \rho\, \mathbf{g}) \tag{4.3}$$

$$\rho = \rho_\infty[1 - \beta(T - T_\infty)] \tag{4.4}$$

where

$$B(q) = \left(1 + \frac{bK\rho}{\mu}\, q\right).$$

Making use of the momentum equation in the energy equation, the viscous dissipation term can be modified as

$$(V \cdot \nabla T) = \nabla \cdot (\alpha_e \nabla T) + \frac{\nu}{K\, c_p} B(q)\,(V)^2. \tag{4.5}$$

The boundary conditions are

$$\left.\begin{array}{lll} y=0 & v=0 & and\ T=T_w \\ y\to\infty, & u=0 & and\ T\to T_\infty \end{array}\right\} \tag{4.6}$$

In the above equations, V is the velocity vector, q is the local speed, K is the permeability, μ is the viscosity, p is the pressure, ρ is density, g is the gravity vector, T is the temperature, α_e is the effective thermal diffusivity, c_p is the specific heat at constant pressure, β is the coefficient of thermal expansion and b is the empirical constant of the porous medium. Eliminating pressure and making use of the boundary layer and Boussenesq approximations, in equations (4.1),(4.2)&(4.5), we get

$$\frac{\partial u}{\partial x}+\frac{\partial v}{\partial y}=0 \tag{4.7}$$

$$\frac{\partial u}{\partial y}+\frac{bK\rho}{\mu}\frac{\partial u^2}{\partial y}=\frac{Kg\beta\rho}{\mu}\frac{\partial T}{\partial y} \tag{4.8}$$

$$u\frac{\partial T}{\partial x}+v\frac{\partial T}{\partial y}=\frac{\partial}{\partial y}\left[(\alpha+\gamma du)\frac{\partial T}{\partial y}\right]+\frac{\nu}{Kc_p}u\left(u+\frac{bK\rho}{\mu}u^2\right) \tag{4.9}$$

In arriving at the above equations, we made use of the simplifications via.,
(1) $uq=u\left(u^2+v^2\right)^{1/2}=u^2\left(1+\frac{v^2}{u^2}\right)^{1/2}\approx u^2$ under the boundary layer approximations
(2) $\frac{\partial p}{\partial y}=0$ inside the boundary layer, so the term $\frac{\nu}{Kc_p}v\left(-\frac{\partial p}{\partial y}\right)$ vanishes in the energy equation, and
(3) $\alpha_e=\alpha+\alpha_d$, α is the stagnant diffusivity, and the dispersion diffusivity α_d is assumed to vary linearly with the stream wise velocity component $\alpha_d=\gamma du$.
The resulting boundary layer equations (4.7)-(4.9), along with the boundary conditions are solved using perturbation technique. We made use of the scales proposed in Bejan and Poulikakos [16] for the flow field and boundary layer thickness. Then the transformation for converting the partial differential equations into non-similar ordinary differential equations are given as

$$\eta=\frac{y}{x}\,{R_x}^{1/4} \tag{4.10}$$

$$\psi=\alpha\,{R_x}^{1/4}\,f(x,\eta) \tag{4.11}$$

$$T-T_\infty=(T_w-T_\infty)\,\theta(x,\eta) \tag{4.12}$$

Here $R_x=\frac{g\beta\theta_w x^2}{b\alpha^2}$ and $\theta_w=T_w-T_\infty$. ψ is the stream function defined so that $u=\frac{d\psi}{dy}$, $v=-\frac{d\psi}{dx}$ and the equation of continuity is satisfied automatically. The transformation (4.10)

- (4.12) reduces the equations (4.7)-(4.9) into

$$Gf''' + 2f'f'' = \theta' \tag{4.13}$$

$$\theta'' + \frac{1}{2}f\theta' + \gamma R_d^{1/2}(f''\theta' + f'\theta'') + Ge_x f'(Gf' + f'^2) = x\left(f'\frac{\partial\theta}{\partial x} - \theta'\frac{\partial f}{\partial x}\right). \tag{4.14}$$

where $G = \frac{\nu}{K}(bgi\theta_w)^{-1/2}$, $R_d = \frac{g\beta\theta_w d^2}{b\alpha^2}$ and $Ge_x = \frac{g\beta x}{c_p}$ Using the integrated form of equation (4.13), the energy equation becomes

$$\theta'' + \frac{1}{2}f\theta' + Ds(f''\theta' + f'\theta'') + \epsilon f'\theta = \epsilon(f'\theta_\epsilon - \theta' f_\epsilon). \tag{4.15}$$

where ϵ $(=Ge_x)$ is the dissipation parameter and Ds $(=\gamma R_d^{1/2})$ is the dispersion parameter. In all these equations the superscript $'$ represents the differentiation with respect to η and subscript ϵ represents the differentiation with respect to ϵ. The boundary conditions become

$$\left.\begin{array}{ll} \eta = 0; & f(\epsilon, 0) = 0 \ \ and \ \ \theta(\epsilon, 0) = 1 \\ \eta \to \infty; & f'(\epsilon, \infty = 0) \ \ and \ \theta(\epsilon, \infty) = 0. \end{array}\right\} \tag{4.16}$$

Now writing the non-dimensional stream function and temperature function in terms of perturbation functions f_m and t_m as

$$\left.\begin{array}{rcl} f(\epsilon, \eta) & = & \Sigma_{m=0}^{\infty}(-1)^m \epsilon^m f_m(\eta) \\ \theta(\epsilon, \eta) & = & \Sigma_{m=0}^{\infty}(-1)^m \epsilon^m t_m(\eta) \end{array}\right\} \tag{4.17}$$

and substituting equations (4.17) into equations (4.13) and (4.15) and equating the coefficients of various powers of ϵ to zero (here we collect terms upto the second power of ϵ), we obtain the following sets of ordinary differential equations :

ϵ^o:

$$\left.\begin{array}{c} Gf_0''' + 2f_0'f_0'' - t_0' = 0 \\ t_0'' + \frac{1}{2}f_0t_0' + Ds(f_0''t_0' + f_0't_0'') = 0 \end{array}\right\} \tag{4.18}$$

with the corresponding boundary conditions

$$f_0(0) = f_0'(\infty) = t_0(0) - 1 = t_0(\infty) = 0$$

ϵ^1:

$$\left.\begin{array}{c} Gf_1''' + 2f_0'f_1'' + 2f_0''f_1' - t_1' = 0 \\ t_1'' + \frac{1}{2}(f_0t_1' + t_0'f_1) + Ds(f_0''t_1' + f_1''t_0' + f_0't_1' + f_1't_0'') - f_0't_0 - (f_0't_1 - f_1t_0') = 0 \end{array}\right\} \tag{4.19}$$

with the corresponding boundary conditions

$$f_1(0) = f_1'(\infty) = t_1(0) = t_1(\infty) = 0$$

ϵ^2:

$$\left.\begin{array}{c} Gf_2''' + 2(f_0'f_2'' + f_1'f_1'' + f_2'f_0'') - t_2' = 0 \\ t_2'' + \frac{1}{2}(f_0t_2' + f_1t_1' + f_2t_0') + Ds(f_0''t_2' + f_1''t_1' + f_2''t_0' + f_0't_2'' + f_1't_1'' + f_2't_0'') \\ -(f_0't_1 + f_1't_0) + (f_1t_1' + 2f_2t_0' - 2f_0't_2 - f_1't_1) = 0 \end{array}\right\} \quad (4.20)$$

with the corresponding boundary conditions

$$f_2(0) = f_2'(\infty) = t_2(0) = t_2(\infty) = 0$$

and so on...

4.3 Results and Discussion

The first set of ordinary differential equations (4.18) deal with the problem without dissipation. This set with $Ds = 0$ was considered by Bejan and Poulikakos [16]. The present analysis covers two cases :

(i)The effect of thermal dispersion in the non-Darcy regime (G=0) and limit Darcy regime ($G \to \infty$), and

(ii)The effect of viscous dissipation in the non-Darcy regime and limit Darcy regime with and without thermal dispersion.

The sets of differential equations (4.18)-(4.20) are solved successively, by giving appropriate initial guess values for $f_i'(0)$, $t_i'(0)$, i=0,1,2 to match the values with the corresponding boundary conditions at $f_i'(\infty)$, $t_i(\infty)$,i=0,1,2. NAG software is used for integrating the corresponding first order system of equations (4.18)-(4.20) and shooting and matching the initial and boundary conditions, the results are observed upto the accuracy of $5.0X10^{-6}$. The results which cover the above two cases are presented in Tables (4.1) and (4.2). Table (4.1) gives the influence of viscous dissipation on non-Darcy, intermediate and limit Darcy regimes when the effect of thermal dispersion is neglected. Table (4.2) gives the influence of viscous dissipation in the three regimes as the value of Ds increases. The percentage decrease in the Nusselt number results for two values of viscous dissipation parameter from zero dissipation values is also shown in the Table (4.3).

In Figures (4.1) and (4.2) the vertical velocity components $f_i'(\eta)$, i = 0,1,2 are plotted for $Ds = 0$ and $Ds = 10$. From Figure (4.2), the curve representing $f_1'$is seen to be more effective for the value of $G = 0.1$ and it becomes thin as we move into the intermediate regime. The slope of the curve f_1' for $G = 0.1$ is maximum at $\eta = 1.07$(approximately) and this value of η increases to 3.8 for the same curve when the dispersion parameter is increased to $Ds = 10$.

From the results obtained, it is observed that the values of $f_i'(0) = 0$, i = 1, 2 and $f_i'(\infty)$ = 0, i = 0,1,2. So there is not much change in the value of $f'(0)$ and is almost equal to $f_1'(0)$ for all values of the parameter G and from Figures (4.3a & 4.3b), it can be observed that the effective vertical velocity

$$f'(\eta) = f_0'(\eta) - \epsilon f_1'(\eta) + \epsilon^2 f_2'(\eta) \tag{4.21}$$

(at ϵ= 0.1) thickens a little from its zero dissipation component, i.e., $f'(\eta) = f_0'(\eta)$ and this deviation increases with increase in the value of dissipation parameter, when $G = 0.1$, $G =$ 10 are plotted.

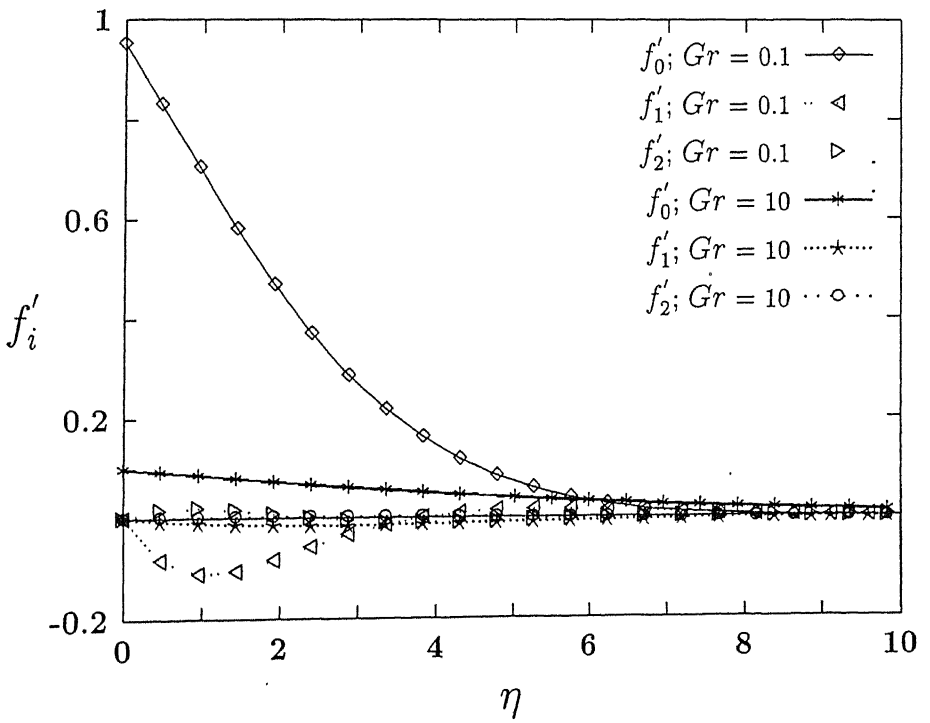

Figure (4.1): Streamwise velocity components when Ds=0.

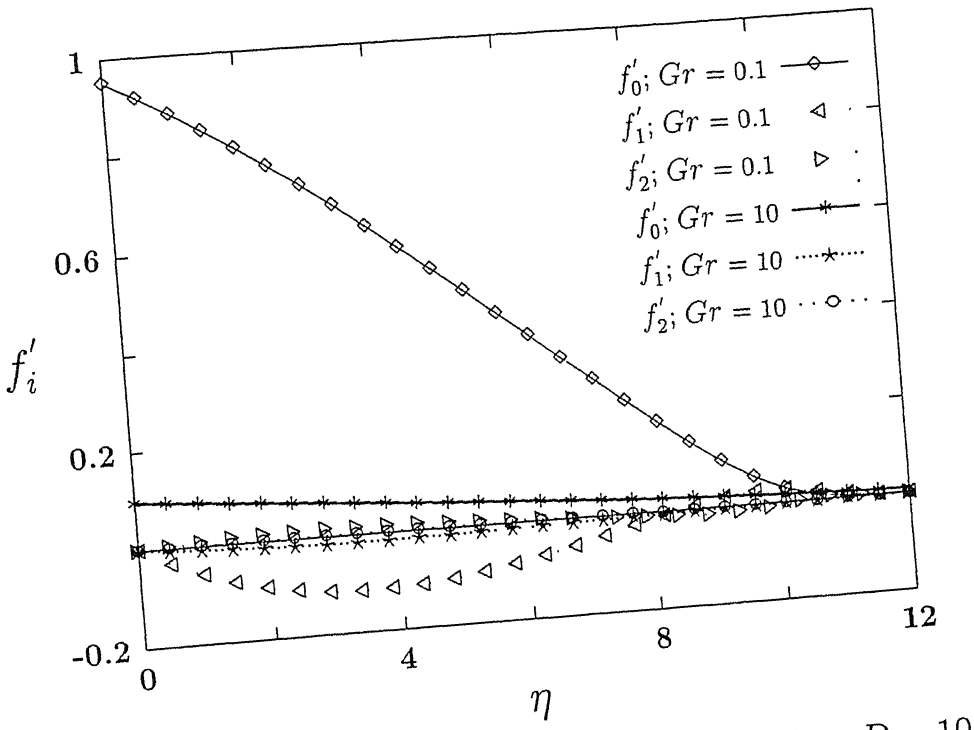

Figure (4.2): Streamwise velocity components when Ds=10.

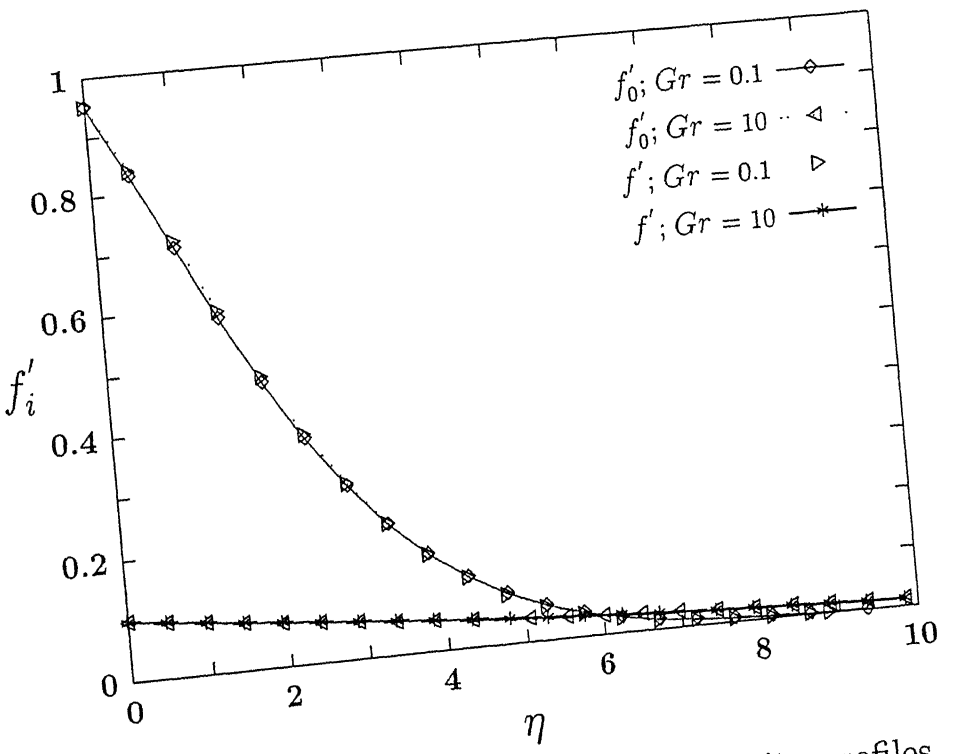

Figure (4.3a): Variation of streamwise velocity profiles with dissipation parameter $\epsilon = 0.1$ when $Ds = 0$.

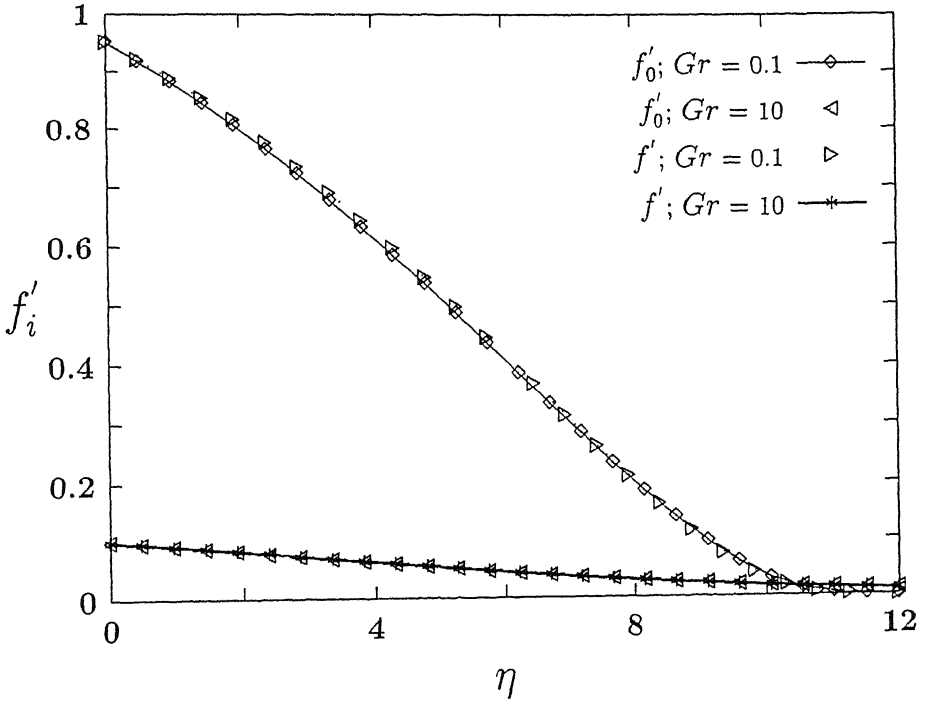

Figure (4.3b): Variation of streamwise velocity profiles with dissipation parameter $\epsilon = 0.1$, when $Ds = 10$.

Similarly the non-dimensional temperature distribution for $t_i(0)$, i = 0,1,2 is plotted in Figures (4.4) and (4.5) for $Ds = 0$ and $Ds = 10$ respectively. From Figures (4.6a) and (4.6b), it can be observed that the effect of viscous dissipation increases as the value of G increases. And it has got pronounced effect as the value of the thermal dispersion parameter increases. The effective temperature distribution is obtained from equation (4.17) at $\epsilon = 0.1$.

Since we have used a series solution for solving the problem and the stream wise derivatives of the dependent variables are not neglected in the governing equations the results obtained here must be very much appropriate. The values for $t_1'(0)$ and $t_2'(0)$ are significant, and the trend shows that even if we consider more terms in the series expansion for f and θ (i.e., after 2nd level of perturbation), the resulting values for $t_3'(\eta)$ etc. and their contribution (i.e.,$-\epsilon^3 t_3'(\eta) + \epsilon^4 t_4'(\eta) - ...$) will be very small in the range of values of ϵ for which the series solution is valid.

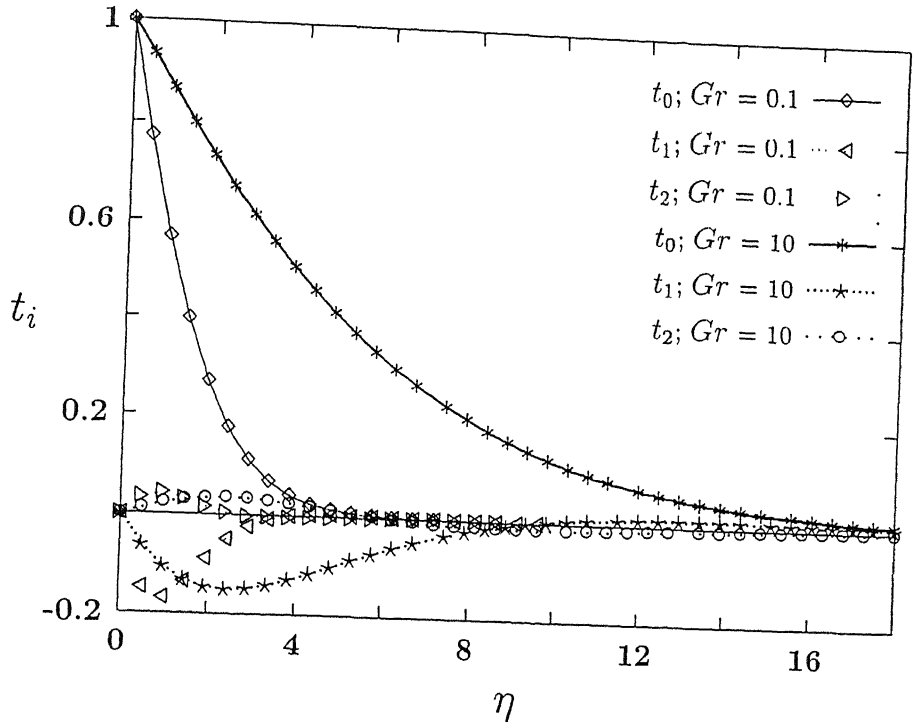

Fig (4.4): Temperature components when $Ds = 0$.

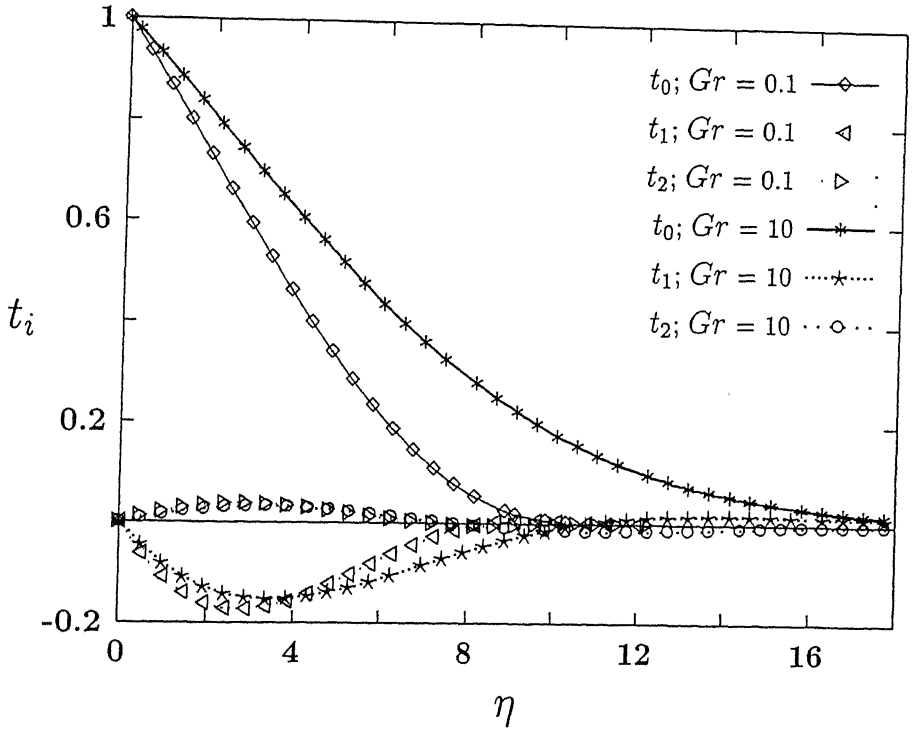

Figure (4.5): Temperature components when $Ds = 10$.

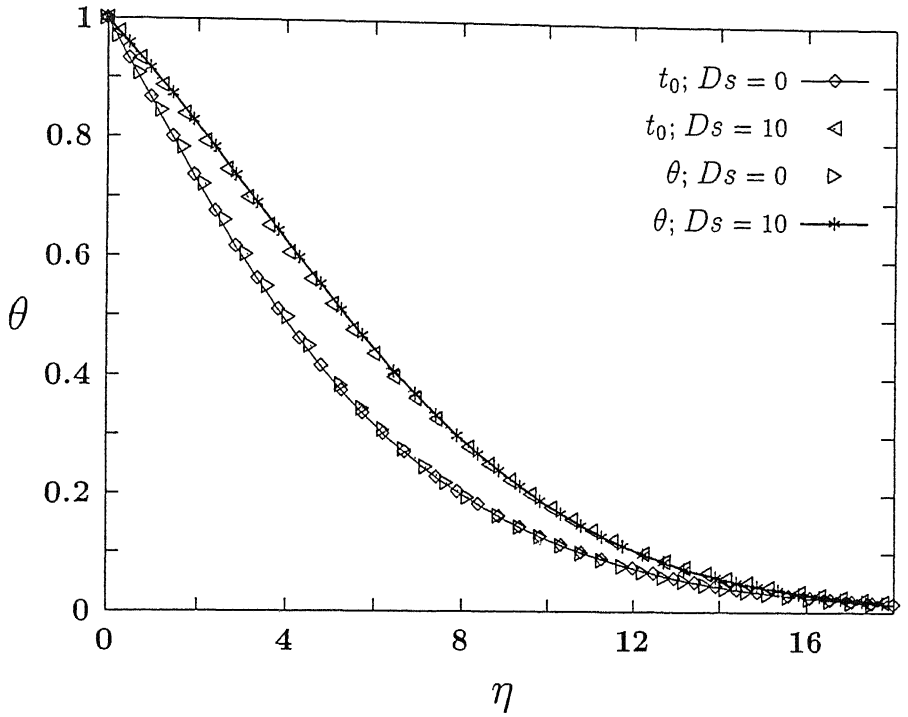

Figure (4.6a): Effect of dissipation ($\epsilon = 0.1$) on temperature profiles with and without dispersion in the limit Darcy regime ($Gr = 10$).

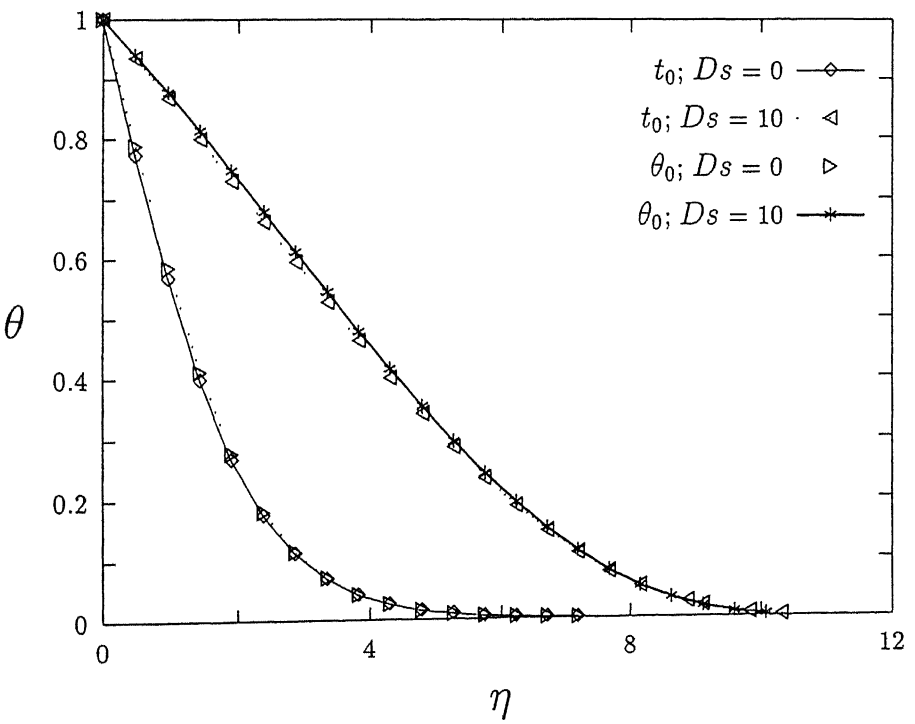

Figure (4.6b): Effect of dissipation on temperature profiles with and without dispersion in the near non-Darcy ($Gr = 0.1$) regime.

The values of $-\theta'(\eta)$ is plotted for $G = 0.1$ and $G = 10$ with increase in dispersion parameter in Figures (4.7a) and (4.7b).

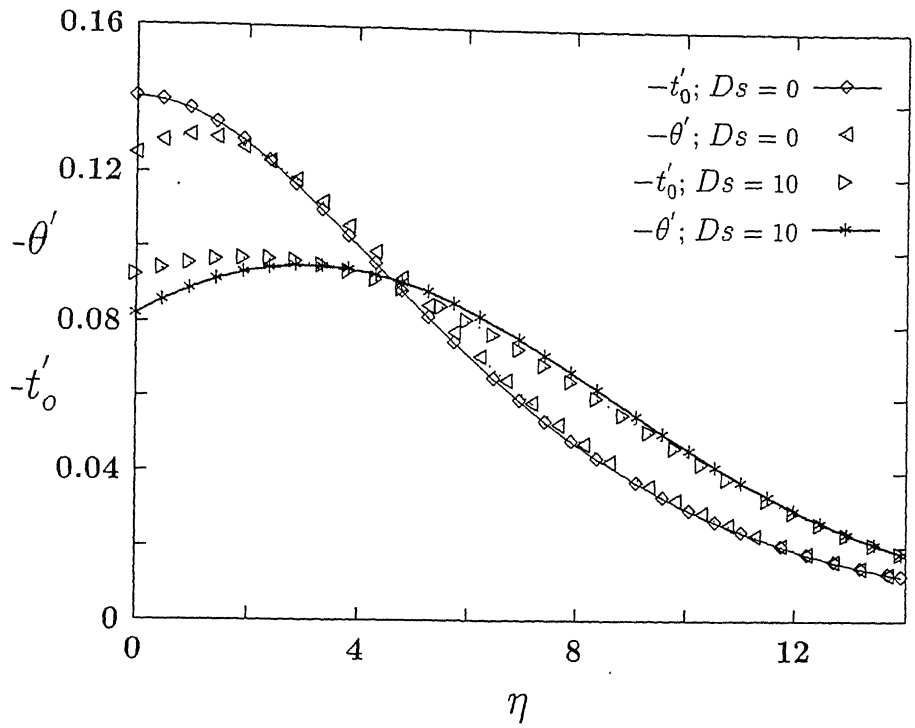

Figure (4.7a): Variation of the '-' temperature gradient when $\epsilon = 0$ and 0.1 in the limit Darcy ($Gr = 10$) regime.

The solid curves correspond to the zero dissipation curves of $-\theta'$ i.e., $-t_0'(0)$ and the dotted curves correspond to effective temperature gradients (negative) when $\epsilon = 0.1$ i.e.,

$$\theta'(\eta) = t_0'(\eta) - \epsilon t_1'(\eta) + \epsilon^2 t_2'(\eta).$$

When $Ds = 0$, the values of $-t_0'(\eta)$ decrease with η steadily, where as the increase in the value of the dispersion parameter increases, $-t_0'(\eta)$ upto certain value of η and comes down to zero; the reasons for this were well explained in Hong and Tien [46]. Consideration of viscous dissipation reveals the increase in temperature gradient $-\theta'$ is more near the wall region in the non-Darcy regime when $Ds = 0$, and this peak is smothened as we go into the intermediate regime and with the increasing values of G and Ds. The effect of viscous dissipation on the '-' ve temperature gradient is shown in the Figures (4.7a) and (4.7b) in the limit Darcy and near non-Darcy regimes respectively.

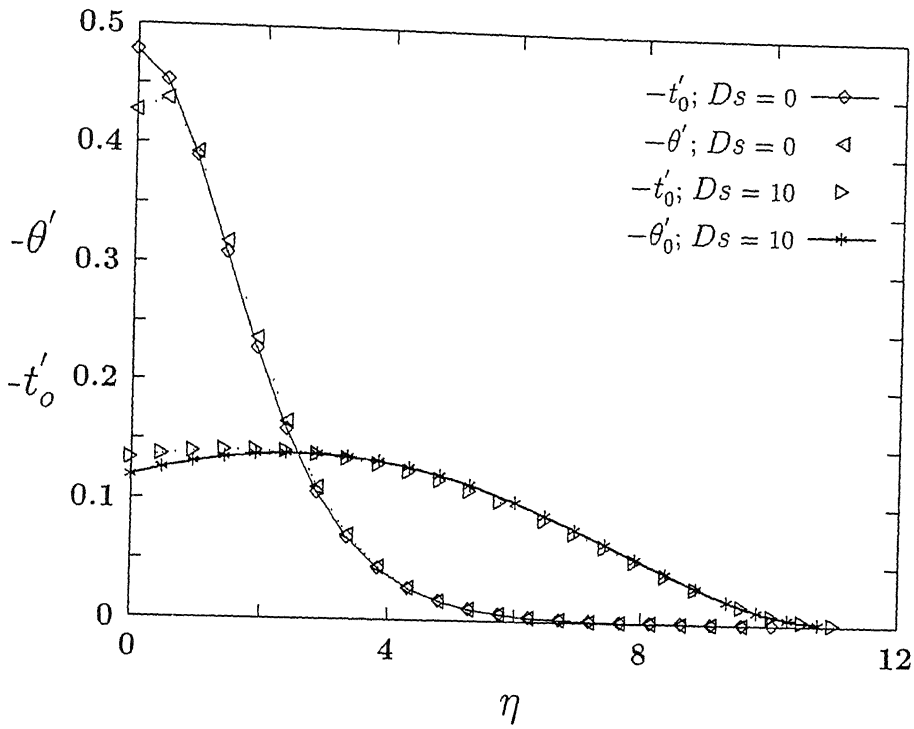

Figure (4.7b): Variation of the '-' temperature gradient when $\epsilon = 0$ and 0.1 in the near non-Darcy ($Gr = 0.1$) regime.

Now the local heat transfer rate from the surface of the plate to the medium is given by

$$q = -k_e \frac{dT}{dy}_{y=0} \tag{4.22}$$

where k_e is the effective thermal conductivity which is the sum of stagnant conductivity and dispersion conductivity (due to mechanical dispersion), and the local Nusselt number Nu_x is given by

$$\frac{Nu_x}{R_x^{1/4}} = [1 + Dsf'(0)]\{-t_0'(\eta) + \epsilon t_1'(\eta) - \epsilon^2 t_2'(\eta)\}. \tag{4.23}$$

The first column under the Nusselt number expression in Table (4.1) is the solution obtained in Bejan and Poulikakos [16] and the second and third columns correspond to the Nusselt number values when the viscous dissipation parameter ϵ takes values 0.01 and 0.1. Table (4.2) gives the combined effect of thermal dispersion and viscous dissipation in all the three regimes under consideration. The thermal dispersion enhances the heat transfer rate while the viscous dissipation tends to lower it and the values of the percentage decrease in the Nusselt number results given in Table (4.3) reveals that

(i) the effect of viscous dissipation increases as we move from non-Darcy to limit Darcy regime.

(ii) the effect of viscous dissipation increases as the value of Ds increases in (a) non-Darcy regime (b) intermediate regime (c) limit Darcy regime.

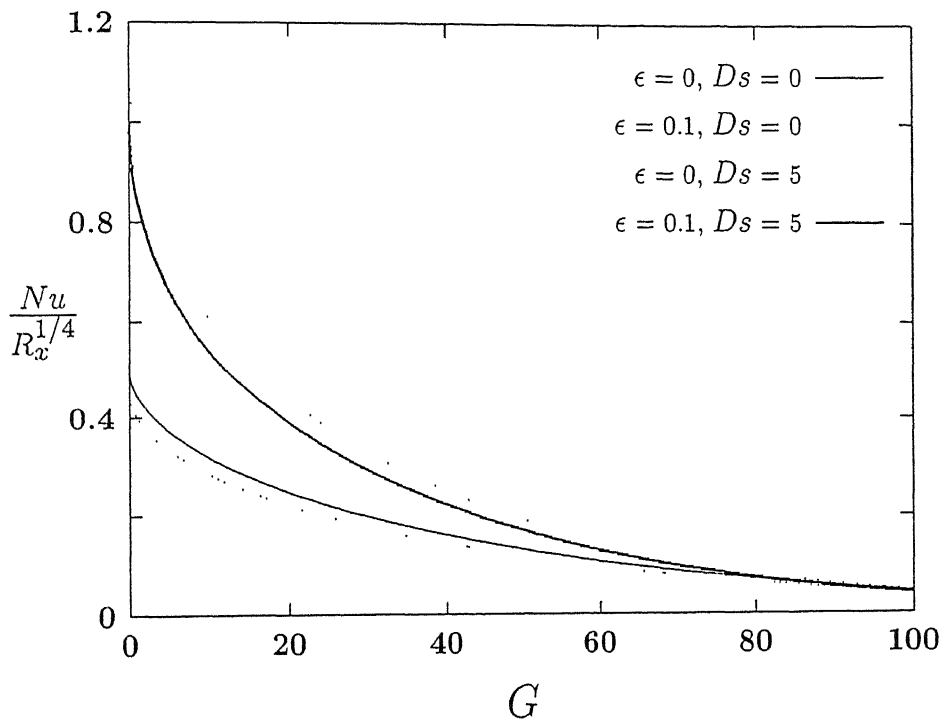

Figure (4.8): $\frac{Nu}{R_x^{1/4}}$ .vs. G for ϵ=0 and ϵ=0.1 and various Ds.

Figure (4.8) gives the clear picture of the influence of viscous dissipation on the Nusselt number. It is seen from this figure that the effect of dissipation increases with thermal dispersion.

					$\frac{Nu}{R_x^{1/4}} = -\theta'(0)$		
G	$f'(0)$	t_0'	t_1'	t_2'	$\epsilon = 0$	$\epsilon = .01$	$\epsilon = .1$
0	1.0	-0.4941	-0.5161	0.0904	0.4941	0.4889	0.4416
0.1	0.9512	-0.4778	-0.5013	0.0881	0.4778	0.4728	0.4268
1.0	0.6180	-0.3658	-0.3904	0.0695	0.3658	0.3619	0.3261
10.0	0.0990	-0.1402	-0.1506	0.0272	0.1402	0.1387	0.1249
∞	0.0100	-0.0460	-0.0468	0.0082	0.0460	0.0455	0.0412

Table 4.1: Decrease in Nusselt number with ϵ when Ds=0;∞=100(here)

					-$\theta'(0)$			$\frac{Nu}{R_x^{1/4}}$		
G	Ds	$-t_0'$	$-t_1'$	t_2'	$\epsilon = 0$	$\epsilon = .01$	$\epsilon = .1$	$\epsilon = 0$	$\epsilon = .01$	$\epsilon = .1$
0	0.2	0.444	0.4656	0.0819	0.444	0.4393	0.3966	0.5328	0.5272	0.4759
	2.0	0.2666	0.2837	0.0510	0.2666	0.2637	0.2377	0.7998	0.7913	0.7132
	5.0	0.1863	0.1968	0.0351	0.1863	0.1843	0.1663	1.1178	1.1059	0.9976
0.1	0.2	0.4311	0.4541	0.0802	0.4311	0.4265	0.3849	0.5131	0.5077	0.4581
	2.0	0.2617	0.2798	0.0502	0.2617	0.2590	0.2332	0.7596	0.7514	0.6769
	5.0	0.1821	0.1959	0.0353	0.1821	0.1802	0.1622	1.0482	1.0369	0.9334
	10.0	0.1335	0.144	0.026	0.1335	0.1321	0.1188	1.4034	1.3882	1.2493
1.0	0.2	0.3406	0.3645	0.0652	0.3406	0.3369	0.3035	0.3827	0.3786	0.3410
	2.0	0.2280	0.2474	0.0449	0.2280	0.2255	0.2028	0.5098	0.5043	0.4535
	5.0	0.1637	0.1791	0.0327	0.1637	0.1619	0.1455	0.6695	0.6621	0.5949
	10.0	0.1216	0.1336	0.0245	0.1216	0.1203	0.1080	0.8731	0.8635	0.7754
10.0	0.2	0.1384	0.1488	0.0269	0.1384	0.1369	0.1233	0.1411	0.1396	0.1257
	2.0	0.1251	0.1351	0.0245	0.1251	0.1238	0.1114	0.1499	0.1483	0.1334
	5.0	0.1093	0.1186	0.0217	0.1093	0.1081	0.0972	0.1634	0.1616	0.1454
	10.0	0.0923	0.1008	0.0185	0.0923	0.0913	0.0820	0.1837	0.1817	0.1632
∞	0.2	0.0459	0.0467	0.0082	0.0459	0.0454	0.0411	0.0460	0.0455	0.0412
	2.0	0.0454	0.0462	0.0081	0.0454	0.0450	0.0407	0.0463	0.0458	0.0415
	5.0	0.0446	0.0454	0.0080	0.0446	0.0441	0.0399	0.0468	0.0463	0.0420
	10.0	0.0433	0.0441	0.0078	0.0433	0.0429	0.0388	0.0476	0.0471	0.0427

Table 4.2: Decrease in Nusselt number with ϵ and Ds;∞=100(here)

G	Ds	% dec when ϵ=0.01	% dec when ϵ=0.1
0	0	1.04635	10.62821
	0.2	1.05106	10.67098
	2.0	1.06276	10.83270
0.1	0	1.05065	10.67601
	0.2	1.05243	10.71721
	2.0	1.07009	10.88392
	5.0	1.0809	10.95401
1.0	0	1.06615	10.86248
	0.2	1.07133	10.89626
	2.0	1.08079	11.04920
	5.0	1.09186	11.13517
	10.0	1.0984	11.18900
10.0	0	1.07704	10.93438
	0.2	1.09112	10.94657
	2.0	1.08093	10.99619
	5.0	1.08323	11.04651
	10.0	1.09436	11.11776

Table 4.3: % Decrease in Nusselt number with ϵ and Ds

Chapter 5

Thermal Dispersion Effects On Non-Darcy Convection Over A Cone [1]

5.1 Introduction

The study of transport phenomena in porous media is gaining more attention because of its wide applicability in extraction of geothermal energy in reservoirs, petroleum industry, temperature controlled reactors, nuclear waste disposal, ceramic processing, and utilization of porous layers for transpiration cooling by water for fire fighting.

In previous chapters we have studied the combined effects of thermal dispersion and mass flux on natural convection. Here, in the present chapter, we studied the effect of thermal dispersion effects on non-Darcy mixed convection over a vertical cone pointing downwards. As mentioned in the chapter 3, that the understanding of the convection about axi-symmetric geometries would be helpful in designing the suitable canesters in the nuclear waste disposal industry, specifically, the mixed convection heat transfer needs special attention because, in many practical problems the buoyancy force is well comparable with the the externally maintained pressure gradient.

Analytical studies on convective heat transfer in porous medium based on the boundary layer approximations begin with Wooding [68], later Cheng and Chang [63], Cheng and

[1] Accepted for publication in the journal "**Advances in Partial Differential Equations**"

Minkowycz [65], and Cheng [61] studied the natural and mixed convection phenomena over horizontal, vertical, and inclined surfaces in a Darcian fluid saturated porous medium. Cheng et al., [66] studied the natural convection about a vertical cone when the curvature effects are neglected. Pop and Cheng [41] in their subsequent study revealed that the curvature effects tend to enhance the heat transfer, but its effect decreases as the Rayleigh number increases. Merkin [42] studied the mixed convection boundary layer flow on a vertical surface in a saturated porous medium. Combined free and forced convection heat transfer about a horizontal cylinder and a sphere has been analysed by Cheng [61]. Minkowycz et al [82] analysed the mixed convection heat transfer from a non-isothermal cylinder and sphere in a saturated porous medium.

In connection with boundary layers on axi-symmetric bodies in a saturated porous media, Fand et al., [71] conducted experiments on a horizontal cylinder. They studied the natural convection process. Later Nakayama and Koyama [19] gave a general similarity transformation for combined convection over non-isothermal two dimensional or axi-symmetric bodies of arbitrary shape. Cheng [12] gave a nice review of mixed convection heat transfer in a Darcian fluid saturated porous medium. When the pore diameter dependent Rayleigh number becomes large enough for the Darcy model to break down, using the Forchheimer extension of Darcy law, Plumb and Huenefeld [56], Bejan and Poulikakos [16] studied the natural convection from a vertical surface. Non-Darcy mixed convection flow over a vertical cylinder has been analysed by Kumari and Nath [53] and in their subsequent study [54] they have studied the mixed convection about a horizontal cylinder and a sphere embedded in a saturated porous medium. A unified similarity treatment is given by Nakayama and Pop [22] for convection problems in Porous medium.

All the above studies neglect thermal dispersion effects. Cheng [60] and Plumb [57] pointed out that when the inertial effects are prevalent, the thermal dispersion effects in Porous medium become very important. Hong et al [47] studied vertical plate natural convection in a non uniform porous medium, and thermal dispersion effects are included in the energy equation. Thermal dispersion effect on non-Darcy convection over horizontal and vertical walls has been studied by Lai and Kulacki [36]-[37]. More recently, Amiri and Vafai [14] confirmed in their study on forced convection flow and heat transfer that the axial dispersion effect can be neglected when compared with the radial dispersion effect.

The similarity solution is not possible for convective heat transfer from any axi-symmetric

geometry except for a vertical cone when thermal dispersion effects are considered. Here in this chapter, similarity solution for non-Darcy mixed convection about an isothermal vertical cone pointing downwards in a fluid saturated porous medium when the free stream velocity is uniform is obtained on the basis of boundary layer approximations. For a fixed cone apex half angle, g_x remains constant and similarity solution is possible. The governing parameter in the mixed convection is $\frac{Ra_x}{Pe_x}$. The limiting case $\frac{Ra_x}{Pe_x} \to 0$ leads the problem into forced convection process. As it will be seen that the similarity solution exists for all power law variations of the wall temperature when the free stream velocity remains uniform and closed form solution for velocity and temperature are obtained for the isothermal wall temperature and uniform free stream flow. In the mixed convection study, both the aiding and opposing flows are considered. The convection domain is divided into pure and mixed regions in terms of $\frac{Ra_x}{Pe_x}$ using the 5% deviation criteria. The effect of thermal dispersion on both aiding and opposing flows is studied. A flow separation phenomenon occurs when the forced and free convection act in opposite directions. The overall heat transfer is enhanced due to the thermal dispersion effects.

5.2 Governing Equations

Consider a vertical cone pointing downwards in a fluid saturated porous medium as shown in the Figure (5.1). The cone is placed with its axis of symmetry vertical and x-measures the distance along the surface of the cone from the apex, x=0 being the leading edge and y measures distance normally outwards. ξ is the cone apex half anlge. The impermeable cone is held at a temperature $T_w = T_\infty + A\, x^n$, greater than the ambient temperature T_∞. The governing equations for the flow and heat transfer in the fluid saturated porous medium are given by

$$\frac{\partial (ru)}{\partial x} + \frac{\partial (rv)}{\partial y} = 0 \tag{5.1}$$

$$u + \frac{C\sqrt{K}}{\nu} u^2 = -\frac{K}{\mu}\left(\frac{\partial p}{\partial x} + \rho g_x\right) \tag{5.2}$$

$$v + \frac{C\sqrt{K}}{\nu} v^2 = -\frac{K}{\mu}\left(\frac{\partial p}{\partial y}\right) \tag{5.3}$$

$$u\frac{\partial T}{\partial x} + v\frac{\partial T}{\partial y} = \frac{\partial}{\partial x}\left(\alpha_x \frac{\partial T}{\partial x}\right) + \frac{\partial}{\partial y}\left(\alpha_y \frac{\partial T}{\partial y}\right) \tag{5.4}$$

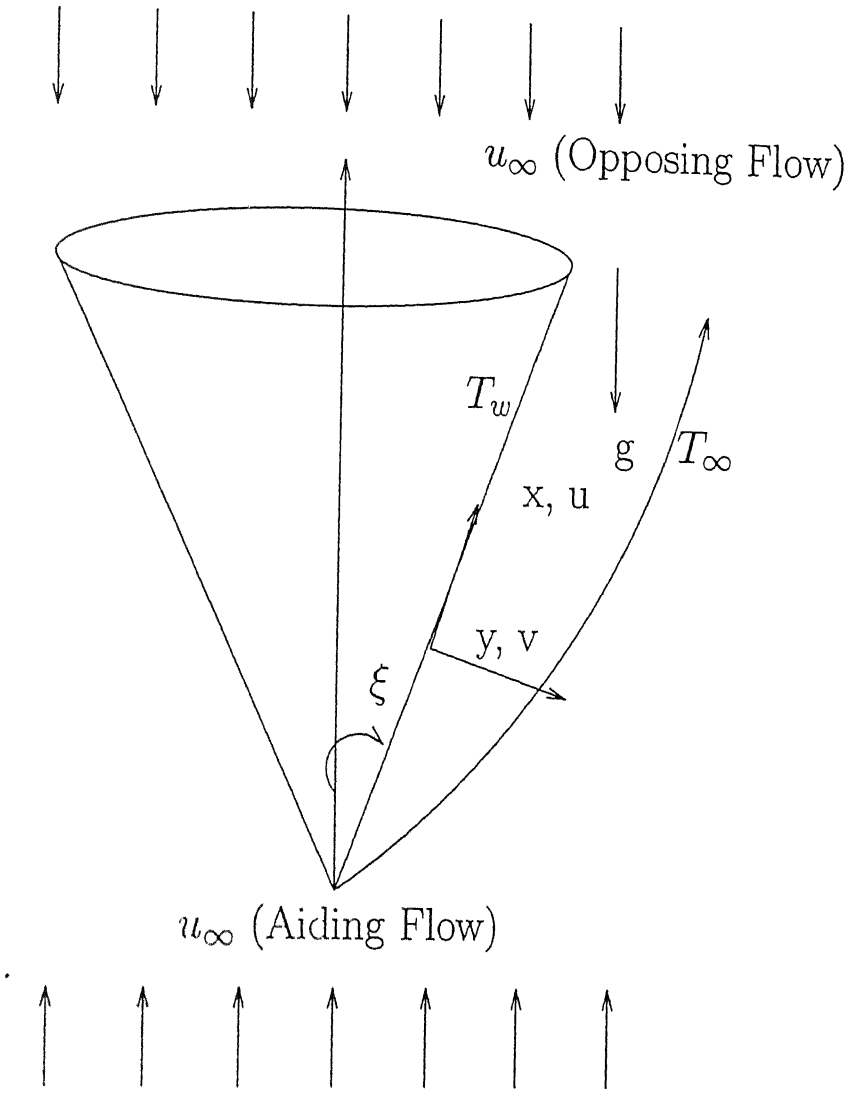

Figure 5.1: Mixed convection - coordinate system

along with the Boussinesq approximation

$$\rho = \rho_\infty[1 - \beta(T - T_\infty)] \tag{5.5}$$

where

$$r(x) = x sin\xi, \tag{5.6}$$

$$g_x = g\left[1 - \left(\frac{\partial r}{\partial x}\right)^2\right]^{1/2} \tag{5.7}$$

and the boundary conditions are

$$\left.\begin{array}{l} y = 0: \; v = 0, \; T_w = T_\infty + A\,x^n \\ y \to \infty: \; u_\infty(x) = Bx^l, \; T \to T_\infty \end{array}\right\}. \tag{5.8}$$

Here x and y are the coordinates along the wall and normal to the wall respectively, u and v are the Darcian velocity components in x and y directions, u_∞ is the free stream velocity, T is the temperature, ρ is the density, p is the pressure, β is the coefficient of thermal expansion, μ is the viscosity of the fluid, ν is the kinematic viscosity of the fluid, K is the permeability constant, C is an empirical constant, g is the acceleration due to gravity, α_x and α_y are the components of thermal diffusivity in x and y directions, r is the curvature of the cone and ξ is the cone apex half angle. The suffixs w and ∞ indicate the conditions at the wall and at the outer edge of the boundary layer respectively. A,B,n and l are real constants.

Experimental and numerical studies on convective heat transfer in porous media show that thermal boundary layers exist adjacent to the heated or cooled bodies. When the thermal boundary layer is thin (i.e., $x >> y \sim \delta_T$, δ_T is the boundary layer thickness), boundary layer approximations analogous to classical boundary layer theory can be applied [7]. Now, applying the boundary layer and Boussinesq approximations and eliminating pressure from the momentum equation, the governing equations will become

$$\frac{\partial u}{\partial y} + \frac{C\sqrt{K}}{\nu}\frac{\partial u^2}{\partial y} = -\left(\frac{K g_x \beta}{\nu}\right)\frac{\partial T}{\partial y} \tag{5.9}$$

$$u\frac{\partial T}{\partial x} + v\frac{\partial T}{\partial y} = \frac{\partial}{\partial y}\left(\alpha_y \frac{\partial T}{\partial y}\right) \tag{5.10}$$

Here α_y is a variable quantity which is the sum of molecular thermal diffusivity α and dispersion thermal diffusivity α_d. Following Plumb [57], the expression for dispersion thermal diffusivity α_d will be $\alpha_d = \gamma\, d\, u$, where γ is the mechanical dispersion coefficient whose value depends on the experiments, and d is the pore diameter.

First we represent the governing equations (5.9) and (5.10) in terms of stream function and temperature formulation. The velocity components u and v can be written in terms of stream function ψ as: $u = \frac{1}{r}\frac{\partial \psi}{\partial y}$ and $v = -\frac{1}{r}\frac{\partial \psi}{\partial x}$. This representation is valid since the expressions for velocity components clearly satisfy the continuity equation. Now the resulting equations are

$$\frac{1}{r}\frac{\partial^2 \psi}{\partial y^2} + \frac{1}{r^2}\frac{C\sqrt{K}}{\nu}\frac{\partial}{\partial y}\left(\frac{\partial \psi}{\partial y}\right)^2 = -\frac{K g_x \beta}{\nu}\frac{\partial T}{\partial y} \tag{5.11}$$

$$\frac{1}{r}\frac{\partial \psi}{\partial y}\frac{\partial T}{\partial x} - \frac{1}{r}\frac{\partial \psi}{\partial x}\frac{\partial T}{\partial y} = \frac{\partial}{\partial y}\left(\left[\alpha + \frac{\gamma d}{r}\frac{\partial \psi}{\partial y}\right]\frac{\partial T}{\partial y}\right). \tag{5.12}$$

From comparison of the order magnitudes of the convection and conduction terms in the energy equation, we get an estimate for the boundary layer thickness δ_T as

$$\delta_T \sim x Pe_x^{-1/2} \tag{5.13}$$

where Pe_x is the Peclet number, given as $Pe_x = \frac{u_\infty x}{\alpha}$. Here, we notice that the maximum velocity is at the outer edge of the boundary layer, and it is the free stream velocity. We take this as the maximum estimate for the velocity and arrive at the above equation. Now, the similarity variable η which is defined as

$$\eta = \frac{y}{\delta_T} \tag{5.14}$$

will become

$$\eta = \frac{y}{x} Pe_x{}^{1/2}. \tag{5.15}$$

From the free stream boundary condition, we get an order magnitude estimate for the stream function as

$$\psi = \alpha r Pe_x^{1/2}, \tag{5.16}$$

and the expression for ψ in the non-dimensional form will be

$$f(\eta) = \frac{\psi}{\alpha r Pe_x{}^{1/2}}. \tag{5.17}$$

Now write the non-dimensional temperature distribution as

$$\theta(\eta) = \frac{T - T_\infty}{T_w - T_\infty}. \tag{5.18}$$

With this transformation set (η, f and θ) the governing equations reduce into the ordinary differential equations as

$$f'' + 2Re\, f' f'' = \pm \frac{Ra_x}{Pe_x} \theta' \tag{5.19}$$

$$\theta'' + \frac{3}{2} f\theta' - n f'\theta + \gamma Pe_d (f''\theta' + f'\theta'') = 0 \tag{5.20}$$

and the boundary conditions become

$$\left.\begin{array}{ll} \eta = 0: & f = 0,\ \theta = 1 \\ \eta \to \infty: & f' = 1,\ \theta = 0 \end{array}\right\}. \tag{5.21}$$

The "+" sign in equation (5.19) denotes aiding flow and the "-" sign denotes the opposing flow. The flow is said to be aiding if the free stream is in the direction of buoyancy, where as the flow is opposing when the free stream is opposing the buoyancy.

5.3 Results and Discussion

In the above ordinary differential equations, the parameter Ra_x is the modified Rayleigh number defined as $\frac{Kg\beta\theta_w x}{\alpha\nu}$ which describes the intensity of buoyancy effects and Pe_x is the Peclet number defined as $\frac{u_\infty x}{\alpha}$, which describes the intensity of the externally maintained pressure gradient. Ra_d, Pe_d represent the pore diameter dependent Rayleigh and Peclet numbers respectively. Re is the Forchheimer coefficient dependent Raynold's number. Now the governing ordinary differential equations will be free from x only for the isothermal wall with uniform free stream. In that case $\frac{Ra_x}{Pe_x}$ will become $\frac{Ra_d}{Pe_d}$ and similarity solution is possible for the mixed convection heat transfer from vertical cone for fixed cone apex half-angle. The governing parameter for the mixed convection process is $\frac{Ra_d}{Pe_d}$.

In the limiting case of $\frac{Ra_x}{Pe_x} \to 0$, the problem will be the non-Darcian forced convection flow and heat transfer, and the equation (5.19) becomes

$$f' + Re\, f'^2 = 1 + Re. \tag{5.22}$$

The solution of the above equation with the appropriate boundary conditions will be

$$f(\eta) = \eta \tag{5.23}$$

Substituting this into the equation (5.20) and integrating twice from $\eta = 0$ to $\eta = \infty$ for the case when $n = 0$ (Isothermal wall case) we get

$$\theta(\eta) = 1 + \theta'(0) \int_0^\eta exp\left(\frac{-3}{4(1+\gamma Pe_d)}\eta^2\right) d\eta \tag{5.24}$$

where

$$\theta'(0) = -\left[\int_0^\infty exp\left(\frac{-3}{4(1+\gamma Pe_d)}\eta^2\right) d\eta\right]^{-1} \tag{5.25}$$

For all the realistic power law variations of wall temperature distribution, the similarity solutions is possible in this limiting case.

For the isothermal wall and uniform free stream flow, the governing equations (5.19)-(5.20) with boundary conditions are solved using Runge-Kutta method with a systematic guessing of $f'(0)$ and $\theta'(0)$. The results obtained are accurate upto the fourth decimal place. The effect of transverse thermal dispersion is studied. For all calculations the value of γ is taken as $1/3$.

In the mixed convection case, for $\xi = 0°$, the problem reduces to the convective heat transfer from a vertical plate, which has been analysed by Lai and Kulacki [37].

For the aiding flow, the velocity and temperature profiles are plotted in Figures (5.2a - 5.2b) and (5.3a - 5.3b) respectively for various values of Re, Pe_d and Ra_d. For fixed values of Re and Pe_d, the increase in the Rayleigh number Ra_d increases the value of the non-dimensional stream wise velocity component.

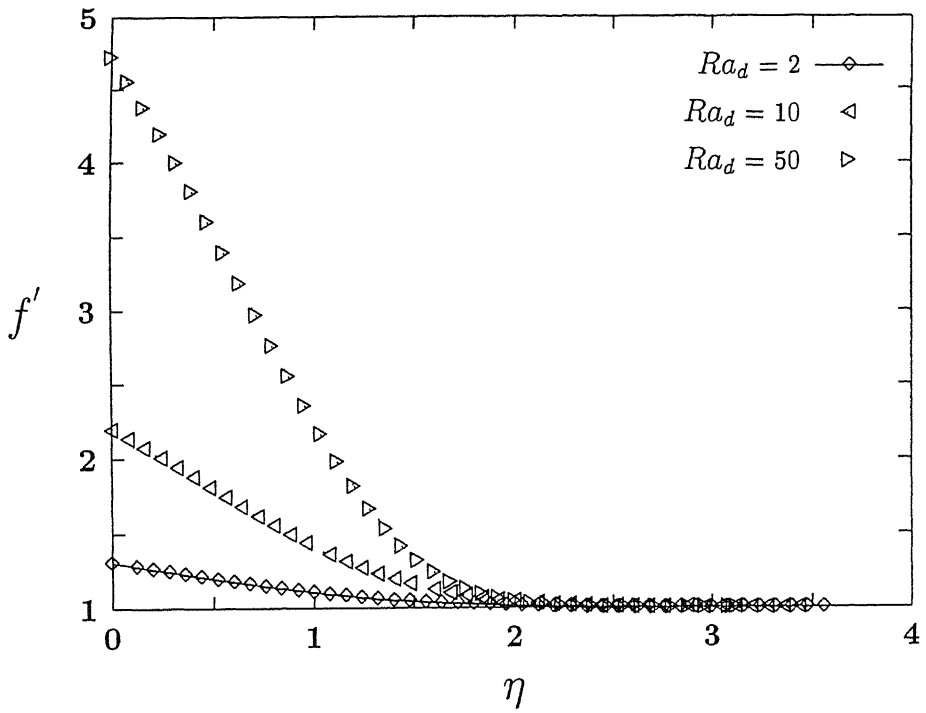

Figure (5.2a): Distribution of stream wise velocity for various Ra_d and fixed $Re = 1.0$ and $Pe_d = 2.0$.

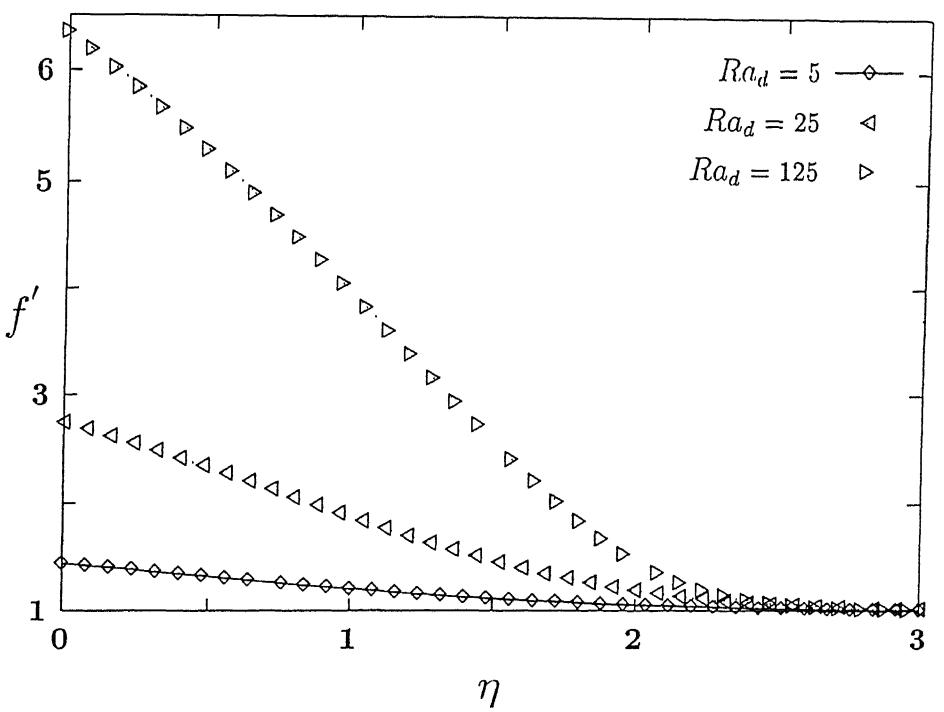

Figure (5.2b): Distribution of stream wise velocity for various Ra_d and fixed $Re = 0.5$ and $Pe = 5.0$

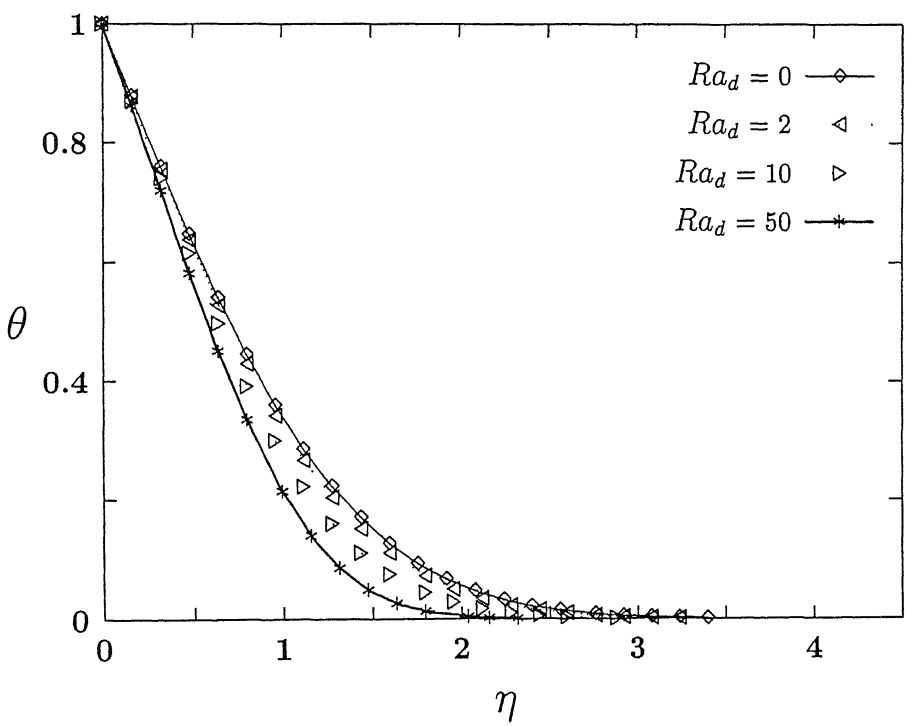

Figure (5.3a): Temperature distribution for various Ra_d for fixed $Re = 1.0$ and $Pe_d = 2.0$.

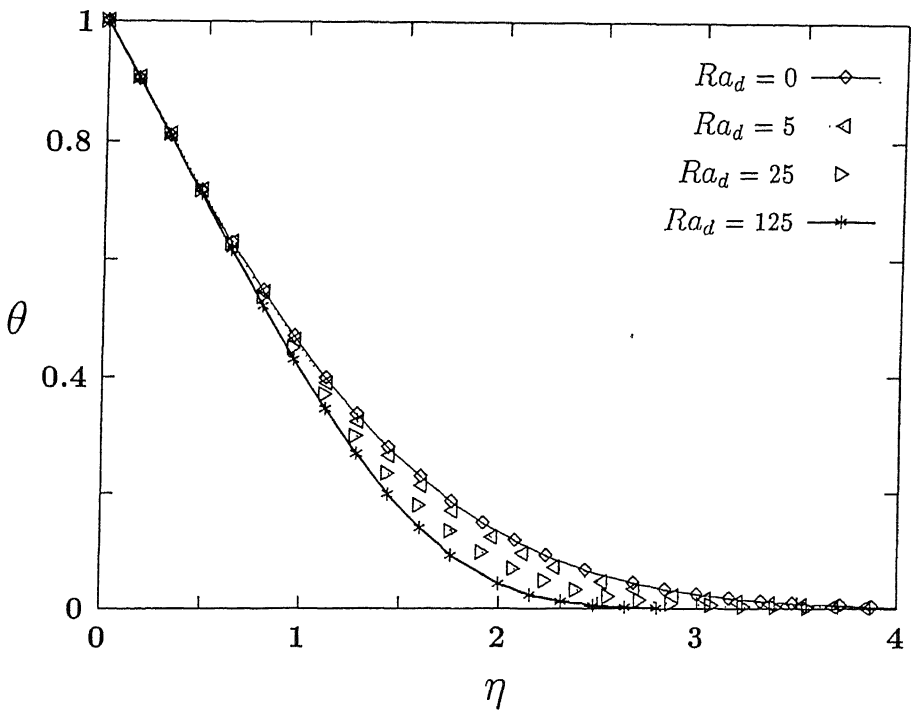

Figure (5.3b): Temperature distribution for various Ra_d for fixed $Re = 0.5$ and $Pe_d = 5.0$

The local heat flux from the surface of the cone into the medium can be obtained from

$$q = -k_e \frac{\partial T}{\partial y}_{|y=0} = -\left([k + k_d] \frac{\partial T}{\partial y} \right)_{|y=0} \tag{5.26}$$

where k_e is the effective thermal conductivity of the porous medium which is the sum of the molecular conductivity k and the dispersion thermal conductivity k_d. The heat flux in terms of Nusselt number is given by

$$\frac{Nu}{Pe_x^{1/2}} = [1 + \gamma\, Pe_d\, f'(0)]\, [-\theta'(0)] \tag{5.27}$$

For the forced convection process $f'(0)$ will be equal to 1, so

$$\frac{Nu}{Pe_x^{1/2}} = [1 + \gamma\, Pe_d]\, [-\theta'(0)] \tag{5.28}$$

Figure (5.4) gives the variation of $\frac{Nu}{Pe_x^{1/2}}$ with n for uniform free stream flow for forced convection process. It is observed that the Nusselt number increases with n. Here $n = 1/2$ is

the constant heat flux case. The effect of thermal dispersion can be studied by varying the value of Pe_d and fixing Re, Ra_d and γ. For fixed Re, with the increase in the value of Pe_d, the heat transfer into the medium increases tremendously.

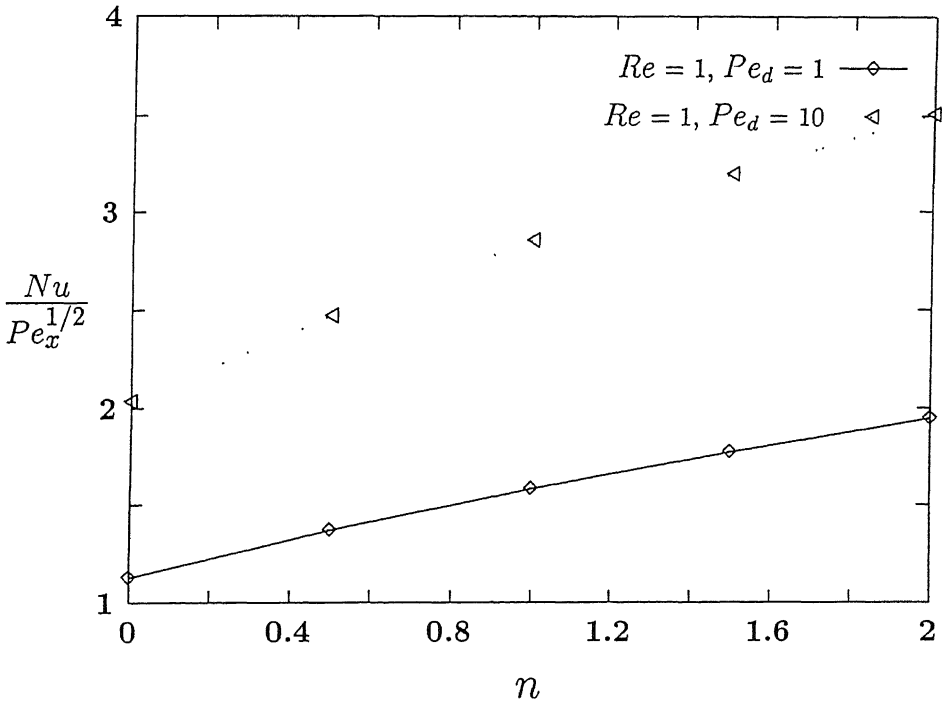

Figure (5.4): Variation of $\frac{Nu}{Pe_x^{1/2}}$ with n for various Pe_d and fixed Re in the forced convection case.

In Figures (5.5a) and (5.5b), the Nusselt number $\frac{Nu}{Pe_x^{1/2}}$ obtained from equation (5.26) is plotted against the governing parameter of the mixed convection process along with the forced and free convection asymptotes for fixed $Re = 1$ and varying $Pe_d = 2$ and 5 respectively. In both the cases, equation (5.27) gives the forced convection asymptote. Free convection asymptote is obtained by solving the corresponding free convection problem described by

$$f'' + 2\frac{ReRa_d}{Pe_d} f' f'' = \theta' \tag{5.29}$$

$$\theta'' + \frac{3}{2} f\theta' + \gamma Ra_d (f''\theta' + f'\theta'') = 0 \tag{5.30}$$

with its corresponding boundary conditions

$$\left.\begin{array}{ll} \eta = 0: & f = 0,\ \theta = 1 \\ \eta \to \infty: & f' = 0,\ \theta = 0 \end{array}\right\}. \tag{5.31}$$

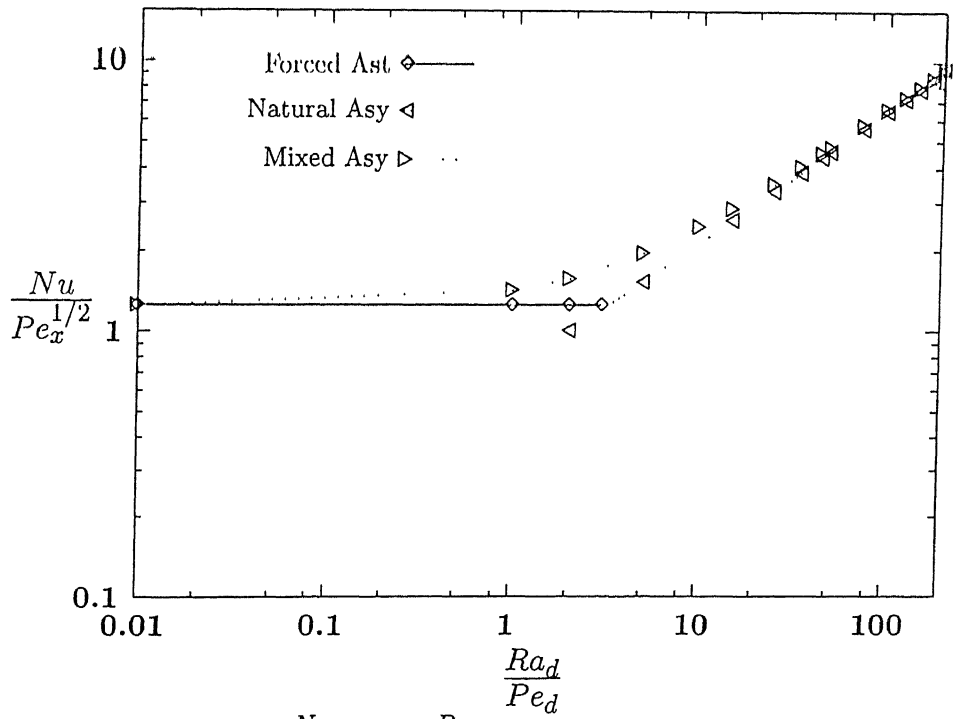

Figure (5.5a): $\frac{Nu}{Pe_x^{1/2}}$ .vs. $\frac{Ra_d}{Pe_d}$ when $Ra_d = 1.0$, $Pe_d = 2.0$.

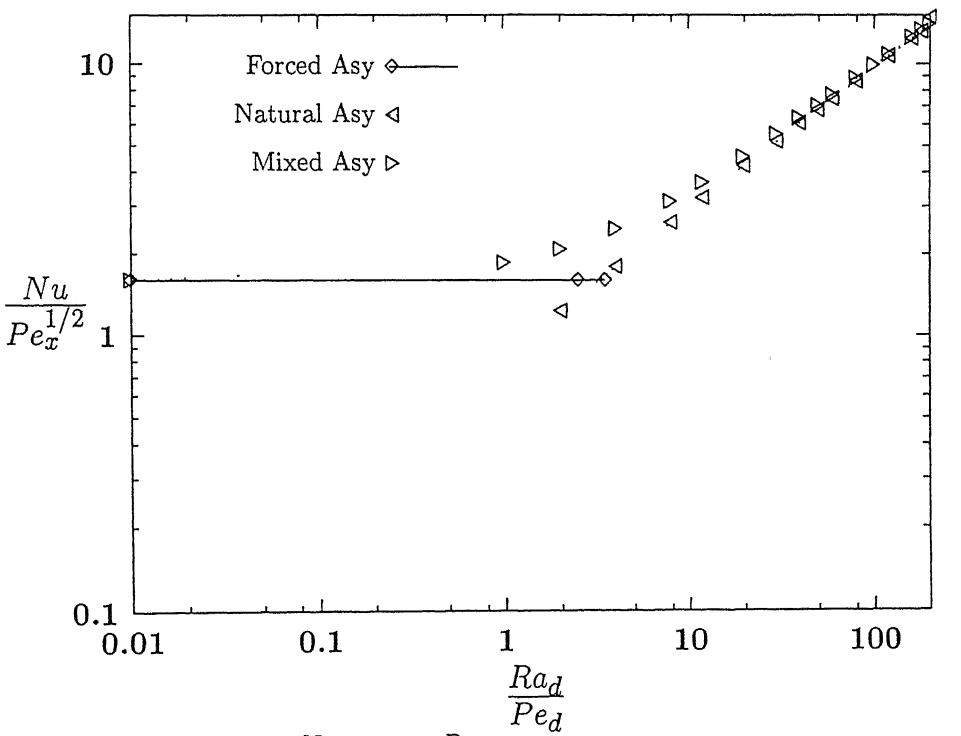

Figure (5.5b): $\frac{Nu}{Pe_x^{1/2}}$ .vs. $\frac{Ra_d}{Pe_d}$ when $Ra_d = 1.0$, $Pe_d = 5.0$.

The Nusselt number expression for the free convection case is

$$\frac{Nu}{Ra_x^{1/2}} = [1 + \gamma\, Ra_d\, f'(0)]\,[-\theta'(0)] \tag{5.32}$$

and rewriting this interms of the mixed convection expression, we get

$$\frac{Nu}{Pe_x^{1/2}} = \frac{Nu}{Ra_x^{1/2}} \left(\frac{Ra_d}{Pe_d}\right)^{1/2}. \tag{5.33}$$

Applying the 5% deviation criteria given in [34], for the local heat transfer rate for the aiding flow revealed that the transverse thermal dispersion effect increases the range of mixed convection flow. For $Re = 1$ with $Pe_d = 2$, the range of $\frac{Ra_d}{Pe_d}$ is subdivided into

$$0 < \frac{Ra_d}{Pe_d} < 0.34 \;\; (forced) \tag{5.34}$$

$$0.34 < \frac{Ra_d}{Pe_d} < 31.5 \;\; (mixed) \tag{5.35}$$

$$31.5 < \frac{Ra_d}{Pe_d} \;\; (natural) \tag{5.36}$$

and for $Re = 1$ with $Pe_d = 5$, the ranges for the pure and mixed convection flows become

$$0 < \frac{Ra_d}{Pe_d} < 0.295 \;\; (forced) \tag{5.37}$$

$$0.295 < \frac{Ra_d}{Pe_d} < 38.5 \;\; (mixed) \tag{5.38}$$

$$38.5 < \frac{Ra_d}{Pe_d} \;\; (natural) \tag{5.39}$$

In the case of opposing flow, flow separation is observed. The velocity and temperature distributions are plotted in Figures (5.6a)-(5.6b). Nusselt number results for the opposing flow are plotted in Figure (5.7).

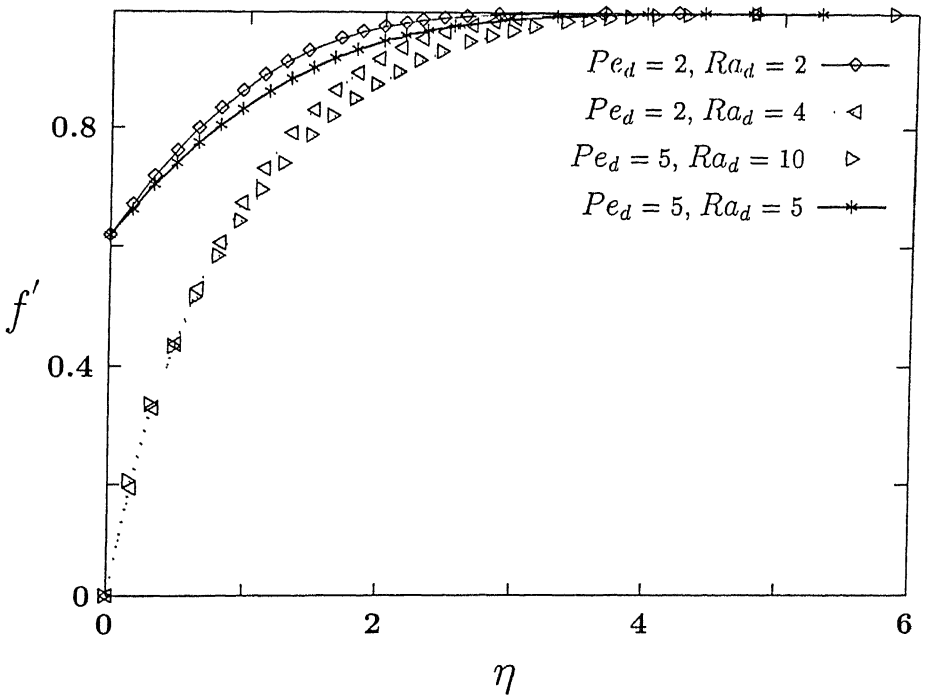

Figure (5.6a): Velocity distribution in the opposing flow when $Re = 1.0$.

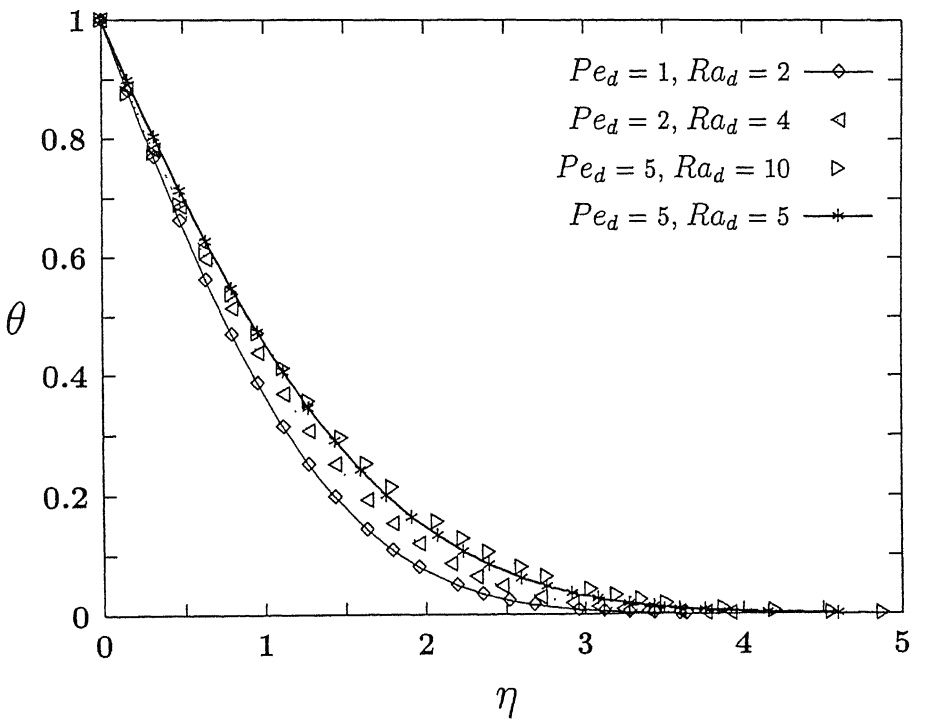

Figure (5.6b): Temperature distribution in the opposing flow when $Re = 1.0$.

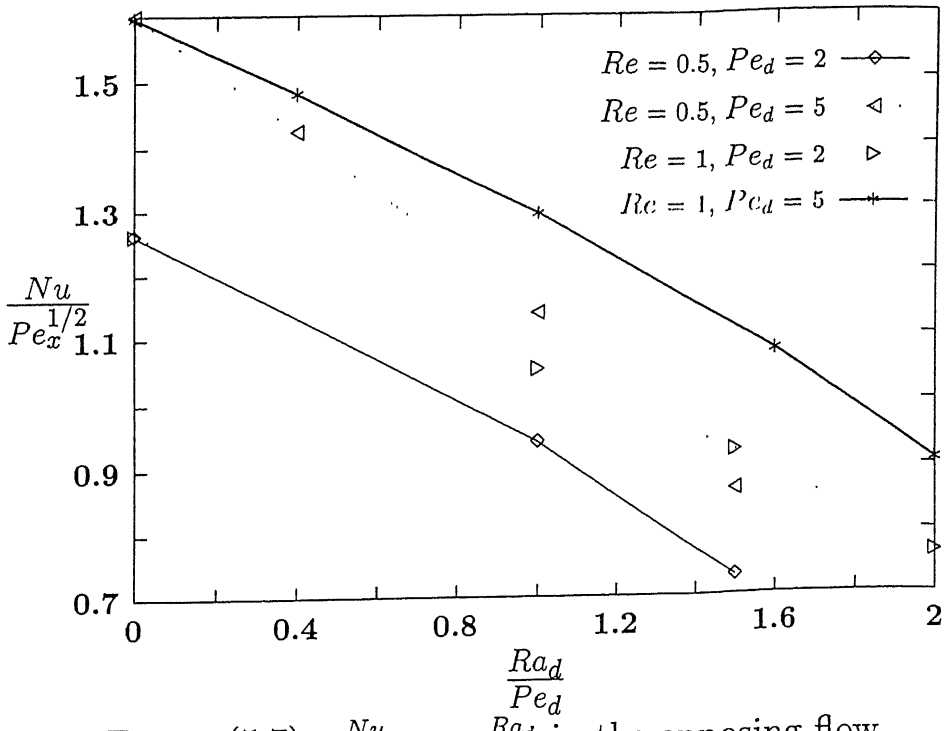

Figure (5.7): $\frac{Nu}{Pe_x^{1/2}}$ .vs. $\frac{Ra_d}{Pe_d}$ in the opposing flow.

The 5% deviation criteria for opposing flows obeys the forced convection ranges in both the cases and the mixed convection ranges will be

$$0.34 < \frac{Ra_d}{Pe_d} \quad (Re = 1, Pe_d = 2). \tag{5.40}$$

$$0.295 < \frac{Ra_d}{Pe_d} \quad (Re = 1, Pe_d = 5). \tag{5.41}$$

Chapter 6

Effect Of Surface Undulations On Natural Convection In A Porous Square Cavity

6.1 Introduction

Study of natural convection in porous enclosures is of great importance in several scientific and engineering applications such as nuclear waste management, transpiration cooling, building thermal insulators, geothermal power plants etc. Two of its interesting configurations are the natural convection in a layer with vertical sides at different temperatures and natural convection in a porous layer heated from below (Horton-Rogers-Lapwood problem). Various flow models (such as Darcy, Forchheimer and Brinkman models) are used to describe the flow and the convective heat transfer in the enclosure. A lot of theoretical and experimental investigations are carried out to understand the natural convection from smooth surfaces in a porous enclosure. Nield and Bejan [7] gives a beautiful review of all these works.

However, in practice one would encounter roughened surfaces in several heat transfer devices such as flat plate solar collectors, flat plate condensers in refrigerators, etc. Large scale non-uniformities are encountered in cavity wall insulating systems and in grain storage containers. So it is essential to understand the effect of surface undulations on natural convection in a porous square cavity. Recently in the context of pure continuum fluid, theoretical and

experimental investigations are carried out to study the effects of surface undulations on free convection. Anderson and Bohn [69] described the two ways by which the natural convection heat transfer coefficient may be altered by introducing surface roughness. Shakerin et al [72] studied the effect of single and repeated rectangular roughness elements on the flow and heat transfer process in an enclosure in the immediate vicinity of the roughness elements. Their observation was that the total heat transfer rate is nearly same as in the smooth wall case inspite of the increased surface area. Many theoretical and experimental studies on this new technique provided us with conflicting results for heat transfer augmentation. Bhavnani and Bergles [76] gave a detailed introduction to all these conflicting results.

Besides these studies, there has been a considerable attention towards the study of spatially periodic boundary imperfections with the boundary layer assumptions. Yao [50] studied the natural convection along an isothermal vertical wavy surface under the boundary layer assumptions. The complex wavy geometry has been transformed into a flat wall and the resulting boundary layer equations are solved using a finite difference scheme. Their results show that the Nusselt number results for the sinusoidal wavy wall is smaller than that of the corresponding flat plate and decreases with the increase in the amplitude of the wavy wall. Similar results were observed for the case of constant wall heat flux from the sinusoidal wavy surface also by Moulic and Yao [75].

The study of the effect of surface roughness or the spatially periodic boundary imperfections on the convective heat transfer in porous medium is not seen in the literature expect for a couple of papers by Riley [33] and Rees and Pop [26]-[27]. Thermal convection in a vertical porous slot was considered by Riley [33]. The vertical walls are assumed to have spatially periodic imperfections (cosine functions are used) and are maintained at different constant temperatures. The analysis is confined to the core flow which is assumed to lie in the conduction regime (i.e., $Ra_l = O(1)$, where Ra_l is the Rayleigh number based upon the length of the vertical slot). It was concluded that heat transfer could be enhanced significantly by considering varicose imperfections rather than sinuous imperfections. Very recently Rees and Pop [26] studied the free convection heat transfer along a vertical isothermal sinusoidal wavy surface under boundary layer assumptions. The governing equations and the associated boundary conditions are transformed to those of a vertical smooth isothermal surface and the resulting ordinary differential equations are solved using a numerical method. Their results show that the local Nusselt number is less than or equal to the corresponding plane heated surface and the total heat transfer rate is unchanged by the presence of surface waves.

The present study initiates the heat transfer from the isothermal vertical sinusoidal wavy wall in the porous square enclosure. The other vertical wall is kept at the ambient temperature. The top and bottom walls are adiabatic. Darcy's law is assumed to be valid in the enclosure. Galerkin finite element method is used. The governing parameters are the Rayleigh number based on the vertical dimension of the cavity, the amplitude, phase of the wave and the number of waves considered in the vertical dimension. It has been observed that these four parameters have crucial effect on the convective heat transfer. The results indicate that the Rayleigh number increases the global heat flux. The amplitude of the wave causes buoyancy loss and the increase in the number of waves considered per vertical dimension of the cavity further increases this loss. Hence the increase in the amplitude and number of waves decreases the global heat flux. The phase of the wave has got a significant effect on the heat transfer results.

6.2 Governing Equations

Consider the Darcian fluid saturated porous square cavity as shown in the Figure (6.1). The left vertical wall of the cavity is isothermal and the remaining three boundaries are plane walls. Four walls are impermeable. The right vertical wall is maintained at the ambient temperature and the horizontal walls are adiabatic. The conservation mass, momentum and energy equations for steady flow and free convective heat transfer in an homogeneous and isotropic porous medium are

$$\frac{\partial u}{\partial x} + \frac{\partial v}{\partial y} = 0 \tag{6.1}$$

$$u = -\frac{K}{\mu}\left(\frac{\partial p}{\partial x}\right) \tag{6.2}$$

$$v = -\frac{K}{\mu}\left(\frac{\partial p}{\partial y} + \rho g\right) \tag{6.3}$$

$$u\frac{\partial T}{\partial x} + v\frac{\partial T}{\partial y} = \alpha\left(\frac{\partial^2 T}{\partial x^2} + \frac{\partial^2 T}{\partial y^2}\right) \tag{6.4}$$

and the equation of state is

$$\rho = \rho_a\left[1 - \beta(T - T_a)\right] \tag{6.5}$$

The corresponding boundary conditions are:

$$\left.\begin{array}{rl} \psi = 0: & T = T_w(const)\ on\ x = a\ sin(\frac{N\pi y}{L} - \phi) \\ \psi = 0: & T = T_a(const)\ on\ x = L \\ \psi = 0: & \frac{\partial T}{\partial y} = 0\ on\ y = 0\ and\ y = L \end{array}\right\} \tag{6.6}$$

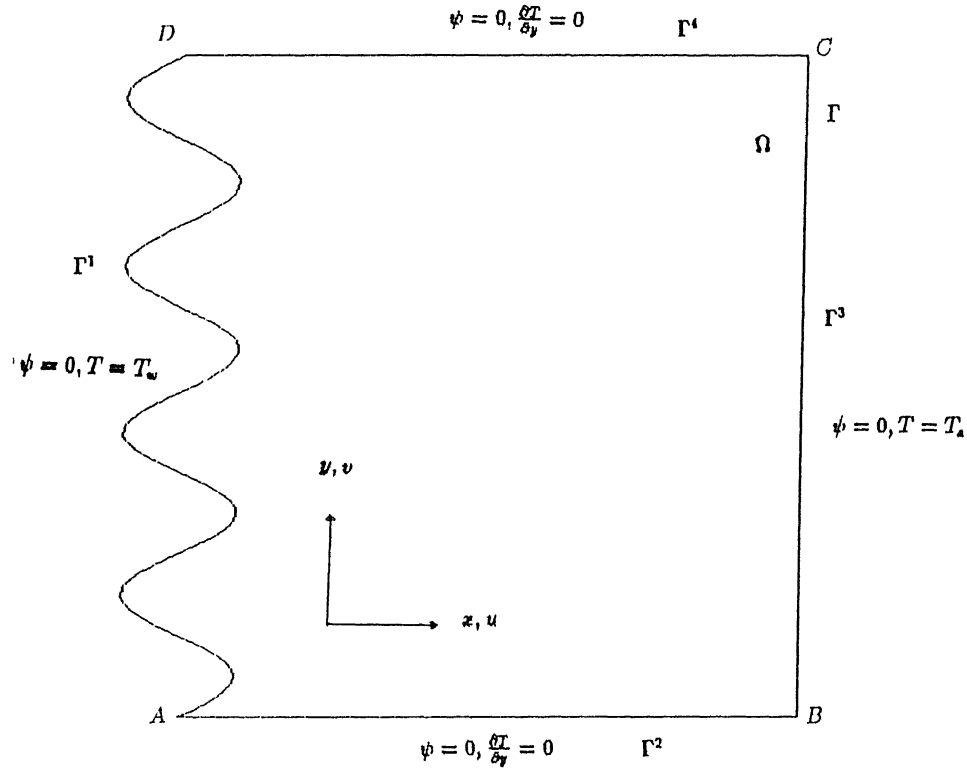

Figure (6.1): Porous square enclosure with uniformly heated vertical wavy wall.

Here x and y are the Cartesian coordinates, u and v are the velocity components in x and y directions, T is the temperature, ρ is the density, p is the pressure, β is the coefficient of thermal expansion, μ is the viscosity of the fluid, K is permeability of the medium, g is the acceleration due to gravity, α is the effective thermal diffusivity.

Eliminating the pressure from the momentum equation and expressing the resulting momentum and energy equations in terms of the stream function and temperature form by making use of the equations $u = -\frac{\partial \psi}{\partial y}$ and $v = \frac{\partial \psi}{\partial x}$, we get

$$\frac{\partial^2 \psi}{\partial x^2} + \frac{\partial^2 \psi}{\partial y^2} = \left(\frac{Kg\beta}{\nu}\right)\frac{\partial T}{\partial x} \tag{6.7}$$

$$\frac{\partial \psi}{\partial x}\frac{\partial T}{\partial y} - \frac{\partial \psi}{\partial y}\frac{\partial T}{\partial x} = \alpha\left[\frac{\partial^2 T}{\partial x^2} + \frac{\partial^2 T}{\partial y^2}\right] \tag{6.8}$$

Now consider the following non-dimensional variables

$$X = \frac{x}{L}, Y = \frac{y}{L}, \Psi = \frac{\psi}{\alpha} \text{ and } \theta = \frac{T - T_a}{T_w - T_a},$$

the above governing equations in terms of these non-dimensional variables will be

$$\frac{\partial^2 \Psi}{\partial X^2} + \frac{\partial^2 \Psi}{\partial Y^2} = Ra \frac{\partial \theta}{\partial X} \tag{6.9}$$

$$\frac{\partial \Psi}{\partial X}\frac{\partial \theta}{\partial Y} - \frac{\partial \Psi}{\partial Y}\frac{\partial \theta}{\partial X} = \frac{\partial^2 \theta}{\partial X^2} + \frac{\partial^2 \theta}{\partial Y^2} \tag{6.10}$$

and the boundary conditions in the non-dimensional variables will be

$$\left.\begin{array}{rl} \Psi = 0: & \theta = 1 \text{ on } X = a\, sin(N\pi Y - \phi) \\ \Psi = 0: & \theta = 0 \text{ on } X = L \\ \Psi = 0: & \frac{\partial \theta}{\partial Y} = 0 \text{ on } Y = 0 \text{ and } Y = L \end{array}\right\} \tag{6.11}$$

The resulting partial differential equations (6.9) - (6.10) along with the hydrodynamic and thermal boundary conditions (6.11) are solved numerically by using Bubnov-Galerkin weighted residual finite element technique.

6.3 Numerical Analysis

The crucial parameters which govern and influence the flow and heat transfer are the modified Rayleigh number Ra based on the vertical dimension of the cavity, the amplitude a and the phase ϕ of the wave (geometrical parameters due to the shape of the wall) and the number of waves N considered in the vertical dimension of the cavity. It has been observed in the continuum fluid boundary layer flow over vertical wavy walls that the crucial and the flow driving buoyancy force is being reduced because of the wavy nature of the wall which inturn reduces the heat transfer into the system. To understand this basic problem in porous enclosure, we analysed the effect of amplitude and Rayleigh number by fixing the phase at 0^o and considering $N = 1$. Later, study is focussed to multiwave case with varying amplitude, phase and Rayleigh number.

Possibility of obtaining an analytical solution for these coupled partial differential equations without any approximations, over the non-planar geometry (even over the planar geometry) is ruled out, the standard finite difference methods with special techniques might yield a good approximate solution for the problem after transforming the non-planar geometry to

a planar one. But straight away, this problem can be attacked using finite element method without any need for transforming the domain.

The domain is discretised into finite number of elements which fit the present geometry considered. Linear rectangular elements can not describe the wavy nature of the wall. The wavy enclosure has been divided into a finite number of eight noded quadratic serendipity elements. Consider the following discretization of the domain and the boundary,

$$\Omega = \cup_e \Omega^e$$

$$\Gamma = \cup_e \Gamma^e$$

So, over a typical element, the approximation to the unknown functions will be

$$\Psi = \sum_{i=1}^{i=8} \Psi_i^e N_i^e$$

$$\theta = \sum_{i=1}^{i=8} \theta_i^e N_i^e$$

where, the shape functions of the typical element are given as (written in terms of the local coordinates)

$$N_i^e(\xi,\eta) = \left\{ \begin{array}{c} (1-\xi)(1-\eta)(-\xi-\eta-1) \\ (1+\xi)(1-\eta)(\xi-\eta-1) \\ (1+\xi)(1+\eta)(\xi+\eta-1) \\ (1-\xi)(1+\eta)(-\xi+\eta-1) \\ 2\,(1-\xi^2)(1-\eta) \\ 2\,(1+\xi)(1-\eta^2) \\ 2\,(1-\xi^2)(1+\eta) \\ 2\,(1-\xi)(1+\eta^2) \end{array} \right\}. \tag{6.12}$$

The serendipity elements have been proven to be very effective in most of the heat transfer applications.

Now the unknown nodal parameters $[\Psi_i^e \;\; \theta_i^e]$, $i = 1$ to 8 are to be determined such that these unknown parameters satisfy the governing equations and specified boundary conditions. This is achieved in a weighted integral sense over a typical elemental volume. The weighted residual weak form of momentum equation and energy equations are obtained as follows: Take all non-zero expressions into one side of the equality and multiply the resulting equations

with a weight functions W_l and integrate the equation over the typical element.

$$\int_{\Omega^e} \left(\nabla^2 \Psi - Ra \frac{\partial \theta}{\partial X} \right) W_l d\Omega^e = 0 \tag{6.13}$$

$$\int_{\Omega^e} \left[\nabla^2 \theta - \left(\frac{\partial \Psi}{\partial X} \frac{\partial \theta}{\partial Y} - \frac{\partial \Psi}{\partial Y} \frac{\partial \theta}{\partial X} \right) \right] W_l d\Omega^e = 0 \tag{6.14}$$

Integrating the second order partial differential terms to reduce the order of differentiation, we get

$$\int_{\Omega^e} \left(\frac{\partial W_l}{\partial X} \frac{\partial \Psi}{\partial X} + \frac{\partial W_l}{\partial Y} \frac{\partial \Psi}{\partial Y} \right) d\Omega^e + Ra \int_{\Omega} W_l \frac{\partial \theta}{\partial X} d\Omega^e = 0 \tag{6.15}$$

$$\int_{\Gamma^{1+3}} W_l \frac{\partial \theta}{\partial n} d\Gamma^{1+3} - \int_{\Omega}^{e} \left(\frac{\partial W_l}{\partial X} \frac{\partial \theta}{\partial X} + \frac{\partial W_l}{\partial Y} \frac{\partial \theta}{\partial Y} \right) d\Omega^e + \int_{\Omega}^{e} \left(\frac{\partial \Psi}{\partial Y} \frac{\partial \theta}{\partial X} - \frac{\partial \Psi}{\partial X} \frac{\partial \theta}{\partial Y} \right) W_l d\Omega^e = 0 \tag{6.16}$$

Introducing the unknown approximations into the above pair of equations, we get elemental momentum equation and energy equations as

$$\left\{ \sum_{k=1}^{k=8} \int_{\Omega^e} \left(\frac{\partial N_l^e}{\partial X} \frac{\partial N_k^e}{\partial X} + \frac{\partial N_l^e}{\partial Y} \frac{\partial N_k^e}{\partial Y} \right) d\Omega^e \right\} \Psi_k^e + \left\{ Ra \sum_{h=1}^{h=8} \int_{\Omega^e} N_l^e \frac{\partial N_h^e}{\partial X} d\Omega^e \right\} \theta_i^e = 0 \tag{6.17}$$

$$\left. \begin{array}{c} \left\{ -\sum_{k=1}^{k=8} \int_{\Omega^e} \left(\frac{\partial N_k^e}{\partial X} \frac{\partial N_k^e}{\partial X} + \frac{\partial N_k^e}{\partial Y} \frac{\partial N_k^e}{\partial Y} \right) d\Omega^e \right\} \theta_i + \\ \sum_{k=1}^{k=8} \left[\sum_{i=1}^{i=8} \left\{ \int_{\Omega^e} \left(\frac{\partial N_k^e}{\partial Y} \frac{\partial N_i^e}{\partial X} N_l^e - \frac{\partial N_k^e}{\partial X} \frac{\partial N_i^e}{\partial Y} N_l^e \right) d\Omega^e \right\} \theta i^e \right] \Psi_k^e = \int_{\Gamma^{1+3}} N_l^e \frac{\partial \theta}{\partial n} d\Gamma^{1+3} \end{array} \right\} \tag{6.18}$$

The above two equations can be put into a Matrix equation as :

$$\mathrm{M^e} \;\; g^e \;\; = \;\; f^e \tag{6.19}$$

where

$$M^e = \begin{bmatrix} A_{lk}^e & B_{lk}^e \\ \\ C_{lki}^e & -A_{lk}^e \end{bmatrix}$$

and g^e is the column vector of unknown nodal parameters

$$g^e = \left[\Psi_k^e \;\; \theta_k^e \right]^T$$

and f^e is the known vector which is given by

$$f^e = \left[r_k^{e^1} \;\; r_k^{e^2} \right]^T .$$

The elements in the above matrix are obtained from the following expressions,

$$A^e_{lk} = \int_{\Omega^e} \left(\frac{\partial N^e_l}{\partial X} \frac{\partial N^e_k}{\partial X} + \frac{\partial N^e_l}{\partial Y} \frac{\partial N^e_k}{\partial Y} \right) d\Omega^e \tag{6.20}$$

$$B^e_{lk} = Ra \int_{\Omega^e} W_l \frac{\partial N^e_k}{\partial X} d\Omega^e \tag{6.21}$$

$$C^e_{lki} = \int_{\Omega^e} \left(\frac{\partial N^e_k}{\partial Y} \frac{\partial N^e_i}{\partial X} N^e_l - \frac{\partial N^e_k}{\partial X} \frac{\partial N^e_i}{\partial Y} N^e_l \right) d\Omega^e \tag{6.22}$$

$$r^{e^1}_l = 0 \tag{6.23}$$

$$r^{e^2}_l = - \int_{\Gamma}^{1+3} N^e_l \frac{\partial \theta}{\partial n} d\Gamma^{1+3}. \tag{6.24}$$

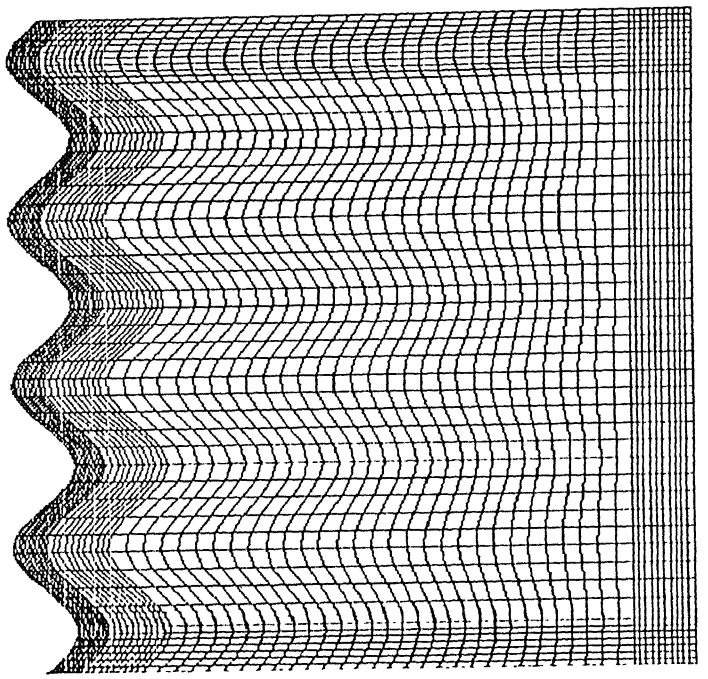

Figure (6.2): Five level graded finite element mesh

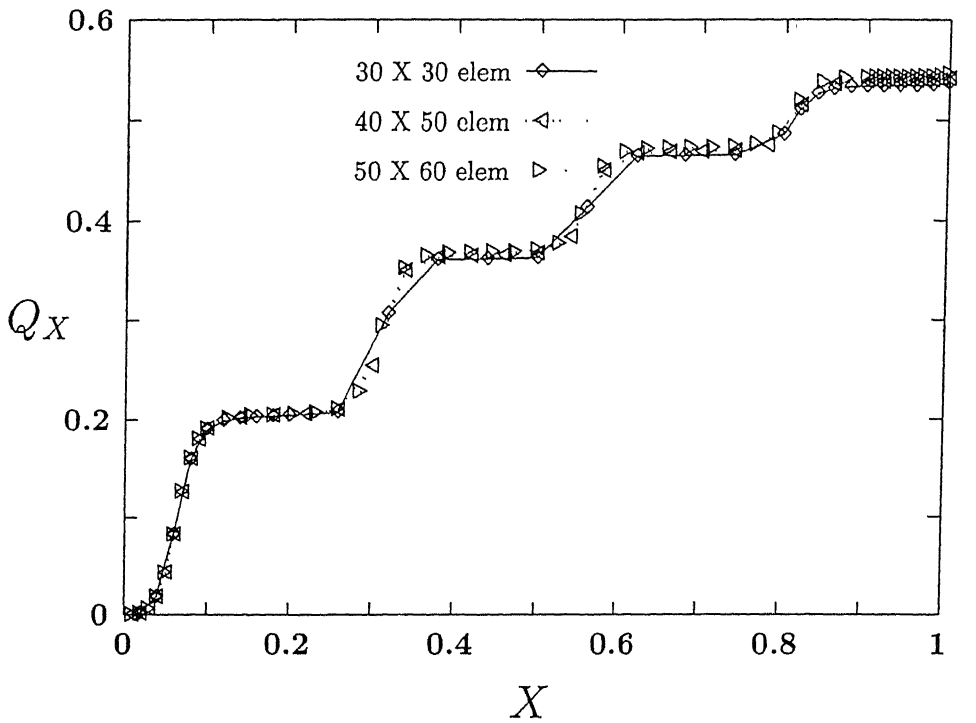

Figure (6.3): Mesh selection using cumulative global heat flux comparison.

Numerical simulations have been carried out on a 60 X 50 finite element graded mesh, with five levels of grading as shown in the Figure (6.2). Eight noded isoparametric quadratic serendipity elements have been used in domain discretization to precisely accommodate the geometrical non-linearities due to the wavy nature of the wall. Simulations have been carried out for the values of the Ra in the convection regime of the flow. The results have been obtained to an error tolerance $\tau = 5X10^{-4}$, where τ is defined as $|\Psi_p^e - \Psi_c^e| \leq \tau$ and $|\theta_p^e - \theta_c^e| \leq \tau$, c and p are the current and previous iteration values respectively.

The local heat flux from the wall to the medium is given by

$$q_X = -k \frac{\partial \theta}{\partial n_{|X = a\ sin(N\pi Y - \phi)}} \tag{6.25}$$

and the cumulative global heat flux has been computed from the formula

$$Q_X = \int_0^X -k \frac{\partial \theta}{\partial n_{|X\ =\ a\ sin(\pi\ Y\ -\ \phi)}} \frac{ds(\xi)}{d\xi} d\xi, \tag{6.26}$$

where n is the outward drawn unit normal vector to the wavy surface and $s(\xi)$ is the arc-length along the surface. The global heat flux can be obtained from taking the upper limit

in the above integral as L (the height of the porous cavity). The cumulative global heat flux results obtained over 3 different meshes are plotted in the Figure (6.3), and from this comparison test, it has been felt that the 50 X 60 graded mesh will be the right choice.

6.4 Results and Discussion

The computational results are presented in the form of streamlines, isotherms and global heat flux plots in order to study the fluid flow and heat transfer phenomenon in the porous square cavity. To begin with, the single sine wave with zero phase has been considered. The heat transfer from wavy wall of varying amplitude and varying Rayleigh number is analysed in this case. In Figures (6.4) and (6.5) streamlines and isotherms for the single wave case are presented.

For a fixed amplitude (a = 0.1), Rayleigh numbers in the range 10 to 50 have been considered for the study. The streamlines presented in the Figures (6.4) depict the fact that the flow becomes intense with increasing values of Ra. Supporting the flow phenomenon depicted by the streamlines, the increase in the range of the variation of the slopes of the isotherms show that increasing Ra favours the convection process. From these Figures it is clearly seen that the wavy nature in both the streamlines and isotherms adjacent to the heated wavy wall and the percolation of this feature deep into medium becomes vivid with the increasing values of the amplitude of the wavy wall (more clear in the multiple wave case).

For a fixed Rayleigh number $Ra = 20$, small amplitude variations (0.05, 0.1, 0.15) are considered for the study. The streamlines and the isotherms corresponding to this study are presented in Figures (6.5). The monotomity of the range of slopes of these isotherms indicate that the increase in amplitudes do not favour the convection process. These figures also indicate that the velocity gradients are high in the regions adjacent to the crest of the wavy wall. Better insight into the convection process is provided by the global heat flux evaluation. The cumulative global heat flux values for both varying Ra and varying a are given in the Figures (6.6) and (6.7). The end values of each curve in both the figures represent the global heat flux value for the corresponding case. These figures clearly indicate that the increase in the amplitude decreases the global heat flux where as the increase in the value of Ra increases the global heat flux.

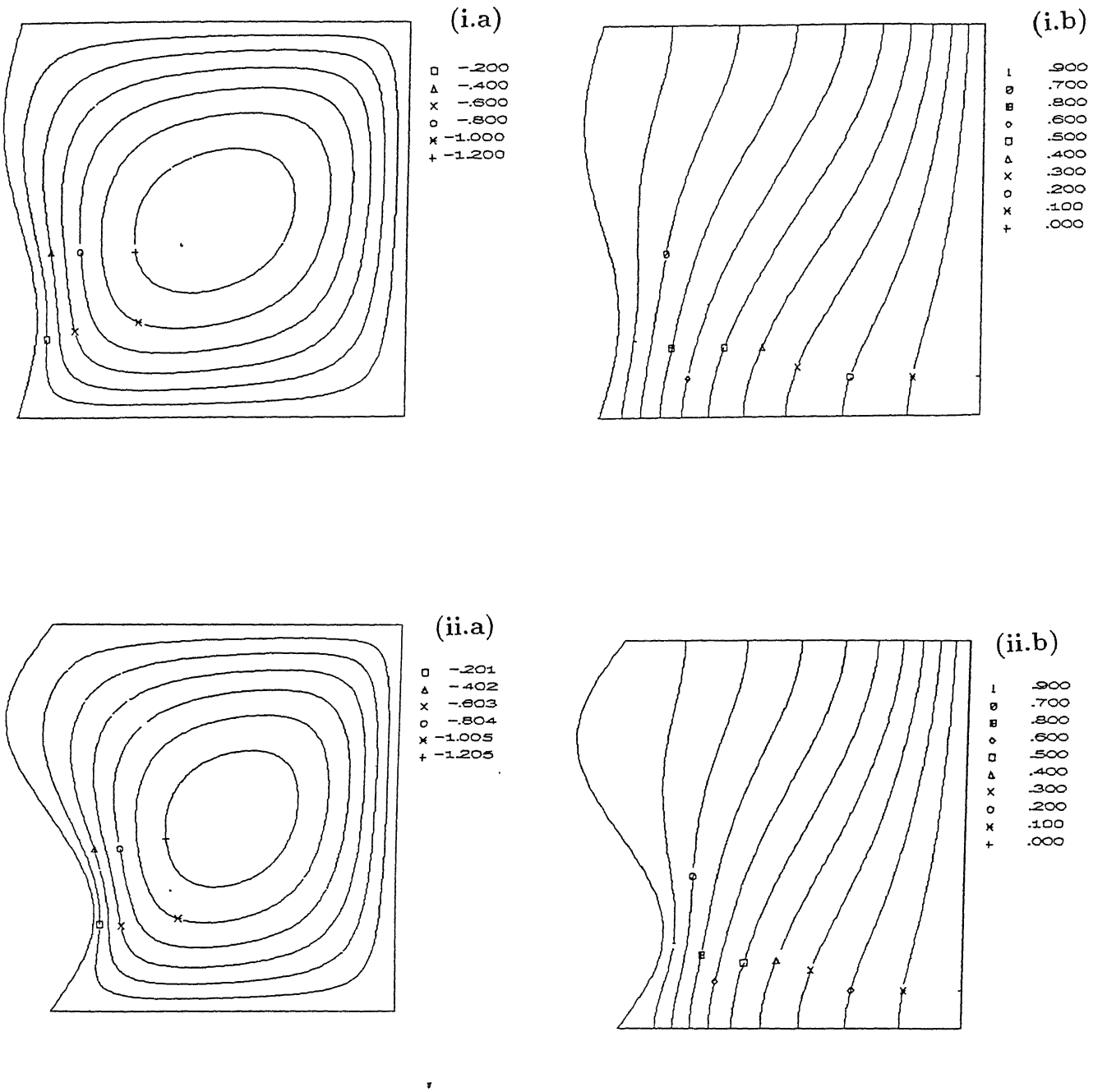

Figure (6.4): (a) Streamlines and (b) Isotherms for single wave case for (i) $Ra = 10$, (ii) $Ra = 50$ with $a = 0.1$ and $\phi = 0°$.

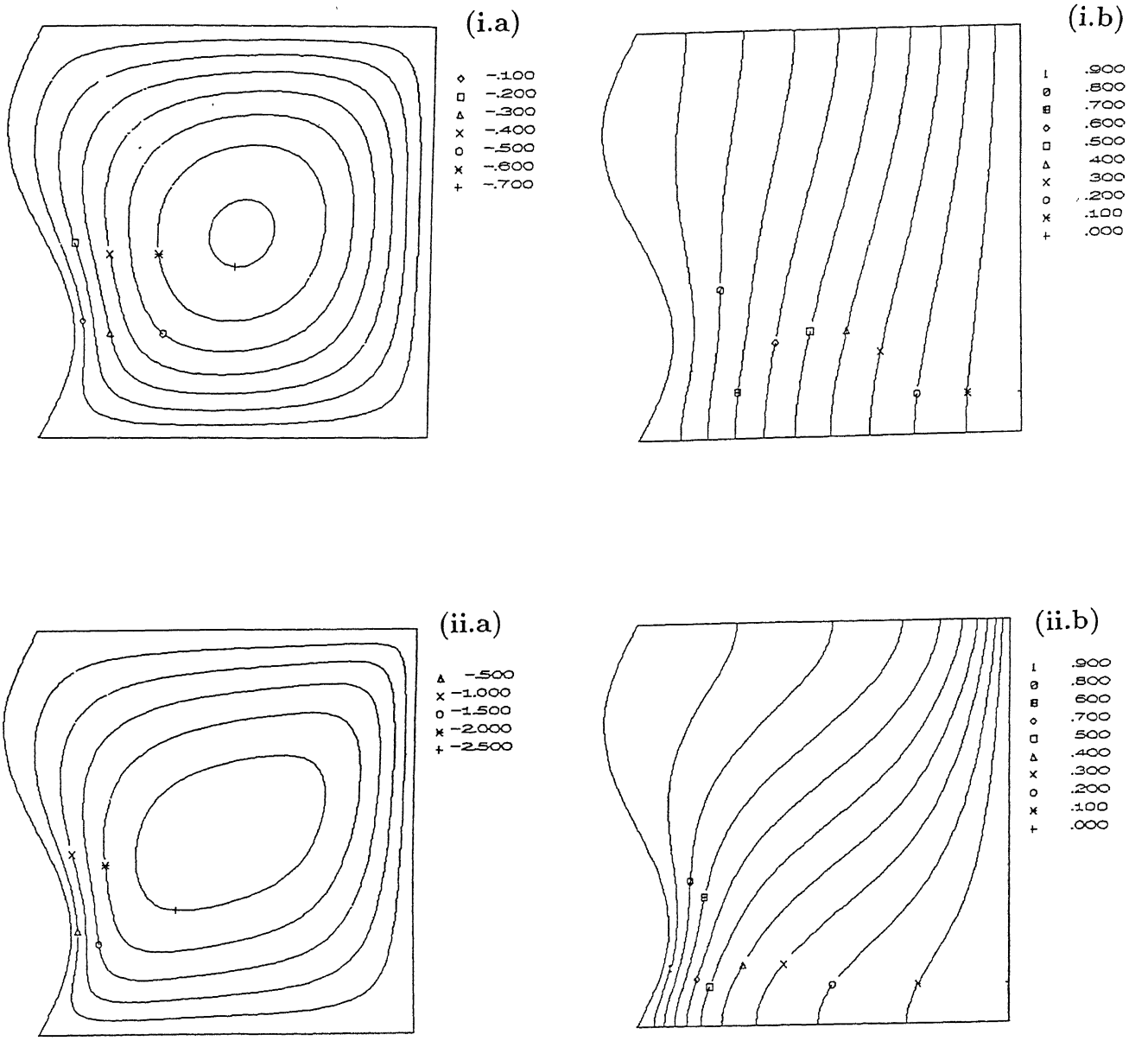

Figure (6.5): (a) Streamlines and (b) Isotherms for single wave case for (i) $a = 0.05$, (ii) $a = 0.15$ with $Ra = 20$ and $\phi = 0^o$.

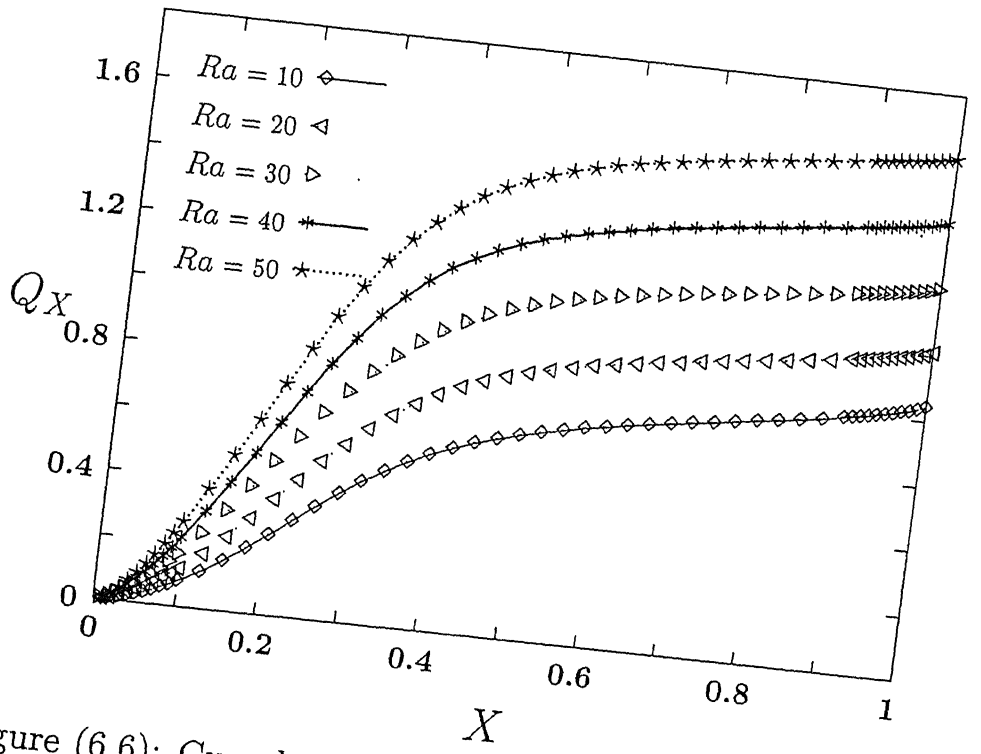

Figure (6.6): Cumulative global heat flux with varyious Ra for single wave case with fixed $a = 0.1$, $\phi = 0^o$.

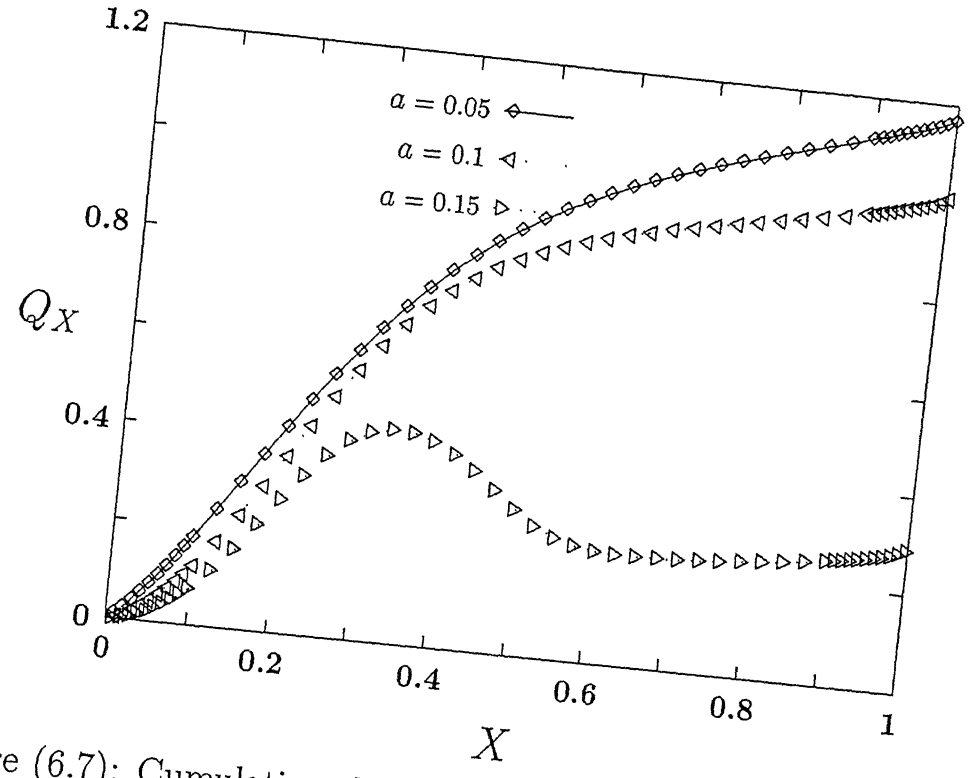

Figure (6.7): Cumulative global heat flux with various amplitudes for single wave with fixed $Ra = 20$, $\phi = 0^o$.

As it has been pointed out by Yao [50], Moulic and Yao [75] and Rees and Pop [26], that the loss in the global heat flux with increasing amplitude can be attributed to the loss in the convection favouring vertical component of the buoyancy force. The vertical component of the buoyancy force is maximum when the heated flat surface is vertical, but in the case of the wavy wall, this buoyancy component is maximum only at the crests of the waves. Consequently, the heat transfer from the vertical wavy wall is less compared to that from a vertical flat plate. This comparison has been done with the multiple number of waves for varying amplitude case, see Figure (6.11)

In the case of multiple waves, the computational simulations have been carried out at varying phases with varying amplitudes and varying Rayleigh numbers. The amplitude is varied from 0.05 to 0.5 fixing $Ra = 50$, $\phi = 0^o$ and $N = 4$. Streamlines and isotherms for this case are presented in Figures (6.8). From these figures it is clear that the wavy nature in both the streamlines and isotherms adjacent to the heated wavy wall, and the percolation of this feature deep into the medium become vivid with increasing values of the amplitude. As in the single wave case, a monotomity in the range of the slopes of isotherms with increasing values of amplitude is observed. The cumulative global heat flux for this varying amplitude case has been plotted in the Figure (6.10). The solid curve which lies above all other curves correspond to the flat plate case. The final value of each curve represent the global heat flux and it can be easily observed that the increase in the amplitude decreases the global heat flux. This decrease is more when compared with that of the single wave case and this highlights the need to probe into the effect of varying N on heat transfer.

For the study of effect of varying Ra (10 - 60), five waves each with amplitude 0.2 at zero phase have been considered. The streamlines and the isotherms are plotted in Figures (6.9). As in the single wave case, the increase in Ra intensifies the flow and favours the convection process. However, the magnitudes of the global heat flux as can be observed from Figure (6.11) being reduced a lot when compared with that of the single wave case Figure (6.6). This also signifies that the number of waves considered per unit length has a tremendous effect on the convective heat transfer in the porous enclosure with the wavy boundary.

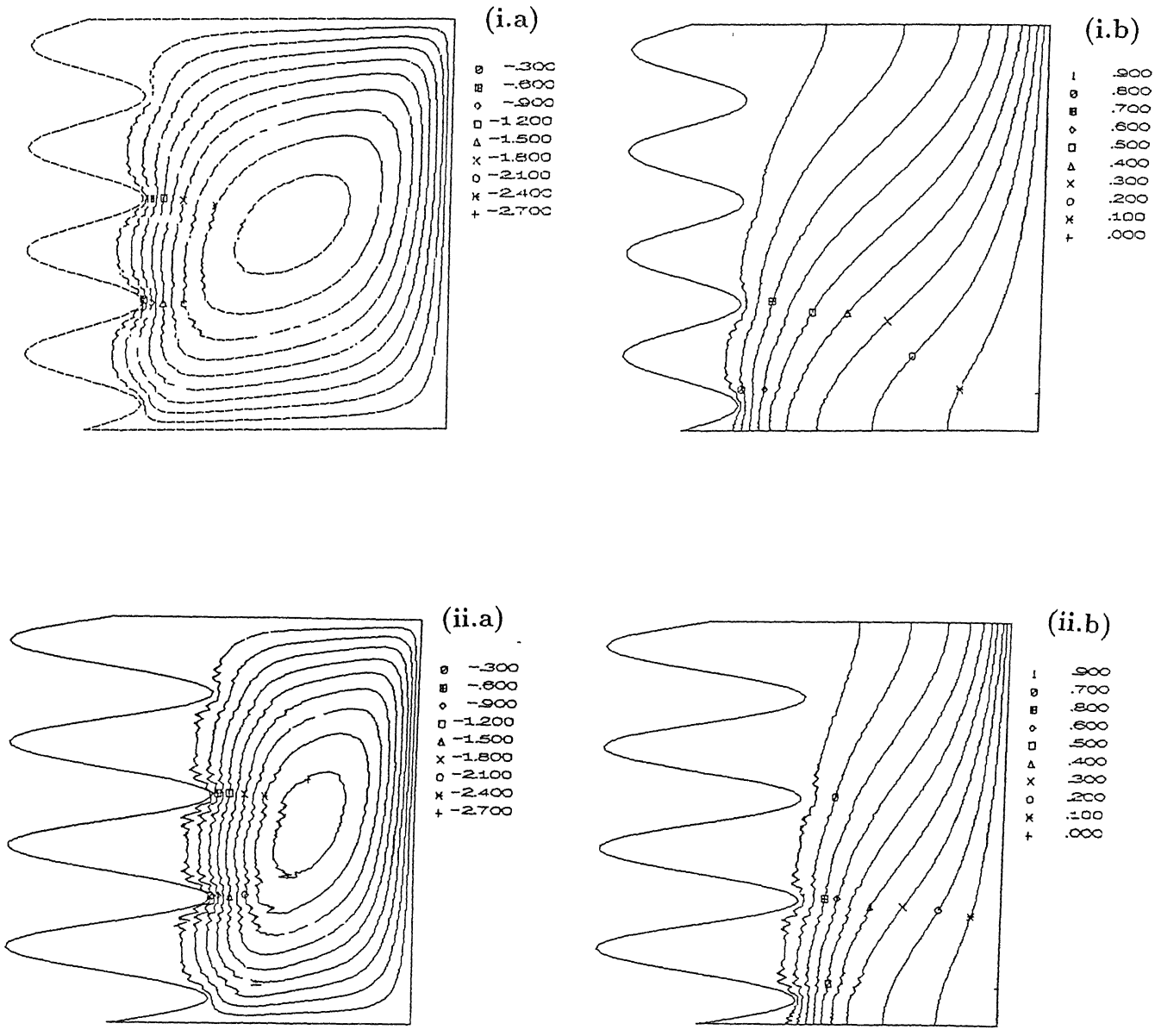

Figure (6.8): (a) Streamlines and (b) Isotherms for multiple waves case for (i) $a = 0.2$, (ii) $a = 0.5$ with $Ra = 50$, $\phi = 0^{\circ}$ and $N = 4$.

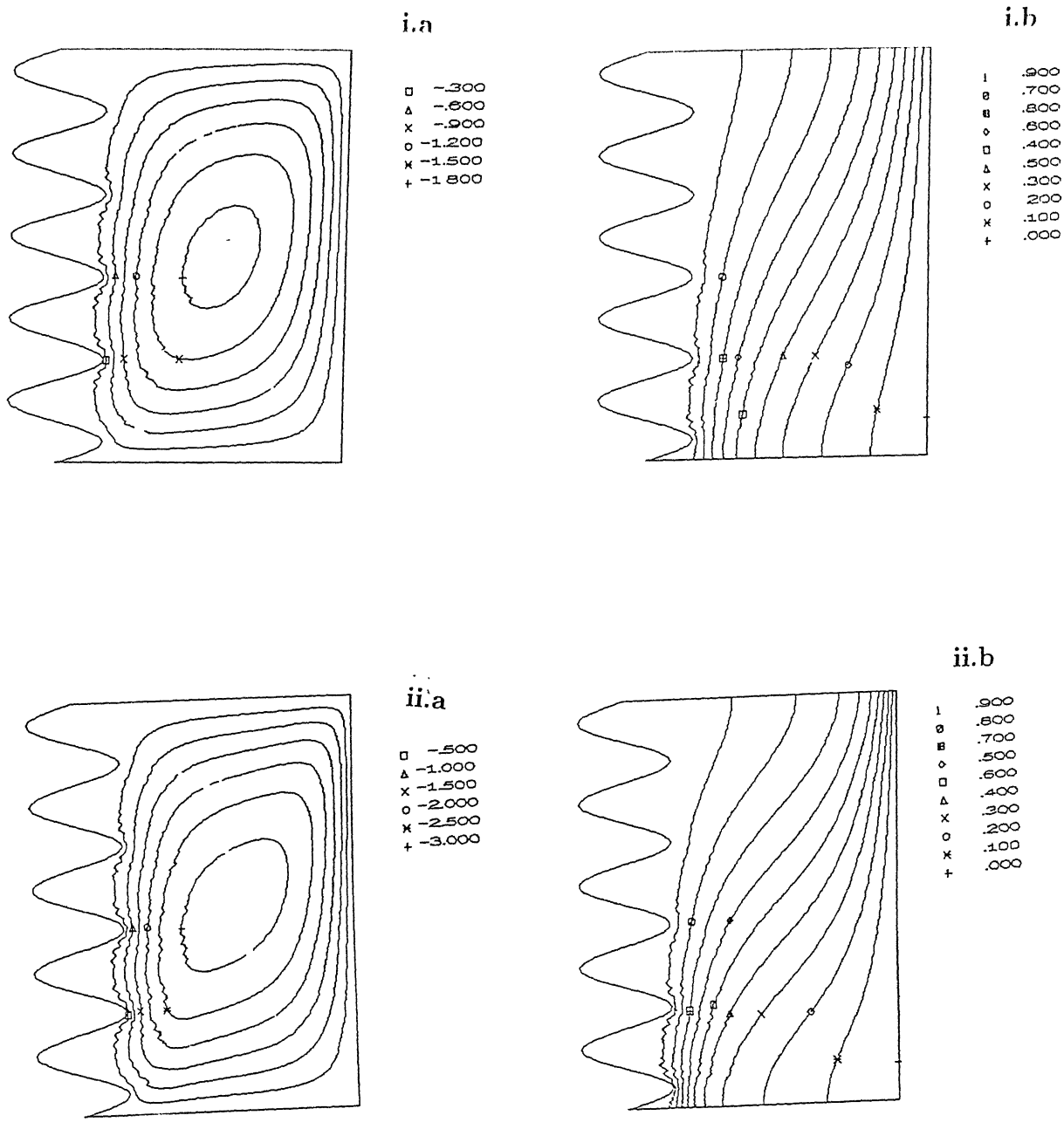

Figure (6.9): (a) Streamlines and (b) Isotherms for multiple waves case for (i) $Ra = 30$, (ii) $Ra = 60$ with $a = 0.2$, $\phi = 0^o$ and $N = 5$.

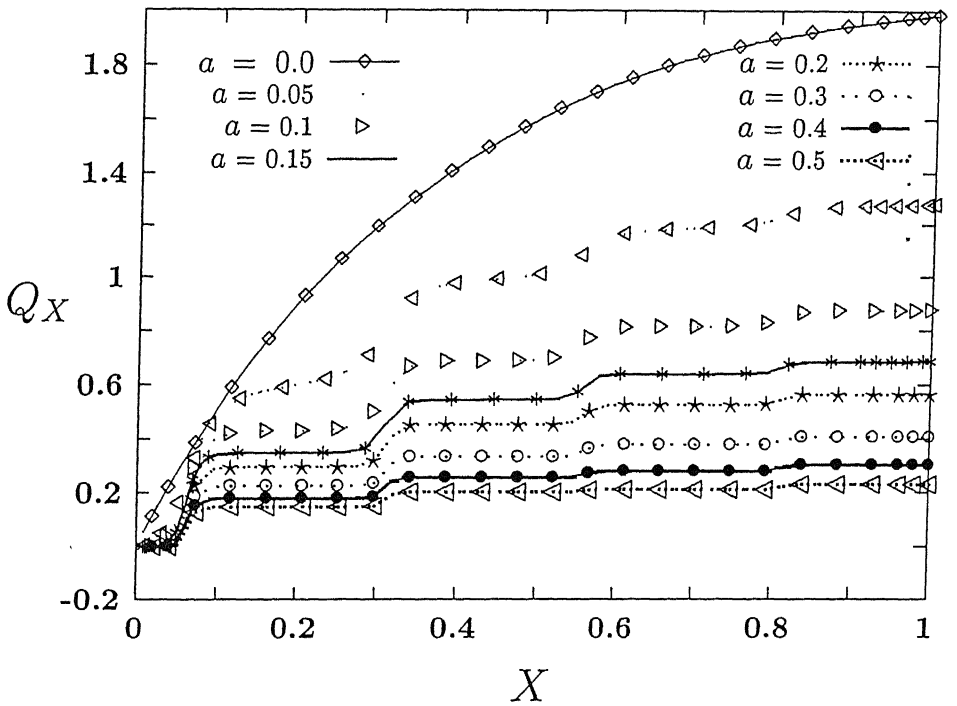

Figure (6.10): Cumulative global heat flux for varyious amplitude with fixed $Ra = 50, \phi = 0^o$ and $N = 4$.

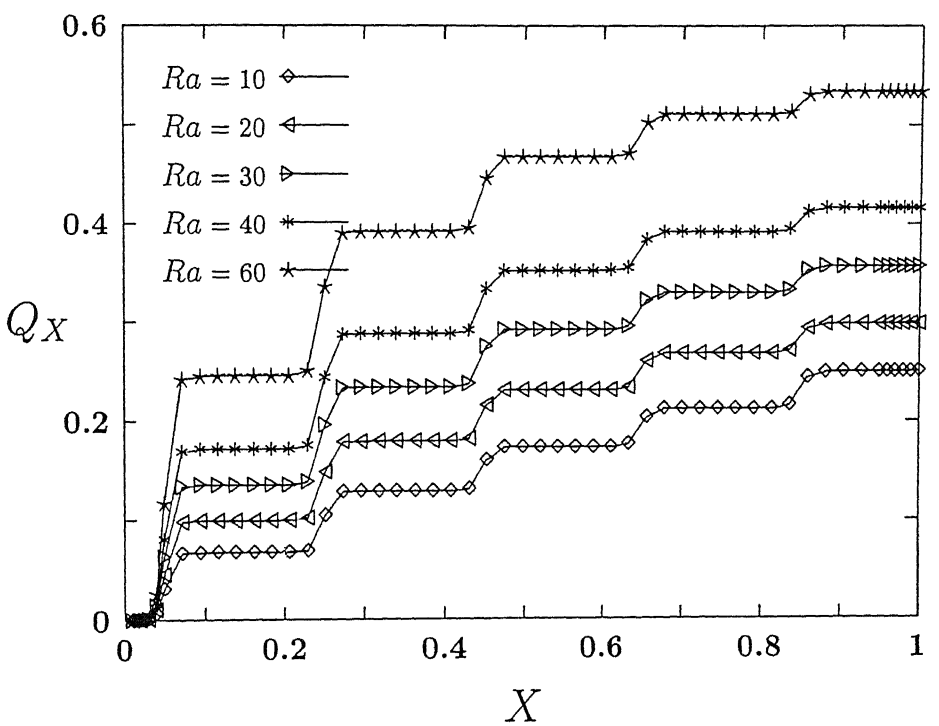

Figure (6.11): Cumulative global heat flux for various Ra with fixed $a = 0.2, \phi = 0^o$ and $N = 5$.

The streamlines, isotherms and cumulative global heat flux in Figures (6.12a), (6.12b) and (6.13) correspond to the study of variable number of waves (2 - 5) each of $a = 0.1$ with zero phase and $Ra = 30$. From these figures it is clear that as the number of the waves increase, the loss of the vertical component of the buoyancy force increases thereby causing a reduction in the convective heat transfer. To a distance from the leading edge of the wavy wall, the cumulative heat flux is increasing with the increase in the value of N, but it continues to lie below further as the distance from the leading edge increases. From the global heat flux results, (the end values of each curve) it is clearly seen that as the number of waves is increasing more, the heat flux into the medium is less. But at the same time, neither separation or reattachment on the wall nor the recirculation zone is observed for the various parameter values considered here.

Finally, the varying phase ($0^o - 315^o$) for fixed amplitude $a = 0.1$ and $Ra = 20$, $N = 4$ has an interesting effect to observe on the global heat flux. As it can be seen from the Figure (6.14), the global heat flux value decreases for increasing phase upto 180^o and then it increases from 180^o. From all these observations, one can choose the optimal values for amplitude, phase, the number of waves per unit length while dealing with wavy boundaries in porous medium.

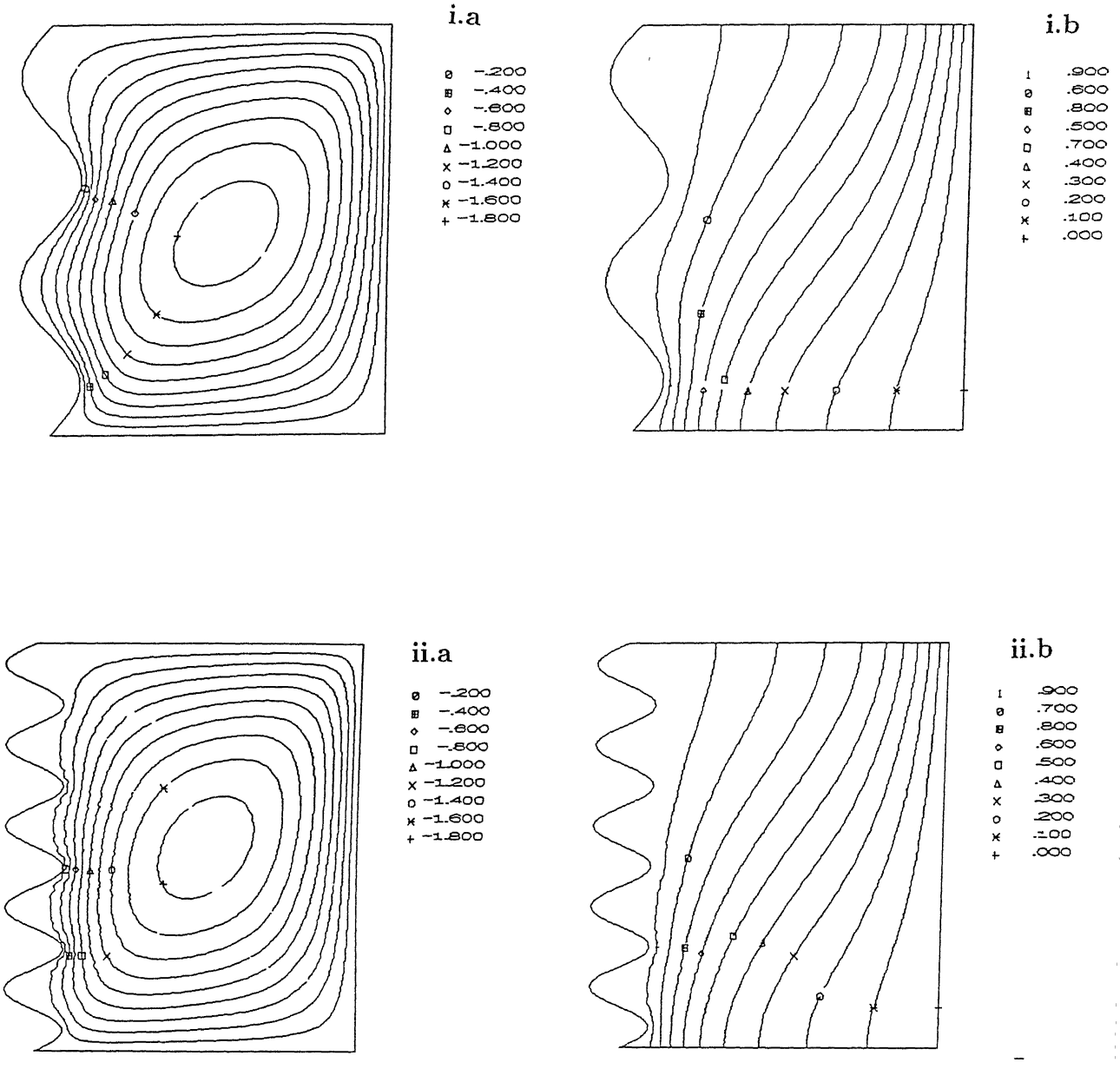

Figure (6.12): (a) Streamlines and (b) Isotherms for multiple waves case for (i) $N = 2$, (ii) $N = 5$ with $a = 0.1$, $\phi = 0^o$ and $Ra = 30$.

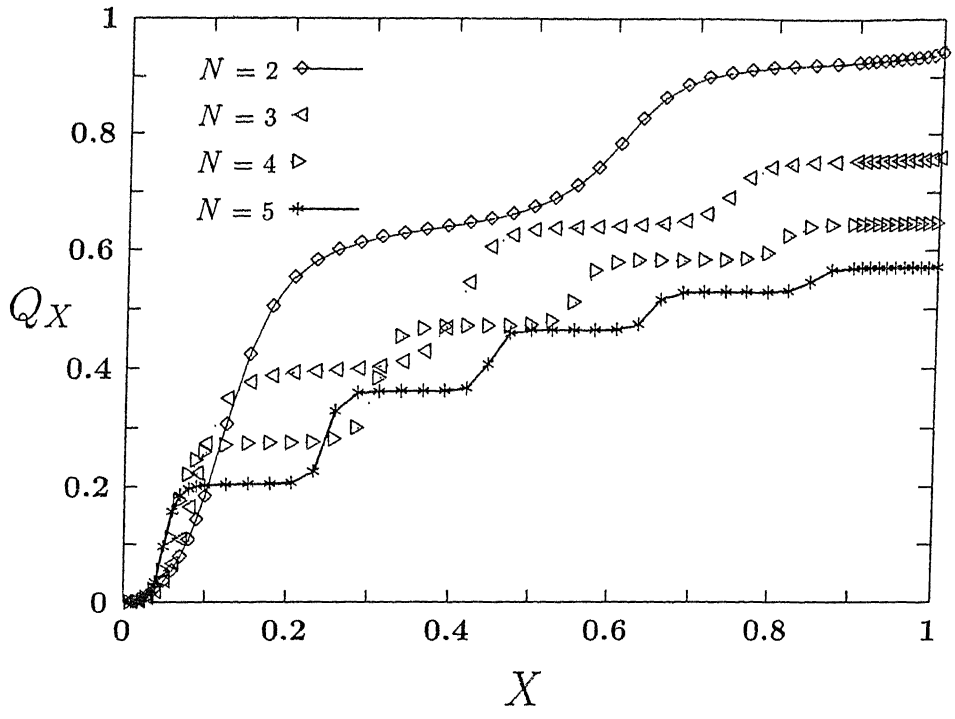

Figure (6.13): Cumulative global heat flux for various N and fixed $a = 0.1, Ra = 30$, and $\phi = 0^o$.

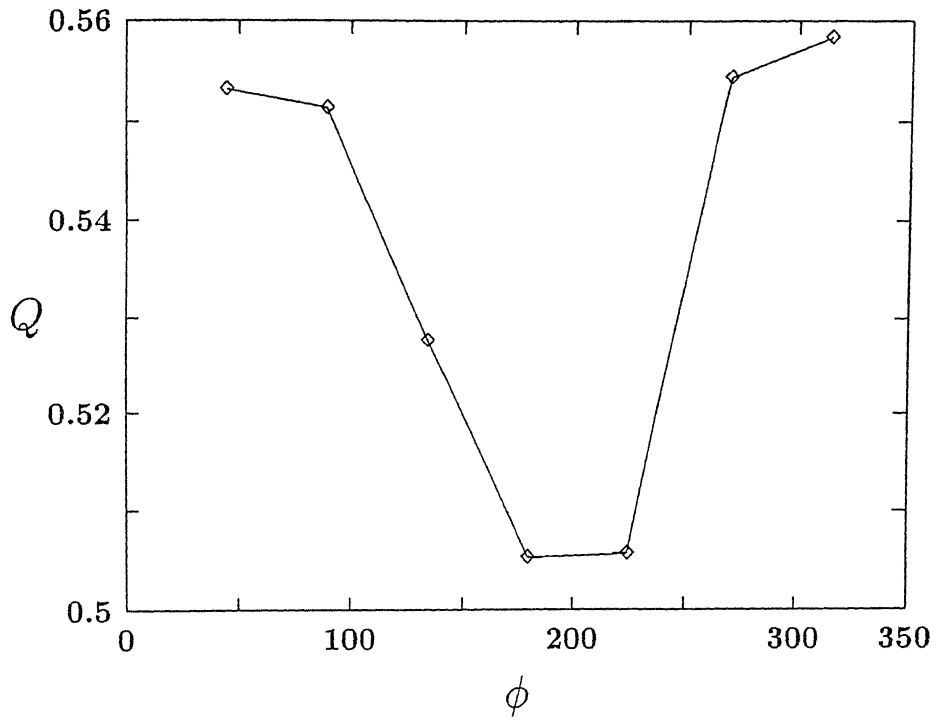

Figure (6.14): Global heat flux Q .vs. ϕ (in degrees).

Chapter 7

Free Convection From A Horizontal Wavy Surface In A Porous Enclosure [1]

7.1 INTRODUCTION

Study of natural convection in porous enclosures is of great importance in several scientific and engineering applications such as nuclear waste management, building thermal insulators, geothermal power plants etc. Many theoretical and experimental investigations have been carried out to understand the natural convection from plane surfaces in a porous enclosure. Nield and Bejan [7] give a beautiful review of all these works. In practice one would encounter roughened surfaces in several heat transfer devices such as flat plate solar collectors, flat plate condensers in refrigerators, etc. Large scale non-uniformities are encountered in cavity wall insulating systems and in grain storage containers.

Very little has been done to understand the effects of the non-uniformities on the convective flow and heat transfer. Yao [50] studied natural convection in a continuum fluid due to a vertical wavy wall at constant temperature. Later Moulic and Yao [75] analysed the same problem with constant heat flux condition. Their studies indicate that the increase in the amplitude of the wave decreases the local heat flux. Rees and Riley [29] studied the Lapwood convection with horizontal plane walls replaced by wavy walls and observed the multicellular convection process for Ra greater than certain critical value. Recently,

[1] Accepted for publication in "**Numerical Heat Transfer**"

Rees and Pop [26], [27],[28] theoretically considered the case of natural convection induced by semi-infinite vertical and horizontal wavy surfaces in saturated porous medium under boundary layer approximations.

In the present investigation, simulation of flow structure and the natural convection due to a uniformly heated horizontal wavy wall in a Darcian fluid saturated porous enclosure is attempted. The wavy wall is assumed to be sinusoidal in structure. The numerical simulation is carried out by using Bubnov Galerkin finite element method. The computational experiments are carried out for various values of the governing parameters (Ra, a, ϕ and N). It is observed that the flow pattern in the enclosure as expected differs greatly from that of the boundary layer flow [27] The global heat flux decreases with increasing values of amplitude. The flow driving buoyancy force is seen to enhance the heat transfer into the system, at the same time, the intensified stream inside the separated region is seen to trap the heat and hinder the heat transfer. Because of this, only marginal changes could be seen in the heat transfer results with the increasing values of Rayleigh number. The results for varying amplitude, phase and Rayleigh number are clearly depicted through the computer generated plots for streamlines, isotherms and cumulative global heat flux profiles.

7.2 Governing Equations

Darcian fluid saturated porous enclosure with sinusoidal wavy wall at the bottom and the three plane walls constituting the other sides as shown in the Figure (7.1) is considered. The bottom wall is maintained at uniform temperature higher than its surrounding temperature and the two vertical walls are adiabatic. The four walls are assumed to be impermeable. The fluid is assumed to be normal Boussinesq fluid.

The governing equations for flow and heat transfer in the enclosure in terms of the dimensionless variables can be written as:

$$\frac{\partial^2 \Psi}{\partial X^2} + \frac{\partial^2 \Psi}{\partial Y^2} = -Ra \frac{\partial \theta}{\partial X} \tag{7.1}$$

$$\frac{\partial \Psi}{\partial Y}\frac{\partial \theta}{\partial X} - \frac{\partial \Psi}{\partial X}\frac{\partial \theta}{\partial Y} = \frac{\partial^2 \theta}{\partial X^2} + \frac{\partial^2 \theta}{\partial Y^2} \tag{7.2}$$

Rees and Pop [26], [27],[28] theoretically considered the case of natural convection induced by semi-infinite vertical and horizontal wavy surfaces in saturated porous medium under boundary layer approximations.

In the present investigation, simulation of flow structure and the natural convection due to a uniformly heated horizontal wavy wall in a Darcian fluid saturated porous enclosure is attempted. The wavy wall is assumed to be sinusoidal in structure. The numerical simulation is carried out by using Bubnov Galerkin finite element method. The computational experiments are carried out for various values of the governing parameters (Ra, a, ϕ and N). It is observed that the flow pattern in the enclosure as expected differs greatly from that of the boundary layer flow [27] The global heat flux decreases with increasing values of amplitude. The flow driving buoyancy force is seen to enhance the heat transfer into the system, at the same time, the intensified stream inside the separated region is seen to trap the heat and hinder the heat transfer. Because of this, only marginal changes could be seen in the heat transfer results with the increasing values of Rayleigh number. The results for varying amplitude, phase and Rayleigh number are clearly depicted through the computer generated plots for streamlines, isotherms and cumulative global heat flux profiles.

7.2 Governing Equations

Darcian fluid saturated porous enclosure with sinusoidal wavy wall at the bottom and the three plane walls constituting the other sides as shown in the Figure (7.1) is considered. The bottom wall is maintained at uniform temperature higher than its surrounding temperature and the two vertical walls are adiabatic. The four walls are assumed to be impermeable. The fluid is assumed to be normal Boussinesq fluid.

The governing equations for flow and heat transfer in the enclosure in terms of the dimensionless variables can be written as:

$$\frac{\partial^2 \Psi}{\partial X^2} + \frac{\partial^2 \Psi}{\partial Y^2} = -Ra \frac{\partial \theta}{\partial X} \tag{7.1}$$

$$\frac{\partial \Psi}{\partial Y}\frac{\partial \theta}{\partial X} - \frac{\partial \Psi}{\partial X}\frac{\partial \theta}{\partial Y} = \frac{\partial^2 \theta}{\partial X^2} + \frac{\partial^2 \theta}{\partial Y^2} \tag{7.2}$$

along with the dimensionless boundary conditions

$$\left.\begin{array}{c} \Psi = 0, \theta = 1 \; on \; Y = a \; \sin(N\pi X - \phi) \\ \Psi = 0, \theta = 0 \; on \; Y = 1 \\ \Psi = 0, \frac{\partial \theta}{\partial X} = 0 \; on \; X = 0 \; and \; X = 1 \end{array}\right\}. \tag{7.3}$$

Here $Ra = \frac{Kg\beta(T_w - T_a)L}{\alpha\nu}$ is the Rayleigh number based on the horizontal dimension of the porous enclosure L.

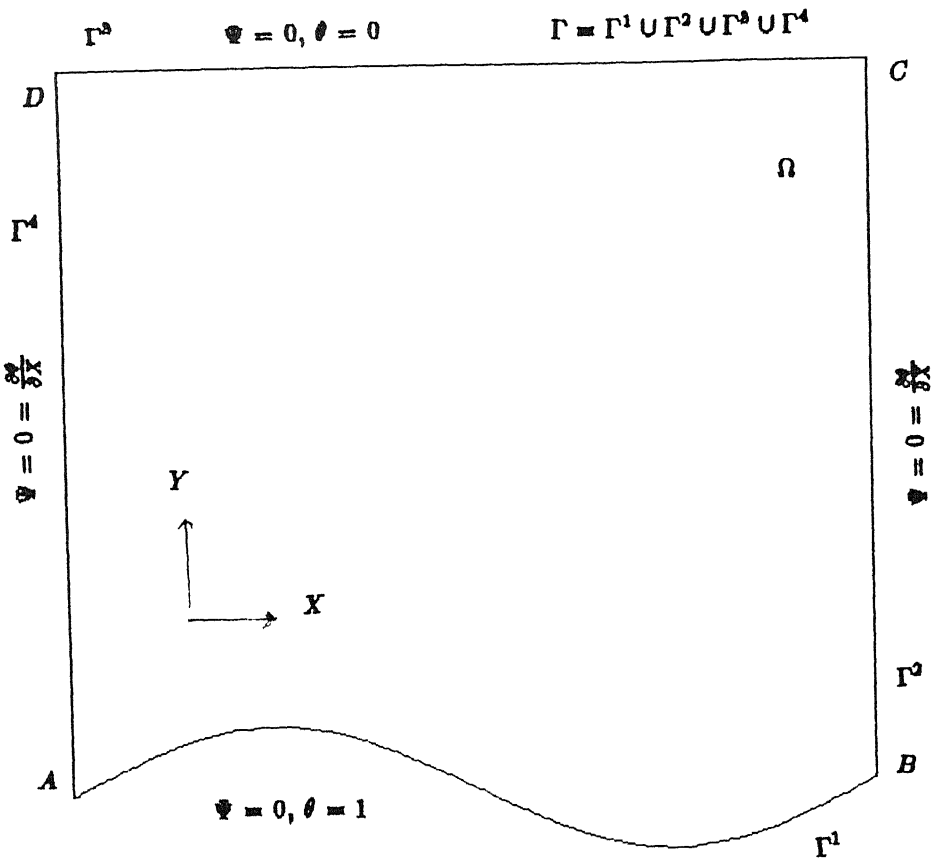

Figure (7.1): Porous square enclosure with uniformly heated horizontal wavy wall.

The dimensionless variables are defined as (ref [27])

$$X = \frac{x}{L}, Y = \frac{y}{L}, \Psi = \frac{\psi}{\alpha} \; and \; \theta = \frac{T - T_a}{T_w - T_a}$$

Here X and Y are the dimensionless Cartesian coordinates with x and y as dimensional

counterparts, L is the horizontal dimension of the cavity, ψ and Ψ are dimensional and dimensionless stream functions, T is the temperature, T_w is the temperature of the wavy wall, T_a is the reference temperature, θ is the dimensionless temperature, ρ is the density, β is the thermal expansion coefficient, ν is the kinematic viscosity of the fluid, K is the permeability, g is the acceleration due to gravity, α is the effective thermal diffusivity, a is the wave amplitude, ϕ is the wave phase, N is the number of waves considered along the horizontal dimension of the cavity.

7.3 Numerical Analysis

The governing partial differential equations (7.1)-(7.2) along with the hydrodynamic and thermal boundary conditions (7.3) are solved numerically by using Bubnov-Galerkin weighted residual finite element technique. To precisely account for the geometrical non-linearity, owing to the wavy nature of the wall, the domain $A\ B\ C\ D$ Figure (7.1) has been discretized using isoparametric quadratic serendipity elements with finer elements near the boundaries.

The Galerkin Weighted Residual form of the momentum and the energy equations are:

$$\int_\Omega \left(\nabla^2\Psi + Ra\frac{\partial\theta}{\partial X}\right) W_l d\Omega = 0 \tag{7.4}$$

$$\int_\Omega \left[\nabla^2\theta - \left(\frac{\partial\Psi}{\partial Y}\frac{\partial\theta}{\partial X} - \frac{\partial\Psi}{\partial X}\frac{\partial\theta}{\partial Y}\right)\right] W_l d\Omega = 0 \tag{7.5}$$

Introducing the following discretization of the domain $(\Omega \cup \Gamma)$ and the element level discretized representation for the stream function and temperature distribution

$$\Omega = \cup_e \Omega^e$$

$$\Psi = \sum_{i=1}^{i=8} \Psi_i^e N_i^e,\ \theta = \sum_{i=1}^{i=8} \theta_i^e N_i^e \ and\ W_l = N_l^e$$

into equations (7.4)-(7.5), we obtain the following elemental matrix over a typical element e as:

$$\mathrm{M^e}\ r^e\ =\ f^e \tag{7.6}$$

where

$$\mathrm{M^e} = \begin{bmatrix} A^e_{lk} & B^e_{lk} \\ \\ C^e_{lki} & A^e_{lk} \end{bmatrix}$$

and r^e is the column vector of unknown nodal parameters

$$r^e = [\Psi^e_k \;\; \theta^e_k]^T$$

and f^e is the known vector which is given by

$$f^e = \left[f^{e^1}_k \;\; f^{e^2}_k\right]^T$$

and the elements in the elemental matrix are obtained from the following representations

$$A^e_{lk} = -\int_{\Omega^e} \left(\frac{\partial N^e_l}{\partial X}\frac{\partial N^e_k}{\partial X} + \frac{\partial N^e_l}{\partial Y}\frac{\partial N^e_k}{\partial Y} \right) d\Omega^e \tag{7.7}$$

$$B^e_{lk} = Ra \int_{\Omega^e} N^e_l \frac{\partial N^e_k}{\partial X} d\Omega^e \tag{7.8}$$

$$C^e_{lki} = \int_{\Omega^e} \sum_{i=1}^{i=8} \left(\frac{\partial N^e_k}{\partial X}\frac{\partial N^e_i}{\partial Y} N^e_l - \frac{\partial N^e_k}{\partial Y}\frac{\partial N^e_i}{\partial X} N^e_l \right) d\Omega^e \tag{7.9}$$

In view of the finite element assembly procedure and the prescribed essential and natural boundary conditions, without any loss of generality, the components of f^e can be written as :

$$f^{e^1}_l = 0 \tag{7.10}$$

$$f^{e^2}_l = -\int_{\Gamma^{2+4} \cap \Gamma^e} N_l \overline{\frac{\partial \theta}{\partial n}} d\Gamma^e \tag{7.11}$$

where the expression under over bar denotes the prescribed normal heat flux.

The cumulative global heat flux has been computed from the formula

$$Q_X = \int_0^X (n. \bigtriangledown T) \frac{ds(\xi)}{d\xi} d\xi \tag{7.12}$$

where n is the unit vector outward drawn normal to the wavy surface and $s(\xi)$ is the arc-length along the surface with the arc length variable ξ. The global heat flux Q can be obtained from the above expression by taking $X = L$ in the integral limit.

Numerical simulations have been carried out on a 50 X 60 graded finite element mesh as shown in Figure (7.2). The results have been obtained with a tolerance of $\tau = 5$ X 10^{-4}

where τ is the absolute difference between two successive iteration values of the unknowns. To ensure the grid independence of the results, the numerical experimentations are carried out on three different mesh systems consisting of 30 X 30, 40 X 50, and 50 X 60 elements. Cumulative global heat flux obtained on these three mesh systems have been compared in Figure (7.3). It clearly shows that the change in cumulative global heat flux becomes negligible as one moves from 30 X 30 mesh system to 50 X 60 mesh system. That is why 50 X 60 mesh system has been chosen for the current numerical simulations.

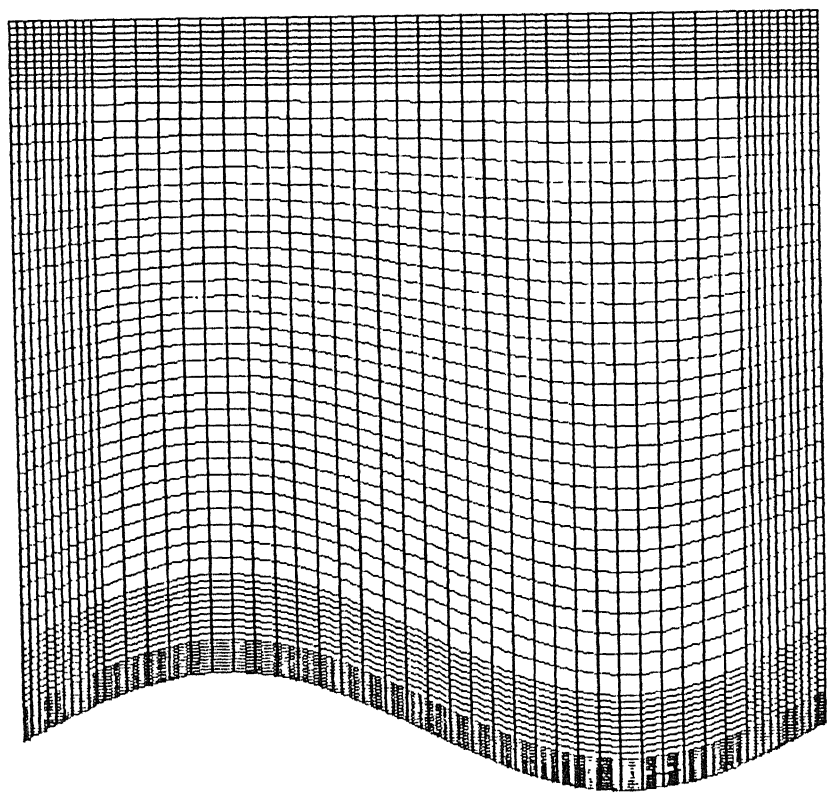

Figure (7.2): Five level graded finite element mesh.

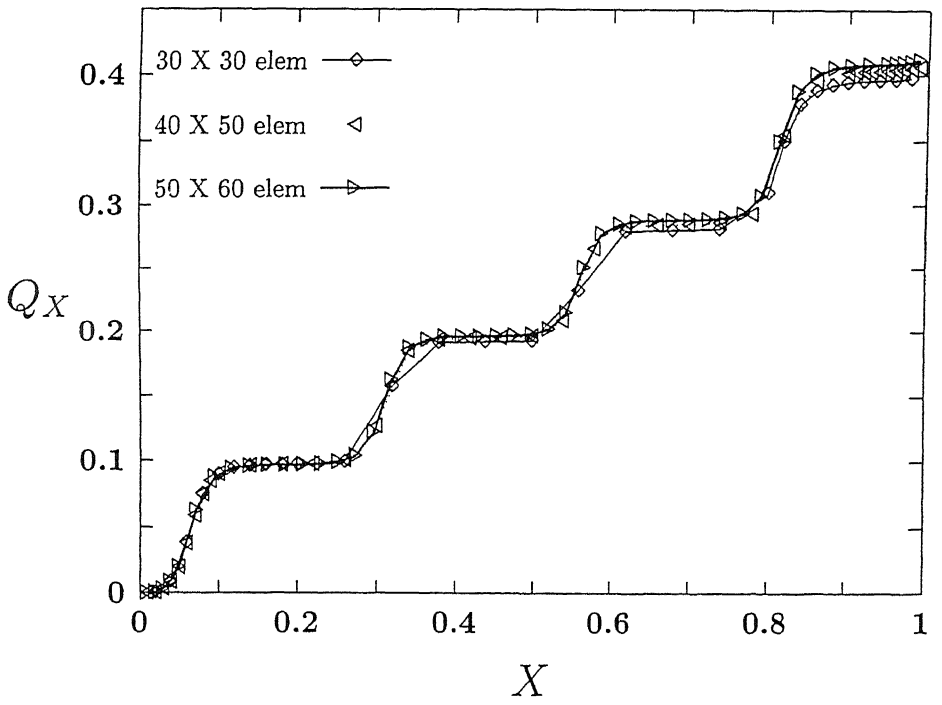

Figure (7.3): Best mesh selection from the comparison curves

7.4 Results and Discussion

The crucial parameters which influence the flow and heat transfer in the porous enclosure are the modified Rayleigh number Ra based on the horizontal dimension of the cavity, the amplitude a and the phase ϕ of the wave and the number of waves N considered along the horizontal dimension. To begin with, the effect of amplitude, phase and Rayleigh number are analysed here by considering $N = 1$. Later, the influence of $N > 1$ on convective heat transfer has been analysed. The computational results are presented in the form of streamlines, isotherms and cumulative global heat flux plots in order to bring out the fluid flow and heat transfer process in the porous square cavity.

The effect of varying amplitude has been analysed for different values of amplitude between 0.05 and 0.15 by fixing Ra at 50 and ϕ at 0°. The results for two of these cases are presented in the Figures (7.4). From the streamline pattern, it is clear that the flow separates on the wall close to the crest of the wave and reattaches near the trough of the wavy wall. As the amplitude increases, this separation zone is seen to grow in size. Also inside this zone, a counter flow is seen. The flow separation and reattachment may be attributed to the change

in the pressure gradient, owing to the non-linear geometry of the bottom wall. The counter flow hinders the heat transfer into the mainstream. This feature becomes amply clear from the cumulative global heat flux plot presented in Figure (7.7). In this figure, comparison is also made with the horizontal flat plate results ($a = 0$; straight line seen in the plot). From this it is clear that the amplitude of the wave reduces the global heat flux into the system. The global heat flux results are presented in the Figure (7.10a). From this figure, it can be clearly seen that the global heat flux decreases as the amplitude of the wave increases.

The varying Ra case has been analysed for $Ra = 1$ to 100 with $a = 0.1$, $\phi = 0^o$ and $N = 1$. For $Ra = 10$ and 25 no flow separation on the wall is observed but for $Ra = 50$, the flow separation and reattachment on the wall is clearly seen and with the increasing Ra, the counter flow inside this separated zone is observed to become intensified. The streamlines and isotherms for this case are given in the Figures (7.5). With increasing Ra, the separation and reattachment points move closer to the leading and the trailing edges of the wavy wall respectively and thus increasingly cover the wavy wall. Also the bulb of the counter flow grows in dimension and extends into the core region of the domain. Such secondary flows are known to hinder the heat transfer into the system. Consequently, the heat transfer enhancing effect of increasing Ra is seen to be countered. That these two opposing factors are competing can be observed clearly from the marginal drifts in the global heat flux plot given in Figure (7.10b). As the value of the Rayleigh number increases the temperature distribution in the enclosure is observed to become wavy in nature due to the presence of the wavy surface.

The streamlines and the isotherms for varying phase are plotted in the Figures (7.6) for fixed $Ra = 50$ and $a = 0.1$. With the phase changing from $0^o - 350^o$, the reattachment point of the separated flow shifts from the bottom wall to the adjacent walls in clockwise direction. Consequently the counter flow zone emerging on the bottom wall grows in size, slowly covering the whole of the domain and thus leading to the manifestation of a cycle of uni and bi-cellular flows. The cumulative global heat flux for varying phases (from 0^o to 350^o) has been plotted in the Figure (7.8) and the global heat flux changes for varying phase has been shown in the Figure (7.10c).

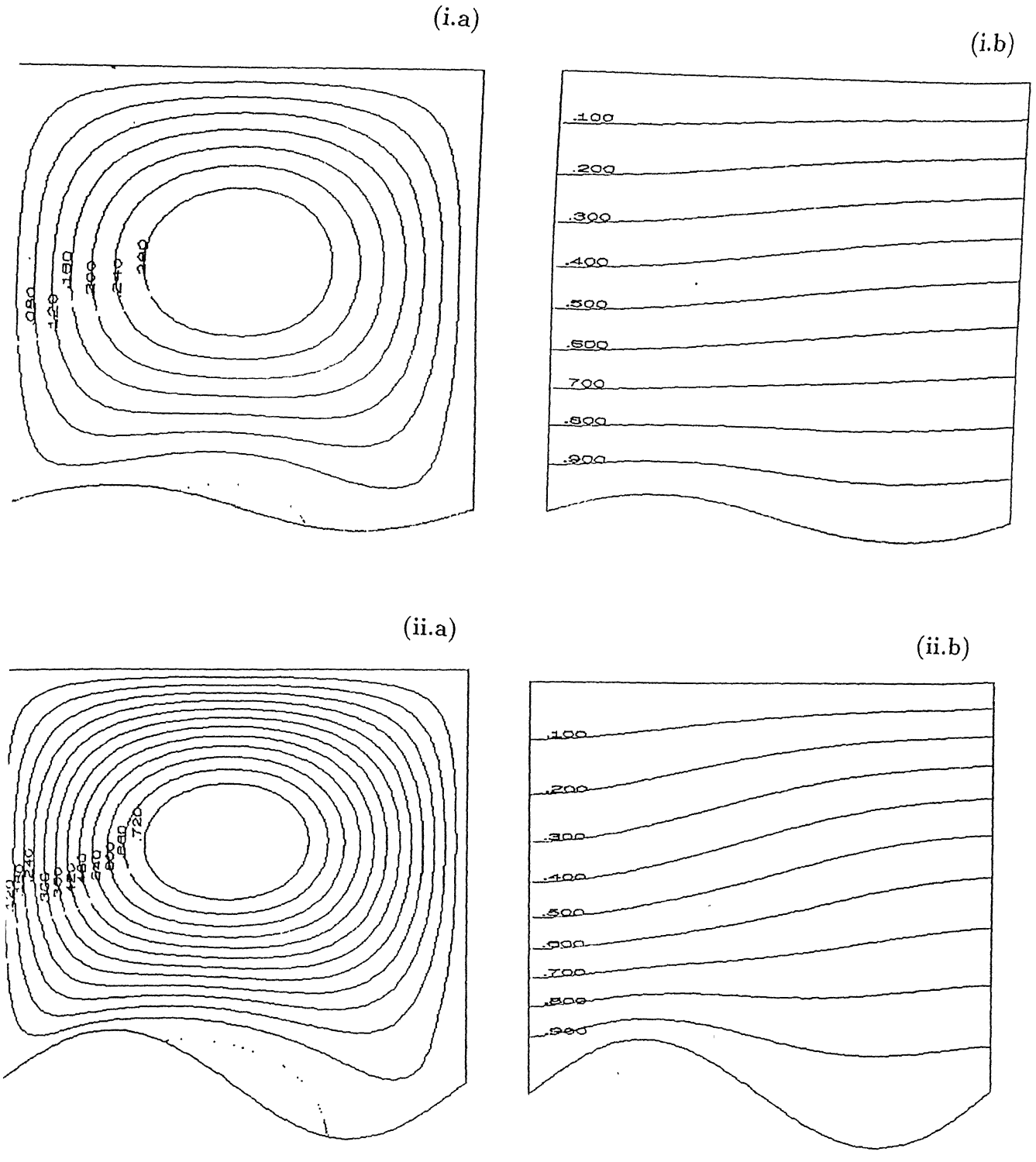

Figure (7.4): (a) Streamlines and (b) Isotherms for varying amplitudes (i) $a = 0.05$, (ii) $a = 0.15$ with $Ra = 50$, $\phi = 0^{o}$ and $N = 1$.

(i.a)

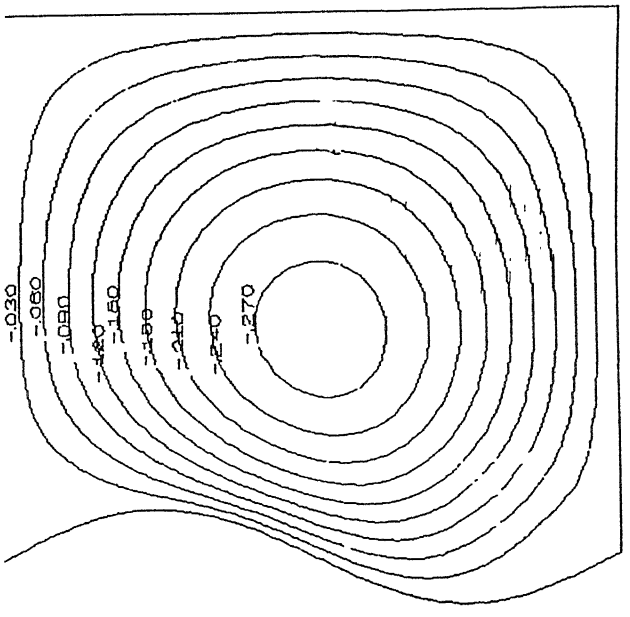
-.030
-.060
-.090
-.120
-.150
-.180
-.210
-.240
-.270

(i.b)

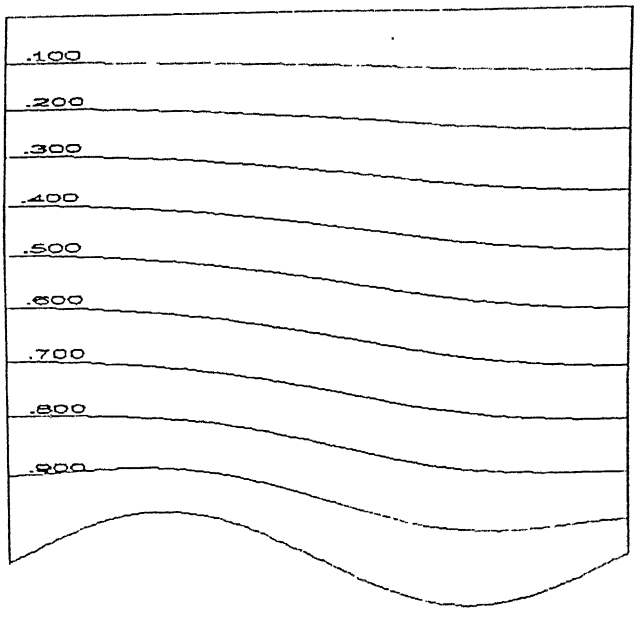
.100
.200
.300
.400
.500
.600
.700
.800
.900

(ii.a)

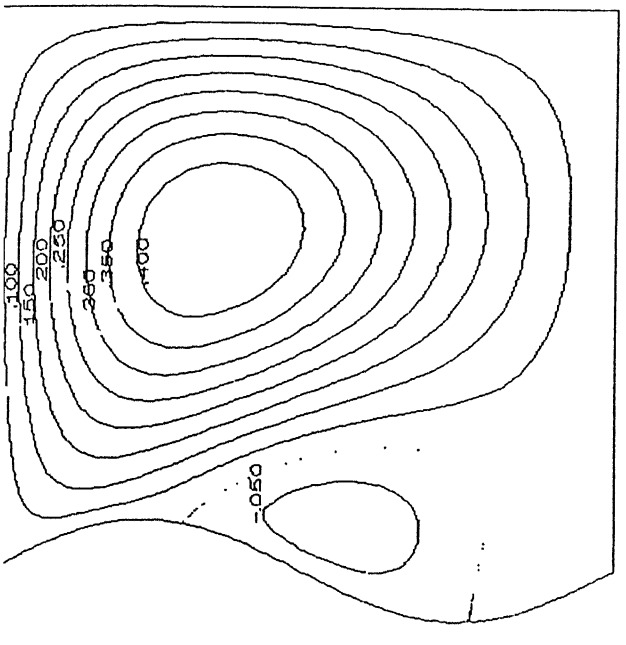
.100
.150
.200
.250
.300
.350
.400
-.050

(ii.b)

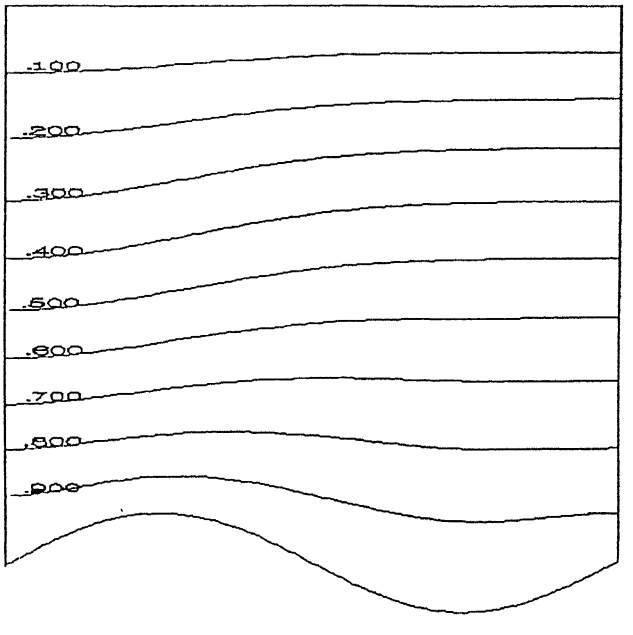
.100
.200
.300
.400
.500
.600
.700
.800
.900

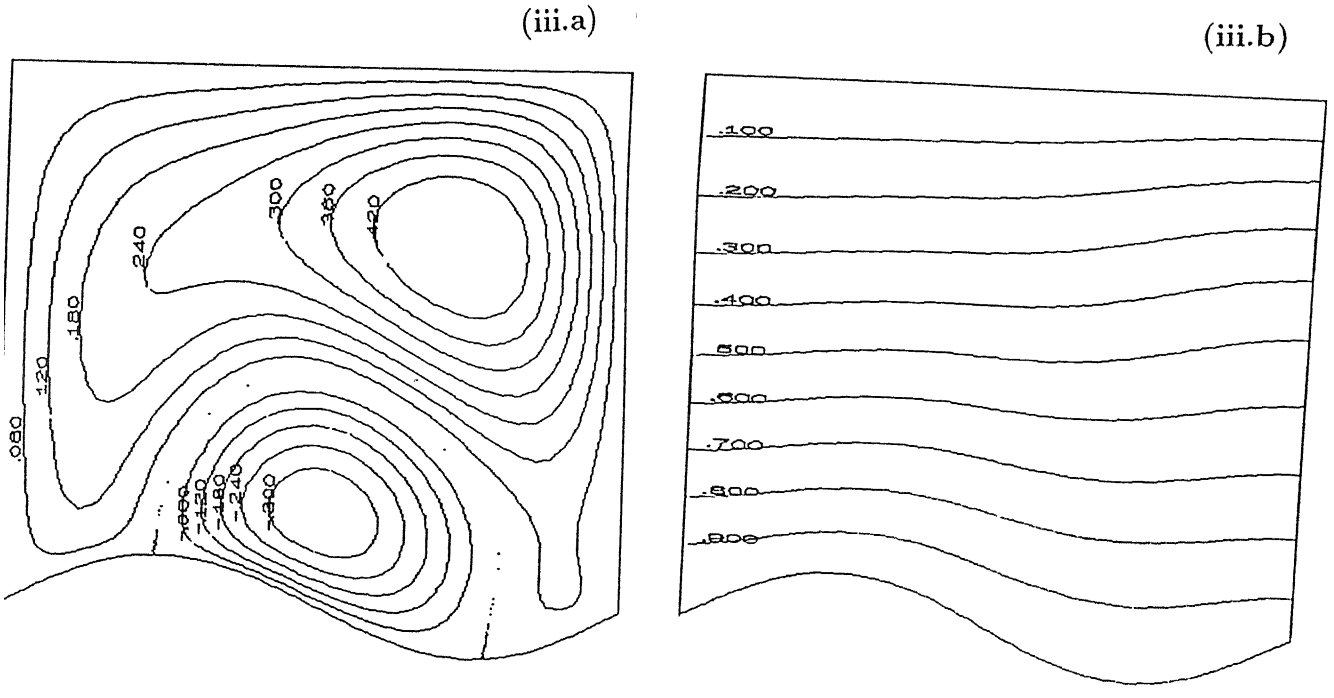

Figure (7.5): (a) Streamlines and (b) Isotherms for varying Rayleigh numbers (i) $Ra = 20$ (ii) $Ra = 60$, (iii) $Ra = 100$ with $a = 0.1$ and $N = 1$.

(i.a)

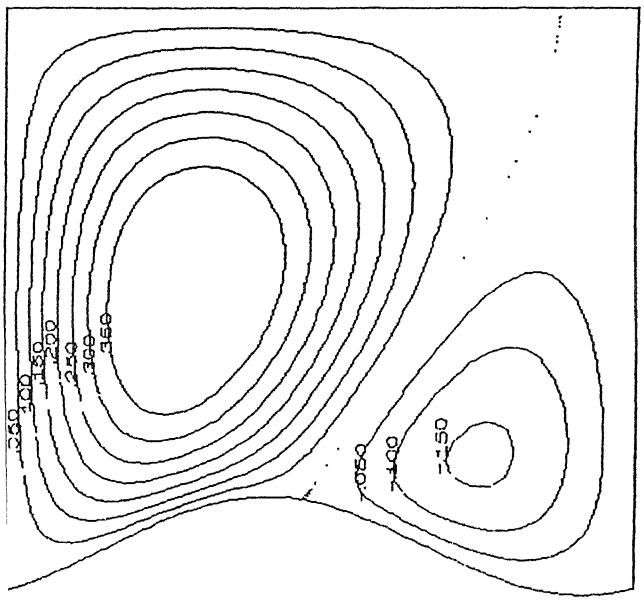
.250
.300
.150
.200
.250
.300
.350
.050
.100
.150

(i.b)

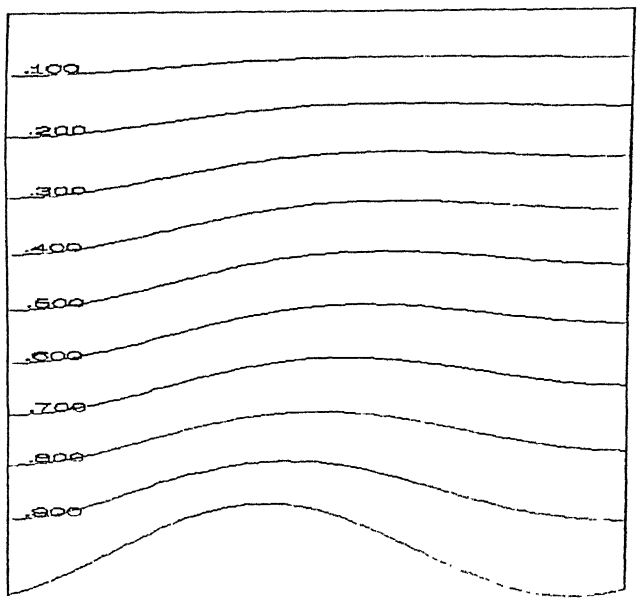
.100
.200
.300
.400
.500
.600
.700
.800
.900

(ii.a)

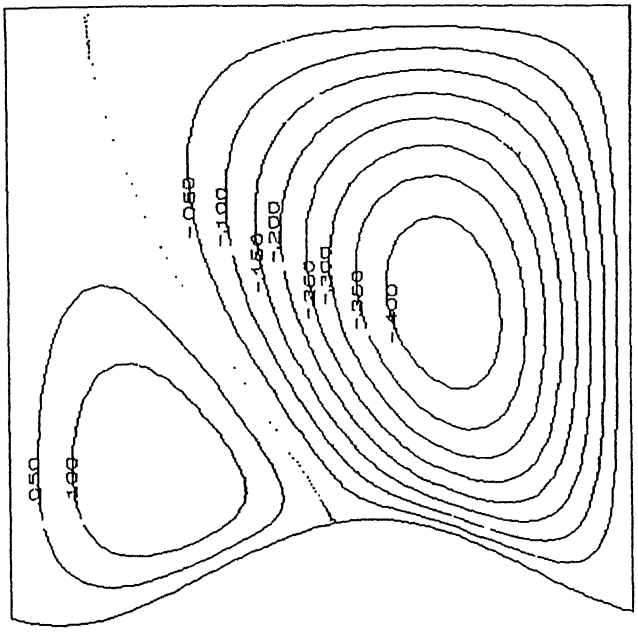
.050
.100
.150
.200
.250
.300
.350
.400
.050
.100

(ii.b)

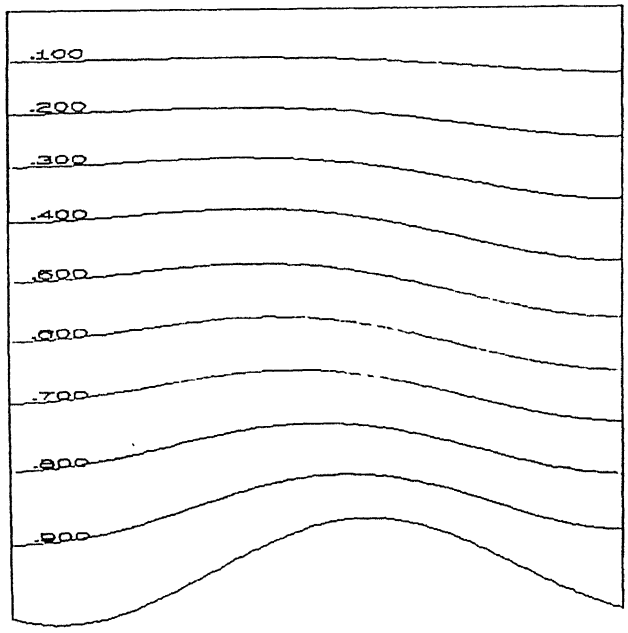
.100
.200
.300
.400
.500
.600
.700
.800
.900

(iii.a)

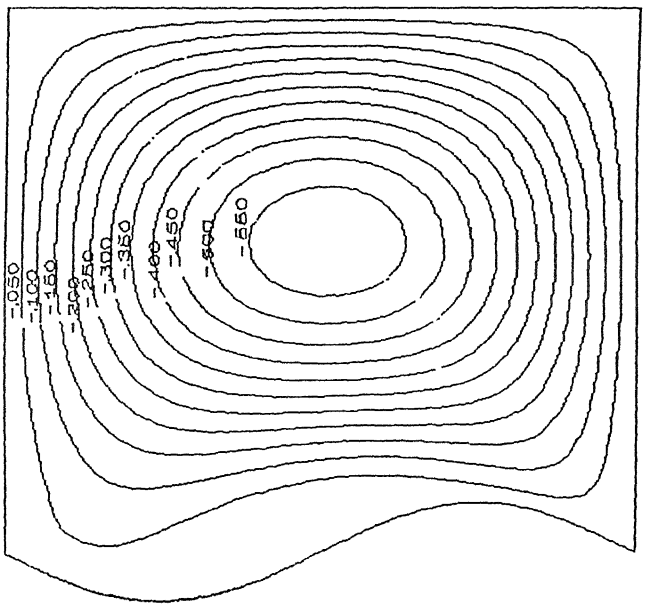

(iii.b)

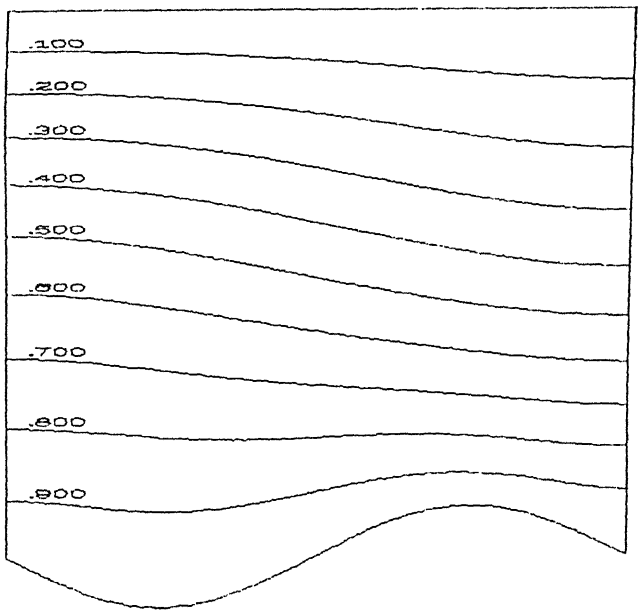

(iv.a)

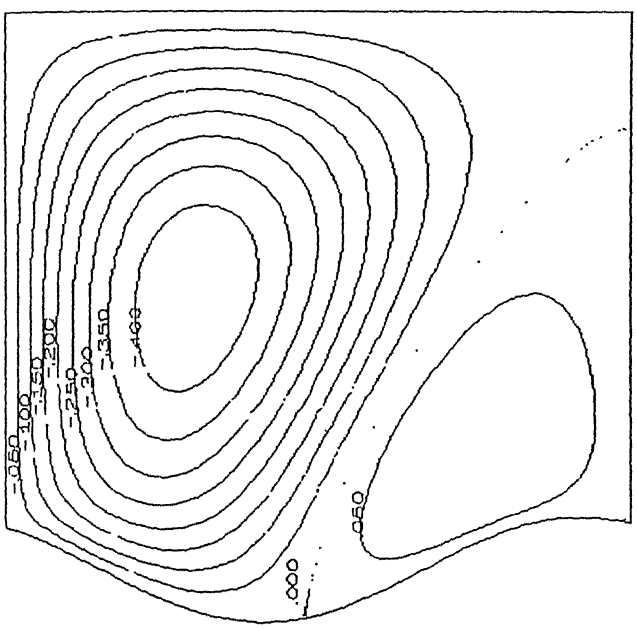

(iv.b)

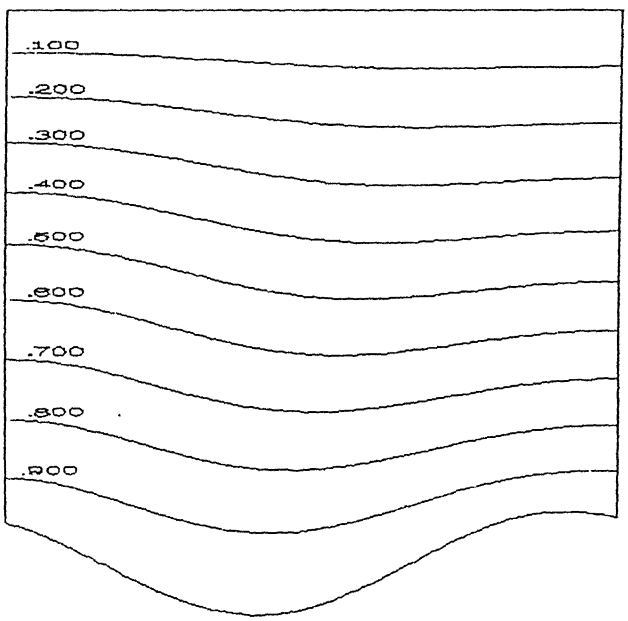

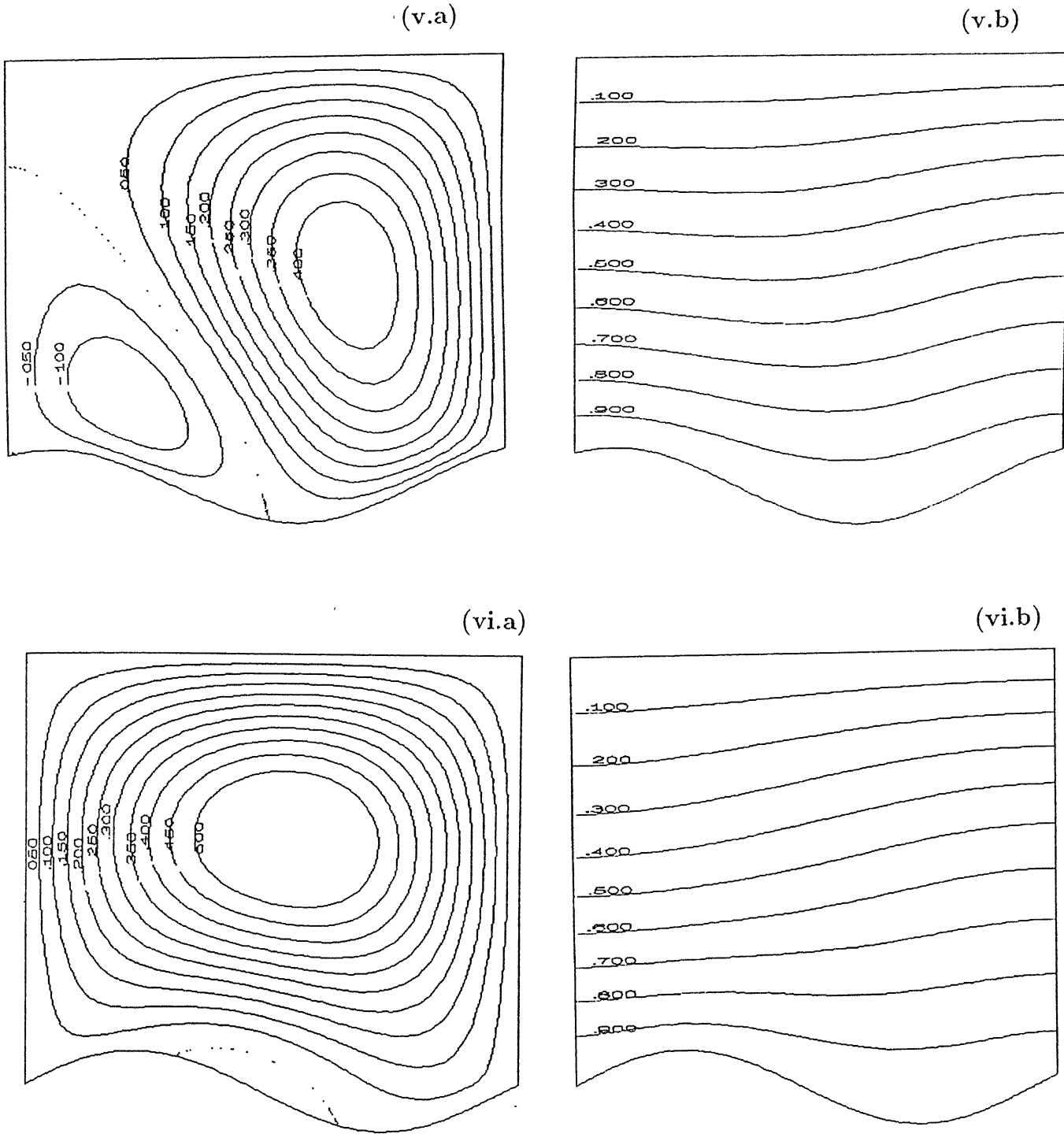

Figure (7.6): (a) Streamlines and (b) Isotherms for varying phase (i) $\phi = 60^o$ (ii) $\phi = 120^o$ (iii) $\phi = 180^o$ (iv) $\phi = 240^o$ (v) $\phi = 300^o$ (vi) $\phi = 350^o$ with $a = 0.1$ $Ra = 50$ and $N = 1$.

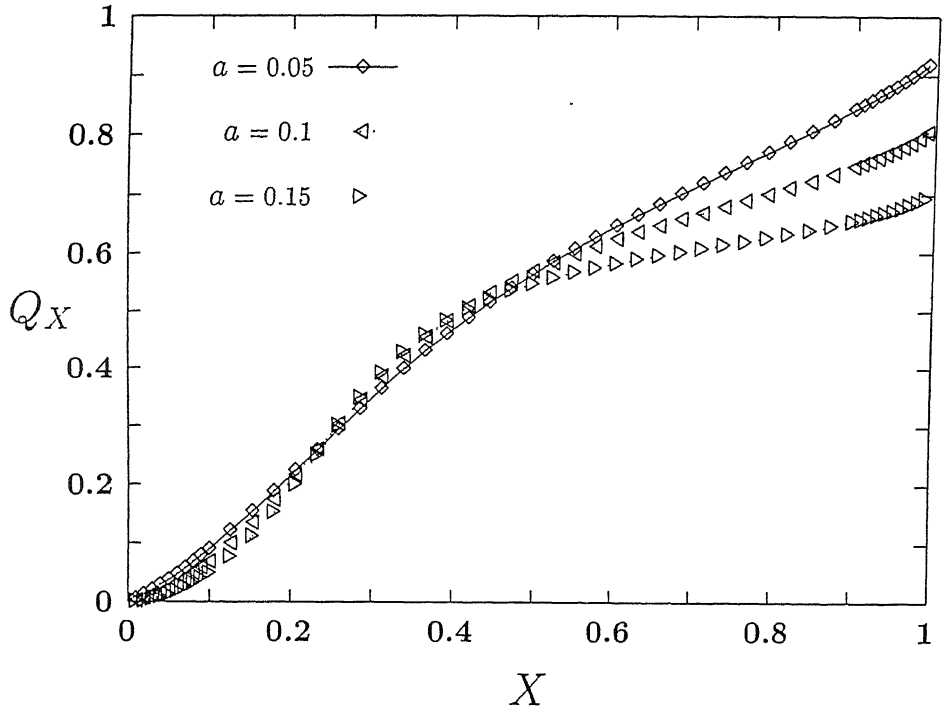

Figure (7.7): Cumulative global heat flux for varying amplitude (0. - 0.15) with fixed $Ra = 50$, $\phi = 0^o$, and $N = 1$.

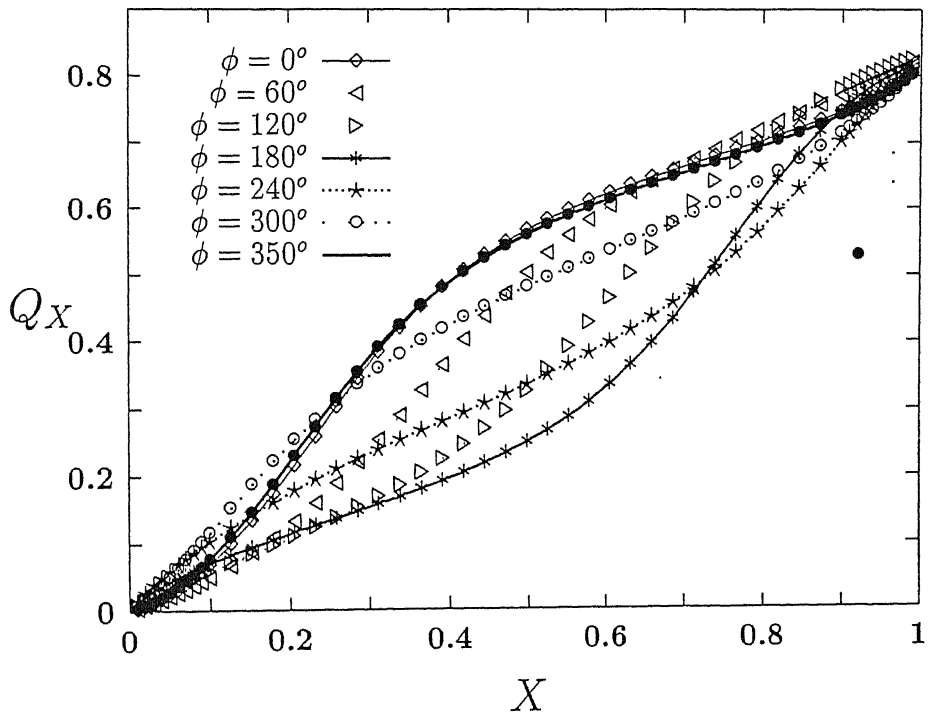

Figure (7.8): Cumulative global heat flux for varying phases from (0^o - 350^o) with fixed $a = 0.1$, $Ra = 50$ and $N = 1$.

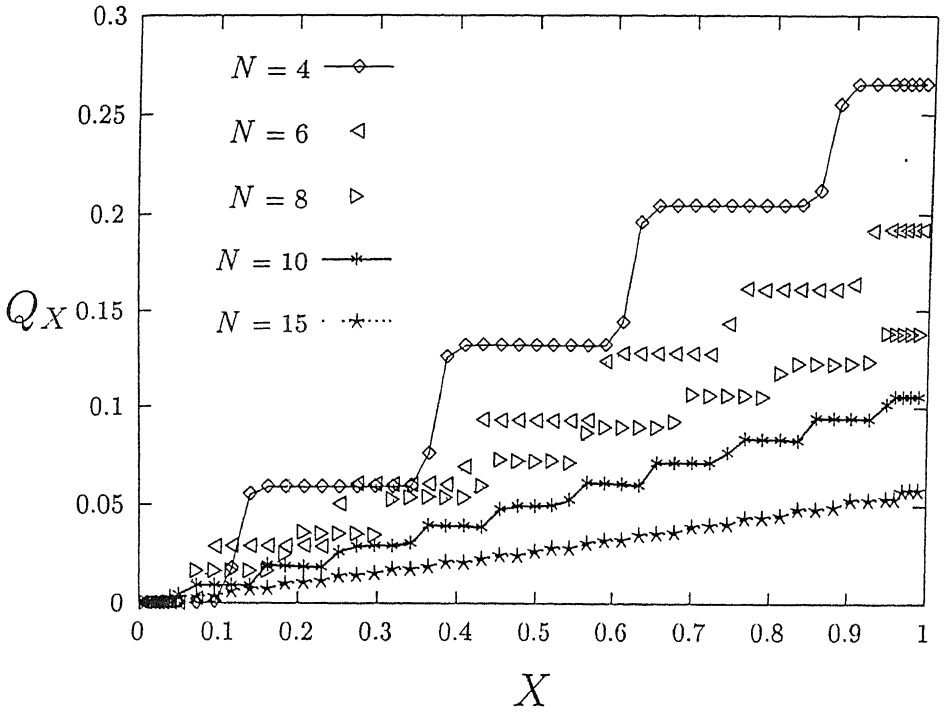

Figure (7.9): Cumulative global heat flux for varying N (= 1 to 4) for fixed $a = 0.1$, $Ra = 50$, and $\phi = 0^o$.

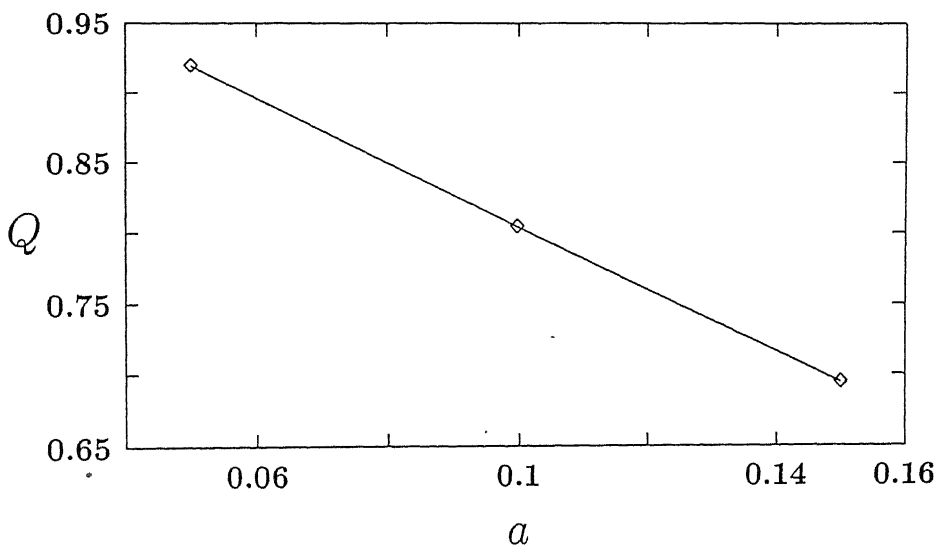

Figure (7.10a): Global Heat Flux .vs. a for fixed Ra,ϕ and N.

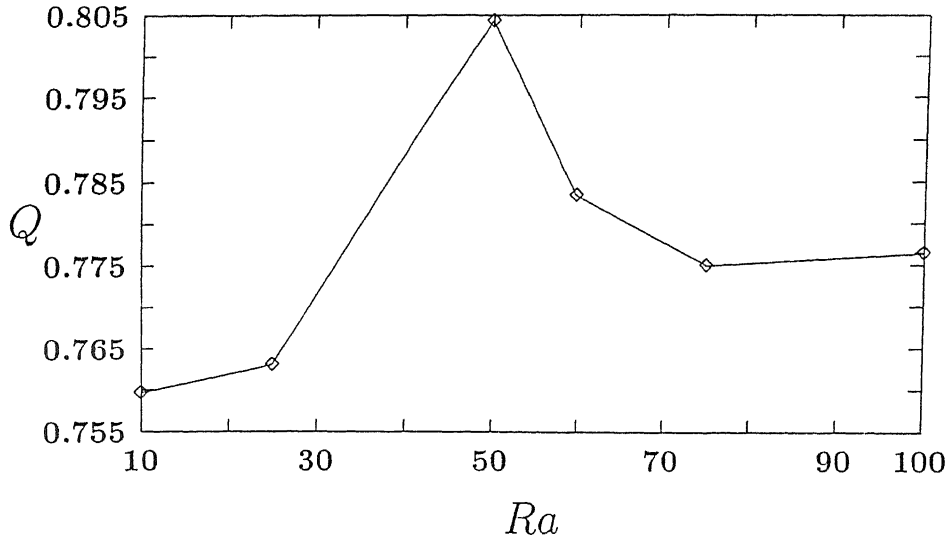

Figure (7.10b): Global Heat Flux .vs. Ra for fixed a,ϕ and N.

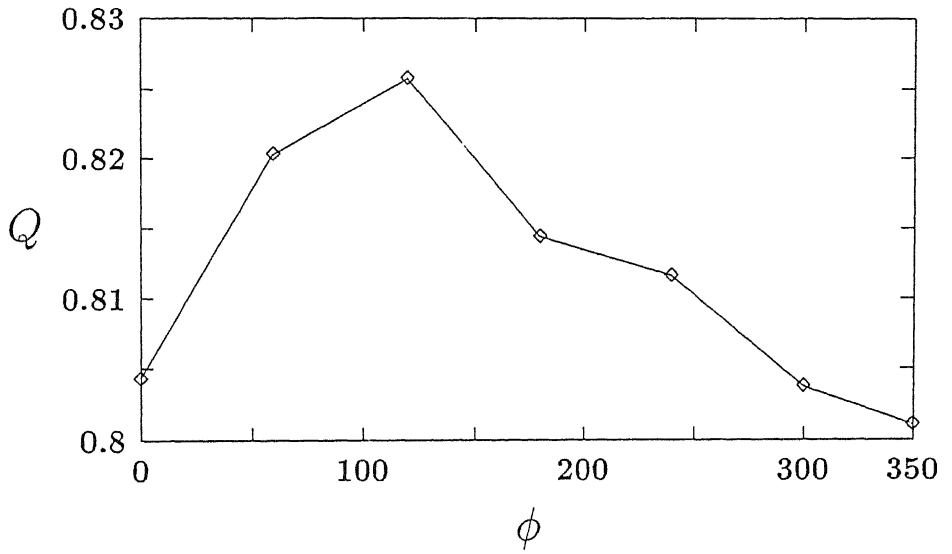

Figure (7.10c): Global heat flux .vs. ϕ for fixed a,Ra and N.

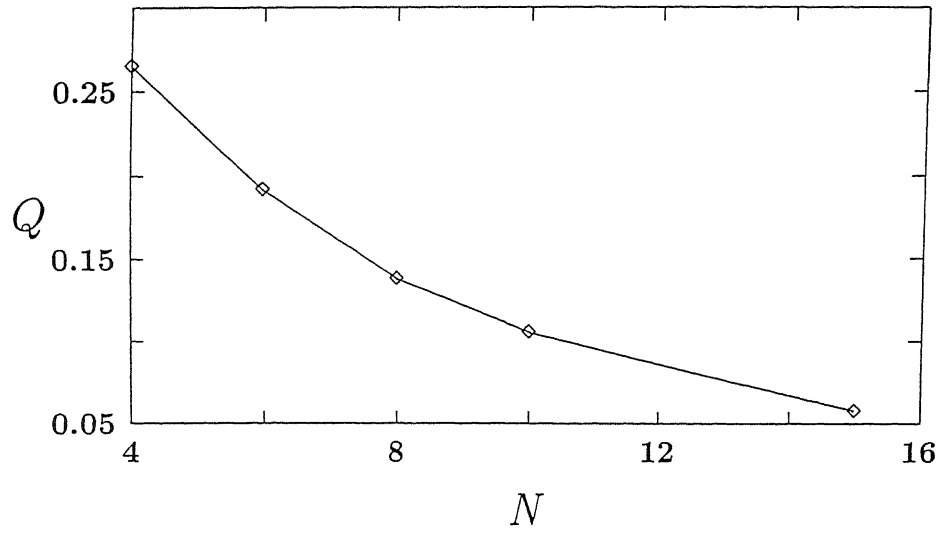

Figure (7.10d): Global heat flux .vs. N for fixed a,Ra and ϕ.

Interestingly, the increase in the value of N changes the heat transfer. The cumulative global heat flux in this case has been plotted in the Figure (7.9). This figure clearly depicts the fact that the increase in the number of waves decreases the global heat flux into the system. The corresponding global heat flux results with varying N are plotted in Figure (7.10d). This decrease may be due to the emergence of increasing number of recirculation zones over these waves.

Bibliography

[1] A. Bejan.: Entropy Generation Through Heat And Fluid Flow. John - Weily & Sons, New York, (1994)

[2] A. Bejan.: Convection Heat Transfer, John - Weily & Sons New York, (1984)

[3] A.V. Shenoy.: Non-Newtonian Fluid Heat Transfer In Porous Media : In Advances In Heat Transfer, Academic Press, New York, 24, (1994) 102-184.

[4] B. Gebhart.: Heat Transfer, McGraw Hill (1971).

[5] C.A.J. Fletcher.: Computational Techniques For Fluid Dynamics. 1 (Fundamental And General Techniques) Springer-Verlag, Berlin, (1977).

[6] C.L. Tucker III and R.B. Dessenberger.: Governing Equations For Flow And Heat Transfer In Stationary Fiber Beds, (In.: Flow And Rheology In Polymor Composits Manufacturing, Edited by S.G.Advani), Elsevier Science B.V. (1994) Chap. 8, Elsevier Science, Amsterdam (1994).

[7] D.A. Nield and A. Bejan.: Convection In Porous Media. New-York, Springer-Verlag (1992).

[8] D.F. Rogers.: Laminar Flow Analysis, Cambridge University Press, (1992).

[9] J. Bear.: Dynamics Of Fluids In Porous Media, American Elsevier Publishing Company Inc. New-York, (1972).

[10] J. Bear and Y. Bechmat.: Introduction To Modelling Of Transport Phenomenon In Poruos Media, Kluwer Academic Publishers, Dordrecht, (1990).

[11] M. Sahimi.: Flow And Transport In Porous Media And Fractured Rock(From Classical Methods To Modern Approaches), VCH, Weinheim, 1995.

[12] P. Cheng.: Heat transfer in geothermal systems : In Advances in Heat Transfer, Academic Press 14 (1978) 1-105.

[13] R.E. Collins.: Flow Of Fluids Through Porous Materials, Reinhold Publishing Corporation, New-York, (1961).

[14] A. Amiri and K. Vafai.: Analysis of dispersion effects and non-thermal equilibrium on non-Darcian variable porosity incompressible flow through porous media, Int J Heat Mass Transfer, 37 (1994) 939-954.

[15] A. Bejan.: The basic scales of natural convection heat and mass transfer in fluids and fluid saturated porous media, Int Comm Heat Mass Transfer, 14 (1987) 107-123.

[16] A. Bejan and D. Poulikakos.: The non-Darcy regime for vertical boundary layer natural convection in a porous medium, Int J Heat Mass Transfer, 27 (1984) 717-722.

[17] A. Nakayama and H. Koyama.: Free convection heat transfer over a non-isothermal body of arbitrary shape embedded in a fluid saturated porous medium, J Heat Transfer, 109 (1987) 125-130.

[18] A. Nakayama and H. Koyama.: Integral treatment of buoyancy induced flows in a porous medium adjacent to horizontal surface with variable wall temperature, Int J Heat Fluid Flow, 8 (1987) 240-242.

[19] A. Nakayama and H. Koyama.: A general similarity transformation for combined free and forced convection flows within a fluid saturated porous medium, J Heat Transfer, 109 (1987) 1041-1045.

[20] A. Nakayama, T. Kokudai and H. Koyama.: An integral treatment for non-Darcy free convection over a vertical flat plate and cone embedded in a fluid saturated porous medium, Warme und Stoffubertrgung, 23 (1988) 337-341.

[21] A. Nakayama, T. Kodudai and H. Koyama.: Forchheimer free convection over a non isothermal body of arbitrary shape in a saturated porous medium, J Heat Transfer, 112 (1990) 511-515.

[22] A. Nakayama and I. Pop.: Free convection over a non-isothermal body in a porous medium with viscous dissipation, Int Comm Heat Mass Transfer, 16 (1989) 173-180.

[23] B. Gebhart.: Effect of viscous dissipation in natural convection, J Fluid Mech, 14 (1962) 225-235.

[24] B. Gebhart and J. Mollendorf.: Viscous dissipation in external natural convection flows, J Fluid Mech, 38 (1969) 97-107.

[25] C.T. Hsu and P. Cheng.: Thermal dispersion in a porous medium, Int J Heat Mass Transfer, 33 (1990) 1587-1597.

[26] D.A.S. Rees and I. Pop.: A note on free convection along a vertical wavy surface in a porous medium, J Heat Transfer, 116 (1994) 505-508.

[27] D.A.S. Rees and I. Pop.: Free convection induced by a horizontal wavy surface in a porous medium, Fluid Dynamics Research, 14 (1994) 151-166.

[28] D.A.S. Rees and I. Pop.: Free convection induced by a vertical wavy surface with uniform heat flux in a porous medium, J Heat Transfer, 117 (1995) 547-550.

[29] D.A.S. Rees and D.S. Riley.: Free convection in an undulating saturated porous layer: Resonant wavelength excitation, J Fluid Mech, 166 (1986) 503-530.

[30] D.B. Ingham.: The non-Darcy free convection boundary layer on axi-symmetric and two-dimensional bodies of arbitrary shape, Int J Heat Mass Transfer, 29 (1986) 1759-1760.

[31] D.B. Ingham and I. Pop.: Natural convection about a heated horizontal cylinder in a porous medium, J Fluid Mech, 184 (1987) 157-181.

[32] D.B. Ingham.: An exact solution for non-Darcy free convection from a horizontal line source, Warme und Stoffubertrag, 22 (1988) 125-127.

[33] D.S. Riley.: Steady two dimensional thermal convection in a vertical porous slot with spatially periodic boundary imperfections, Int J Heat Mass Transfer, 31 (1988) 2365-2380.

[34] E.M. Sparrow, R. Eichhorn and J.L. Gregg.: Combined forced and free convection in a boundary layer flow, Phy Fluids, 2 (1959) 319-328.

[35] F.C. Lai and F.A. Kulacki.: Non-Darcy convection from horizontal impermeable surfaces in saturated porous media, Int J Heat Mass Transfer, 30 (1987) 2289-2192.

[36] F.C. Lai and F.A. Kulacki.: Thermal dispersion effects on non-Darcy convection over horizontal surfaces in saturated porous media, Int J Heat Mass Transfer, 32 (1989) 971-976.

[37] F.C. Lai and F.A. Kulacki.: Non-Darcy mixed convection along a vertical wall in saturated porous medium, J Heat Transfer, 113 (1991) 252-255.

[38] G. Ramanaiah and G. Malarvizhi.: Non-Darcy regime mixed convection on vertical plates in saturated porous media with lateral mass flux, Acta Mechanica, 81 (1990) 191-200.

[39] G. Ramanaiah and G. Malarvizhi.: Non-Darcy axi-symmetric free convection on permeable horizontal surfaces in a saturated porous medium, Int J Heat Fluid Flow, 12 (1991) 89-91.

[40] H.M. Badr and I. Pop.: Combined convection from an isothermal horizontal rod buried in a porous medium, Int J Heat Mass Transfer, 31 (1988) 2527-2541.

[41] I. Pop and P. Cheng.: An integral method for free convection on a Darcian fluid about a cone with curvature effects, Int Comm Heat Mass Transfer, 13 (1986) 433-438.

[42] J.H. Merkin.: Mixed convection boundary layer flow on a vertical surface in a saturated porous medium, J Engg Maths, 14 (1980) 301-313.

[43] J.H. Merkin.: Free convection boundary layers in a saturated porous medium with lateral mass flux, Int J Heat Mass Transfer, 21 (1978) 1499-1504.

[44] J.H. Merkin.: Free convection boundary layers on axi-symmetric and two dimensional bodies of arbitrary shape in a saturated porous medium, Int J Heat Mass Transfer, 22 (1979) 1461-1462.

[45] J.J. Fried and M.A. Combarnous.: Dispersion in porous media : In Advances in Heat Transfer, Academic Press, New-York, 7 (1971).

[46] J.T. Hong and C.L. Tien.: Analysis of thermal dispersion effect on vertical plate natural convection in porous media, Int J Heat Mass Transfer, 30 (1987) 143-150.

[47] J.T. Hong, Y. Yamada and C.L. Tien.: Effects of non-Darcian and non-uniform porosity on vertical plate natural convection in porous media, J Heat Transfer, 109 (1987) 356-361.

[48] K.S. Chen and J.R. Ho.: Effects of flow inertia on vertical natural convection in saturated porous media, Int J Heat Mass Transfer, 29 (1986) 753-759.

[49] K. Vafai and C.L. Tien.: Boundary and inertia effects on flow and heat transfer in porous media, Int J Heat Mass Transfer, 24 (1980) 195-203.

[50] L.S. Yao.: Natural convection along a vertical wavy surface, J Heat Transfer, 105 (1983) 465-468.

[51] M.J. Huang and C.K.Chen.: Effects of surface mass transfer on free convection flow over vertical cylinder embedded in a saturated porous medium, J Energy Resources Tech, 107 (1985) 394-396.

[52] M.J. Huang, A.K. Yin, L.Y. Chou and C.K. Chen.: Mixed convection over a horizontal cylinder or a sphere embedded in a saturated porous medium, J Heat Transfer, 108 (1986) 469-471.

[53] M. Kumari and G. Nath.: Non-Darcy mixed convection boundary layer flow on a vertical cylinder in a saturated porous medium, Int J Heat Mass Transform 32 (1989) 183-187.

[54] M. Kumari and G. Nath.: Non-Darcy mixed convection flow over a non-isothermal cylinder and sphere embedded in a saturated porous medium, J Heat Transfer, 112 (1990) 518-523.

[55] M. Poreh.: The dispersivity tensor in the isotropic and axi-symmetric mediums, J Geophysical Research, 70 (1965) 3909-3913.

[56] O. Plumb and J.C. Huenefeld.: Non-Darcy natural convection from heated surfaces in saturated porous medium, Int J Heat Mass Transfer, 24 (1981) 765-768.

[57] O. Plumb.: The effect of thermal dispersion on heat transfer in packed bed boundary layers. Proceedings of Ist ASME/JSME Thermal Engineering Joint Conference, 2 (1983) 17-21.

[58] P. Cheng.: The influence of lateral mass flux on free convection boundary layers in a saturated porous medium, Int J Heat Mass Transfer, 20 (1977) 201-206.

[59] P. Cheng.: Convective heat transfer in porous layers by integral methods, Lett Heat Mass Transfer, 5 (1978) 243-252.

[60] P. Cheng.: Thermal dispersion effects in non-Darcian convective flows in a saturated porous Medium, Lett Heat Mass Transfer, 8 (1981) 267-270.

[61] P. Cheng.: Mixed convection about a horizontal cylinder and a sphere in a fluid saturated porous medium, Int J Heat Mass Transfer, 25 (1982) 1245-1247.

[62] P. Cheng and D. Vortmeyer.: Transverse thermal dispersion and wall channelling in a packed bed with forced convective flow, Chemical Engg Science, 43 (1988) 2523-2532.

[63] P. Cheng and I.D. Chang.: Buoyancy induced flows in a saturated porous medium adjacent to impermeable horizontal surfaces, Int J Heat Mass Transfer, 19 (1976) 1267-1272.

[64] P. Cheng and W.C. Chau.: Similarity solutions for convection of ground water adjacent to horizontal impermeable surfaces with axi-symmetric temperature distribution, Water Resources Res, 13 (1977) 768-772.

[65] P. Cheng and W.J. Minkowycz.: Free convection about a vertical flat plate embedded in a porous medium with application to heat transfer from a dike, J Geo Research, 82 (1977) 2040-2044.

[66] P. Cheng, T.T. Le and I. Pop.: Natural convection of a Darcian fluid about a cone, Int Comm Heat Mass Transfer, 12 (1985) 705-717.

[67] P. Singh and K. Sharma.: Integral method for free convection in thermally stratified porous medium, Acta Mechanica, 83 (1990) 157-163.

[68] R.A. Wooding.: Convection in a saturated porous medium at large Rayleigh or Peclet number, J Fluid Mech, 15 (1963) 527-544.

[69] R. Anderson and M. Bohn.: Heat transfer enhancement in natural convection enclosure flow, J Heat Transfer, 108 (1986) 330-336.

[70] R.M. Fand and J. Brucker.: A correlation for heat transfer by natural convection from horizontal cylinders that accounts for viscous dissipation, Int J Heat Mass Transfer, 26 (1983) 709-726.

[71] R.M Fand, T.E. Steinberger and P. Cheng.: Natural convection heat transfer from a horizontal cylinder embedded in a porous medium, Int J Heat Mass Transfer, 29 (1986) 119-133.

[72] S. Shakerin, M. Bohn and R.I. Loehrke.: Natural convection in an enclosure with discrete roughness elements on a vertical heated wall, Int J Heat Mass Transfer, 31 (1988) 1423-1430.

[73] Jhonson and P. Cheng.: Possible similarity solutions for free convection boundary layers adjacent to flat plates in porous media, Int J Heat Mass Transfer, 21 (1977) 709-718.

[74] S. Ergun.: Fluid flow through packed columns, Chem Engg Progress, 48 (1952) 89-94.

[75] S.G. Moulic and L.S.Yao.: Natural convection along a vertical wavy surface with uniform heat flux, J Heat Transfer, 111 (1989) 1106-1108.

[76] S.H. Bhavnani and A.E. Bergles.: Effect of surface geometry and orientation on laminar natural convection heat transfer from a vertical flat plate with transverse roughness elements, Int J Heat Mass Transfer 33 (1990) 965-981.

[77] W.B. Hooper, T.S. Chen and B.F. Armaly.: Mixed convection from a vertical plate in porous media with surface injection or suction, Num Heat Transfer, 25 (1994) 317-329.

[78] W.J. Minkowycz and P. Cheng.: Free convection about a vertical cylinder embedded in a porous medium, Int J Heat Mass Transfer, 19 (1976) 805-813.

[79] W.J. Minkowycz and P. Cheng.: Local non-similar solutions for free convective flow with uniform lateral mass flux in a porous medium, Lett Heat Transfer, 9 (1982) 159-168.

[80] W.J. Minkowycz, P. Cheng and F. Moalem.: The effect of surface mass transfer on buoyancy induced Darcian flow adjacent to a horizontal heated surface, Int Comm Heat Mass Transfer, 12 (1985) 55-65.

[81] W.J. Minkowycz, P. Cheng and C.H. Chang.: Mixed convection about a non-isothermal cylinder and sphere in a porous medium, Num Heat Transfer, 8 (1985) 349-359.

[82] W.J. Minkowycz, P. Cheng and C.H. Chang.: Mixed convection about non-isothermal cylinders and spheres in a porous medium, Numer Heat Transfer, 8 (1985) 349-359.

Date Slip

This book is to be returned on the date last stamped.

A 123671

.....	.....
.....	.....
.....	.....
.....	.....
.....	.....
.....	.....
.....	.....
.....	.....
.....	.....
.....	.....
.....	.....
.....	.....